Teknillinen korkeakoulu
Laivalaboratorio

Helsinki University of Technology
Ship Laboratory

Espoo 2006

M-292

MODEL TESTS FOR THE PROGRESSIVE FLOODING OF A BOX-SHAPED BARGE

Pekka Ruponen

TEKNILLINEN KORKEAKOULU
TEKNISKA HÖGSKOLAN
HELSINKI UNIVERSITY OF TECHNOLOGY

M-292

MODEL TESTS FOR THE PROGRESSIVE FLOODING OF A BOX-SHAPED BARGE

Pekka Ruponen

Helsinki University of Technology
Ship Laboratory

Teknillinen korkeakoulu
Laivalaboratorio

Espoo 2006

Distribution:
Helsinki University of Technology
Ship Laboratory
P.O.Box 5300
FI-02015 TKK, Finland
Tel. +358 9 451 3501
Fax +358 9 451 4173
Email: Leila.silonsaari@tkk.fi

ISBN 921-22-8228-3
ISSN 1456-3045

Picaset Oy
Helsinki 2006

Contents

Nomenclature

A	area (of an opening)
$\overline{\mathrm{B_0M_0}}$	initial metacentric radius
C_d	discharge coefficient
e	lever
g	acceleration due to gravity
$\overline{\mathrm{GM_0}}$	initial metacentric height
H	water height
I_T	moment of inertia
$\overline{\mathrm{KB_0}}$	vertical center of buoyancy (initial value)
$\overline{\mathrm{KG}}$	vertical center of gravity
m	mass
M	moment
p	air pressure
Q	volumetric flow
S	area of free surface
t	time
T	draft
	time period
T_ϕ	natural period of roll motion
u	flow velocity
V	volume (in general)
V_w	volume of floodwater
x, y, z	Cartesian co-ordinate system, origin in the intact center of gravity
Δ	buoyancy force
ϕ	heel angle
ρ	density of water
ω	angular frequency

ω_e	natural frequency of roll motion
ξ	critical damping ratio
θ	trim angle
ψ	yaw angle
∇	volume of the buoyancy

Abbreviations

COG	center of gravity
HUT	Helsinki University of Technology
TTF	time-to-flood
WT	watertight

Introduction

This report describes the model tests for the progressive flooding of a box-shaped barge. The tests were performed in the towing tank of HUT Ship Laboratory in January 2006. The research was jointly funded by Napa Ltd and HUT Ship Laboratory.

The aim of the tests was to provide experimental data for the validation of numerical simulation methods for progressive flooding of passenger ships since public and detailed measurement data is not currently available.

The shape of the hull is very simple; basically the model is a box-shaped barge with a chamfer in the bilge. The nominal scale of the model is 1:10. The main emphasis was in the modelling and instrumentation of the flooded compartments in order to get as much information on the flooding process as possible. The eight flooded compartments are located slightly forward from the midsection of the model in order to ensure sufficient trim in the flooded condition.

Water heights were measured in every flooded compartment. Furthermore, air pressures in the double bottom compartments and the floating position of the model were recorded. Six different flooding cases were investigated. The average discharge coefficients for all openings were evaluated experimentally by draining water through the openings.

All dimensions in this report are given as mm in model scale unless otherwise stated. The motions of the model are presented in a right-handed co-ordinate system, fixed with the center of gravity of the intact model, COG. The angular motions are presented in degrees.

Finally, the author would like to express his gratitude to Mr. Pentti Tukia and the rest of the personnel at the workshop of HUT Ship Laboratory for their effort on this project.

1 Description of the Model

1.1 Background

The aim of the tests was to provide experimental data for the validation of numerical simulation methods (e,g, *Ruponen, 2006*), not to model the flooding of any particular ship. Therefore, a simple box-shaped barge was used for easy manufacturing. The internal subdivision was built so that the model would trim during the tests. Furthermore, it was ensured that air pockets could be formed, at least in the double bottom compartments.

1.2 Main Dimensions

The model is relatively large in order to achieve large water heights and air pressures. Thus the accuracy of the measurements is somewhat better. The overall length of the model is 4.0 m and the draft in the intact condition is 0.5 m. All main dimensions of the model are given in Figure 1.1 and Table 1.1. The nominal scale of the model is 1:10.

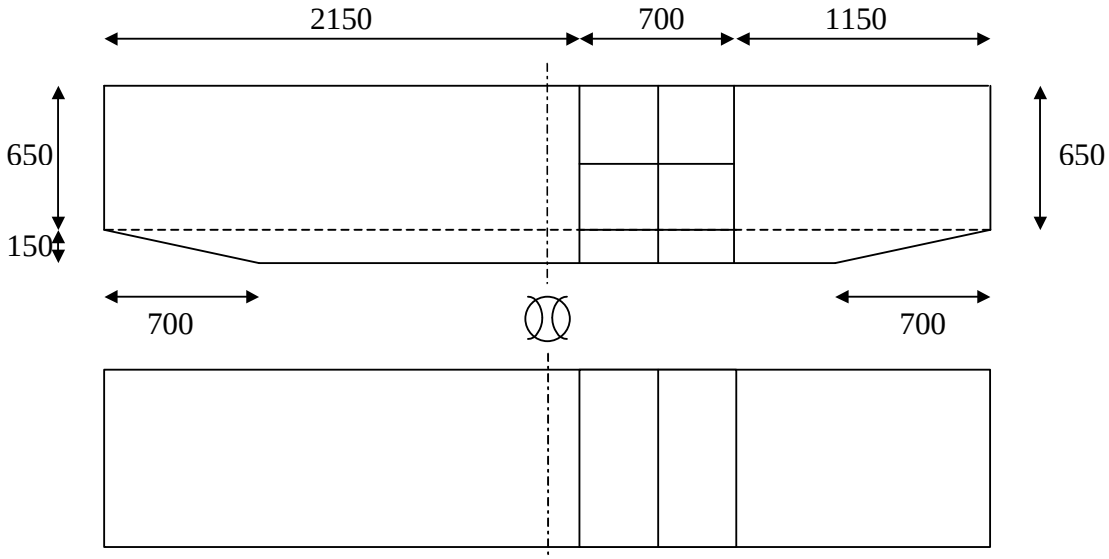

Figure 1.1 General view of the model

Table 1.1 Main dimensions of the model

Length over all:	4.000 m
Breadth:	0.800 m
Height (excluding the “backbone” structure):	0.800 m
Design draft:	0.500 m
Block coefficient at design draft:	0.906
Volume of buoyancy:	1.450 m^3

The forward and aft blocks were constructed of wood, while the mid-section with the flooded compartments was built of see-through plexiglass. The thickness of the sheets is 10 mm. The sheets were joined together with screws and the seams were tightened with silicon. So the structure of the mid-section was both watertight and airtight.

In order to avoid high tensions in the plexiglass mid-section during flooding, a steel-structured backbone was fitted to the top of the model. In addition, two aluminium T-beams were installed on the bottom of the model in order to further increase the rigidity of the combined structure. Therefore, the plexiglass block rested between the bow and stern structures without any direct connection. The seams were tightened with silicon in order to avoid flooding between the blocks of the model. The bow and stern blocks and the support structures are shown in Figure 1.2 and the finished model in Figure 1.3.

Figure 1.2 The bow and stern sections, connected with the backbone structure

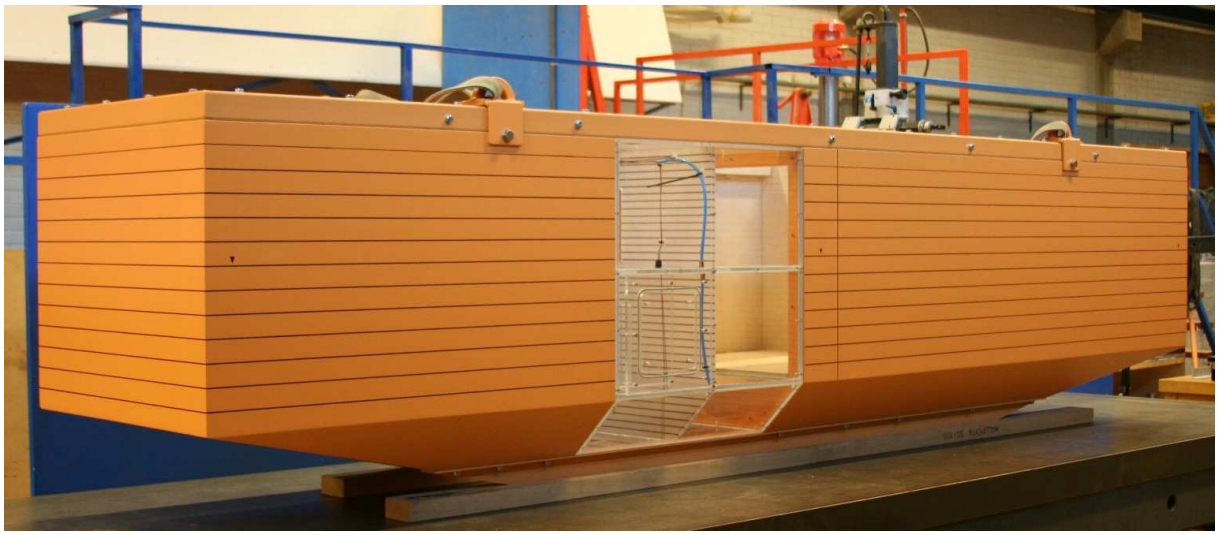

Figure 1.3 The finished model before the tests

1.3 Flooded Compartments

The block for the flooded compartments was manufactured separately from see-through plexiglass (thickness 10 mm). The size of the compartments and the internal openings were selected so that the flooding process would be similar to progressive flooding inside a passenger ship.

The compartments are divided by two decks and a transverse watertight bulkhead. The double bottom is constructed to be not only watertight but also airtight. This is necessary as the aim of the tests is to validate a simulation method that is capable of handling air pressures and airflows as well (*Ruponen, 2006*). The compartments on the lower deck and on the upper deck (excluding the side compartments) can be considered as practically fully vented since the openings on the top of each compartment are larger than the flooding openings. The side compartments are ventilated with small pipes (see section 2.5).

A removable plate is used for closing the top of the compartments on the upper deck in order to increase the strength of the plexiglass structure. The top plate is equipped with ventilation holes and holes for the sensor cables and discharging and ventilation pipes. The plexiglass block with the instrumentation is shown in Figure 1.4. The dimensions of the rooms and the openings are presented in Figure 1.5, Figure 1.6 and Figure 1.7.

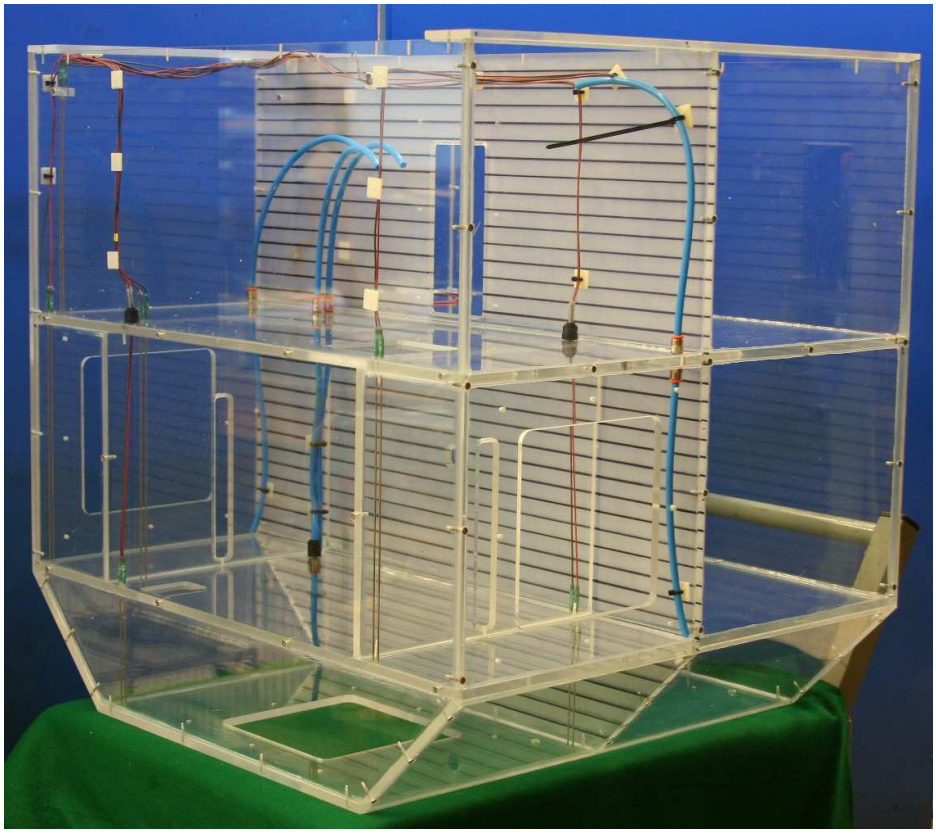

Figure 1.4 The mid-section of the model with the instrumentation

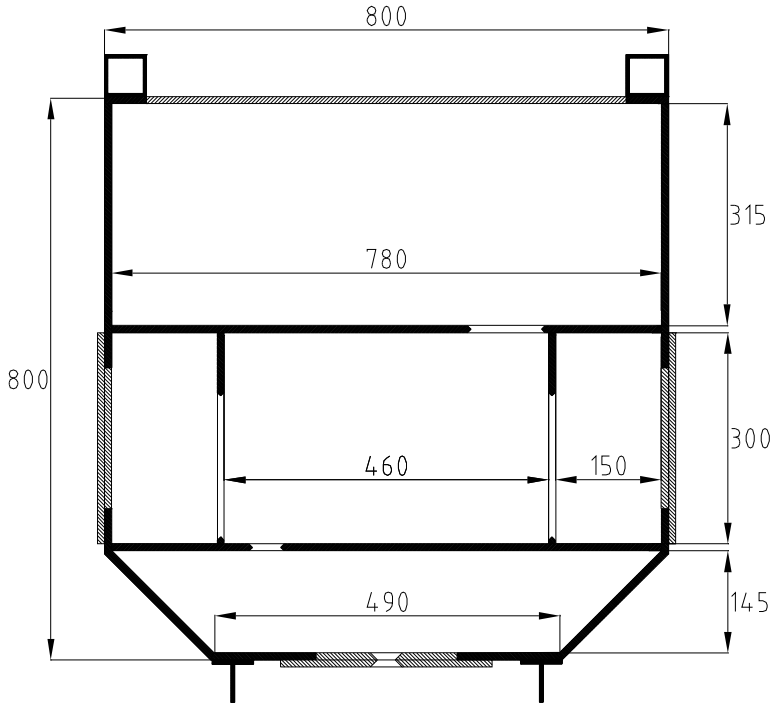

Figure 1.5 Cross-section of the forward compartment

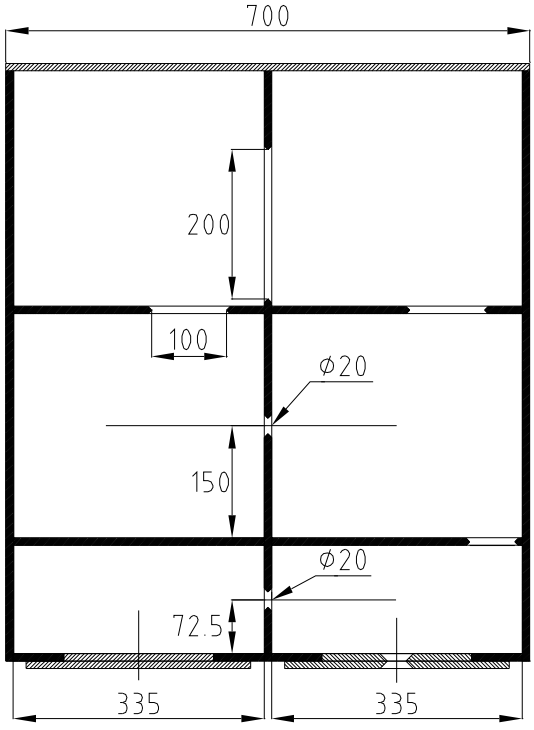

Figure 1.6 Side view of the compartments

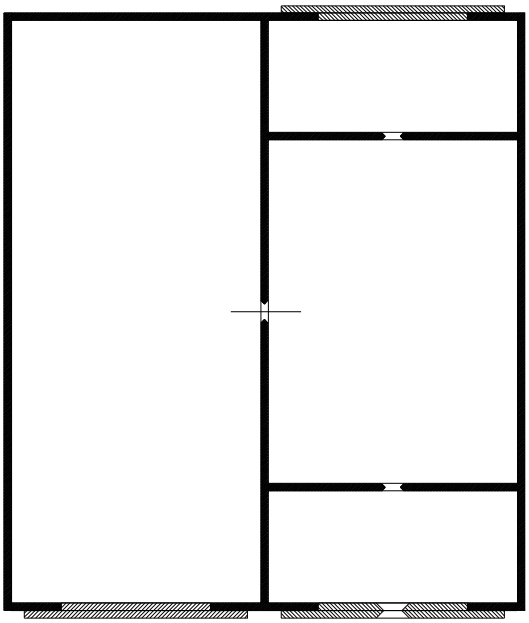

Figure 1.7 View of the lower deck from above

Figure 1.8 The mid-section installed in the model

1.4 Identification of the Flooded Compartments

The compartments of the model are identified with the same name throughout the report. The names of the rooms are based on the following principle. “DB” means double bottom and “R” means a room above the double bottom. The first number denotes the watertight compartment, so that “1” is the aft compartment and “2” is the forward compartment. The second number marks the deck; “1” is the lower deck (tank top) and “2” is the upper deck. Additional letters “P” and “S” refer to “port side” and “starboard side”, respectively. This is needed for the identification of the side compartments on the lower deck. All the flooded compartments and their identifications are presented in Figure 1.9.

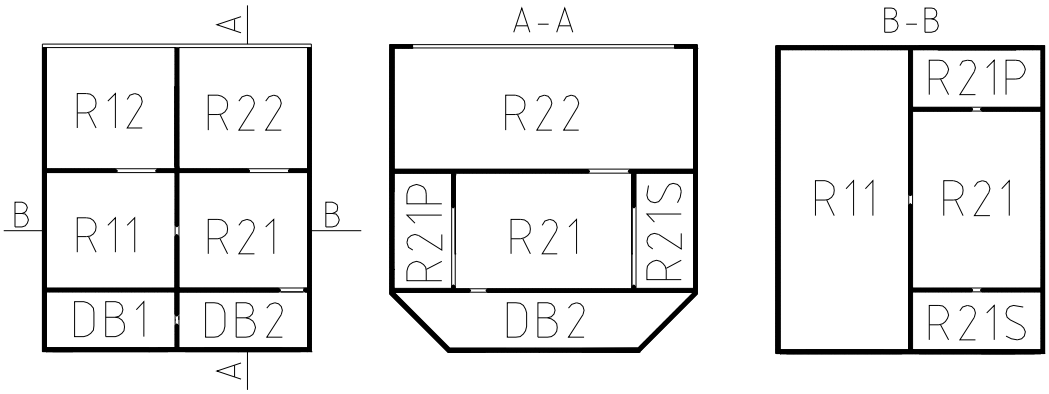

Figure 1.9 Identification of the flooded compartments

1.5 Openings

1.5.1 Damage Openings

Structure

The damage openings were constructed on separate plates (Figure 1.10) in order to be able to change the size and location of the openings. Furthermore, the “opening plates” acted as maintenance openings for the instrumentation inside the compartments.

Two different rectangular-shaped damage openings were tested. The dimensions are given in Table 1.2. The openings were sharp-crested. For structural reasons a small rounding (radius approximately 3 mm) was used in the corners of the openings.

The plates were attached to the model with screws and the tightness was ensured with an O-ring (see Figure 1.11). Plates without opening were used to close the maintenance openings.

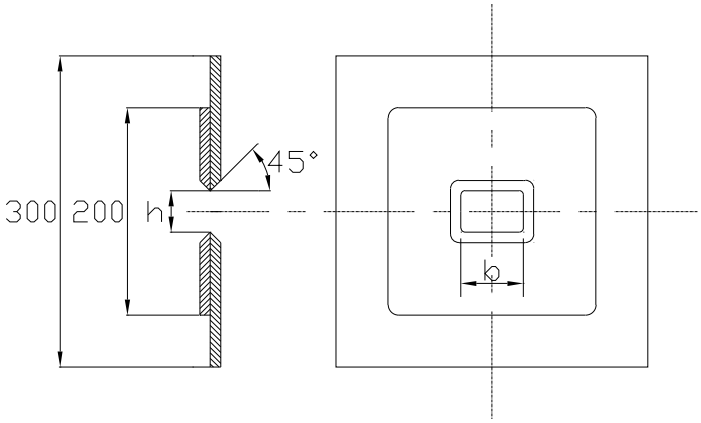

Figure 1.10 Dimensions and structure of the opening plates

Table 1.2 Dimensions of the damage openings

	Breadth	**Height**	**Area**
Large damage hole	60 mm	40 mm	24.0 cm^2
Small damage hole	25 mm	25 mm	6.25 cm^2

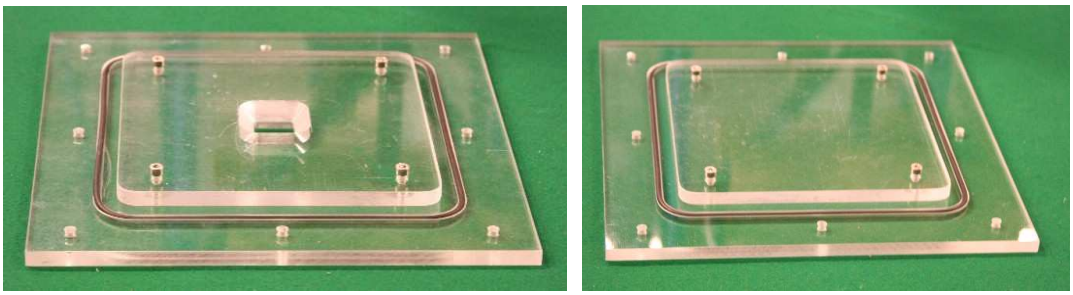

Figure 1.11 Plate with the small damage hole (left) and a cover for a maintenance opening (right)

Opening Mechanism

A tight plug was used to close the damage opening prior to a test. The flooding was started when the plug was carefully pulled out. Possible disturbances to the model are considered to be minimal, since the plug is very small when compared to the size of the model. A picture of the damage opening, closed with the plug is presented in Figure 1.12. In the bottom damage tests, the plug was pulled out by dropping a weight that was tied to the plug with a string.

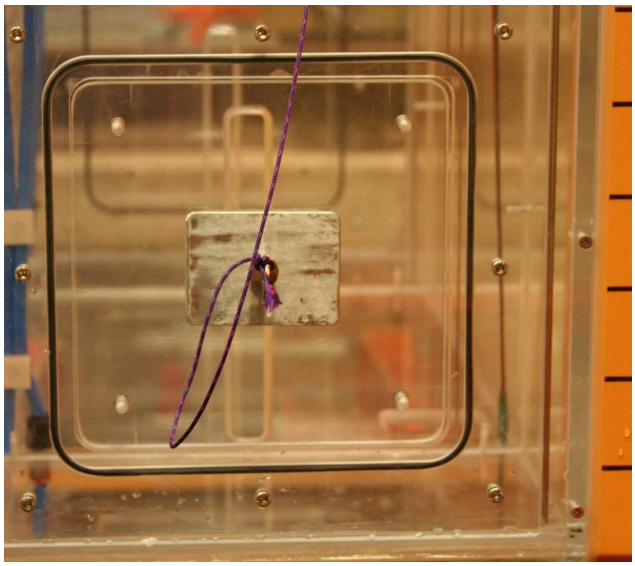

Figure 1.12 Damage opening, closed with the plug

1.5.2 Internal Openings

General

All internal openings are in the model are sharp-crested and either rectangular-shaped or circle-shaped. The open “doors” have a threshold of 10 mm, measured from the deck.

For structural reasons a small rounding (radius approximately 3 mm) was used in the corners of the rectangular-shaped openings.

Double bottom

A small circle-shaped opening that represents a broken pipe connects the compartments DB1 and DB2 in the double bottom. The diameter of the opening is 20 mm and it is located in the middle of the transverse bulkhead, both in vertical and transverse direction. This small opening ensures that a relatively large air pocket is formed in the aft double bottom compartment (DB1).

The forward double bottom compartment DB2 is connected to the lower deck (R21) by a small opening (40 mm $\times$ 60 mm) that represents a manhole. This opening can be closed with a small steel plate and a rubber seal.

Longitudinal bulkheads

The openings in the longitudinal bulkheads, connecting the rooms R21P and R21S to the room R21, represent partly open or leaking fire doors. Hence these openings are narrow and

tall. The size is 20 mm × 200 mm. The openings are located in the centers of the bulkheads in longitudinal direction.

Transverse bulkhead

On the lower deck, the compartments R11 and R21 are connected by a small circle-shaped opening in the transverse bulkhead. The opening represents a damaged pipe and its diameter is 20 mm. It is located on the centerline and in the middle between the lower and upper decks.

On the upper deck, the compartments R12 and R22 are connected by a large rectangular-shaped opening in the transverse bulkhead. This opening represents an open watertight door and its dimensions are 80 mm × 200 mm and it is located on the centerline. This opening is normally closed with a tight plexiglass plate but it was opened for one test.

Deck

On both WT-compartments, there is a large opening (100 mm × 100 mm) in the upper deck. The centers of the openings are located 180 mm from the centerline on the port side of the model and 100 mm aft from the nearest transverse bulkhead. These openings represent staircases and they ensure that the main compartments on the lower deck (R11 and R21) are practically fully vented.

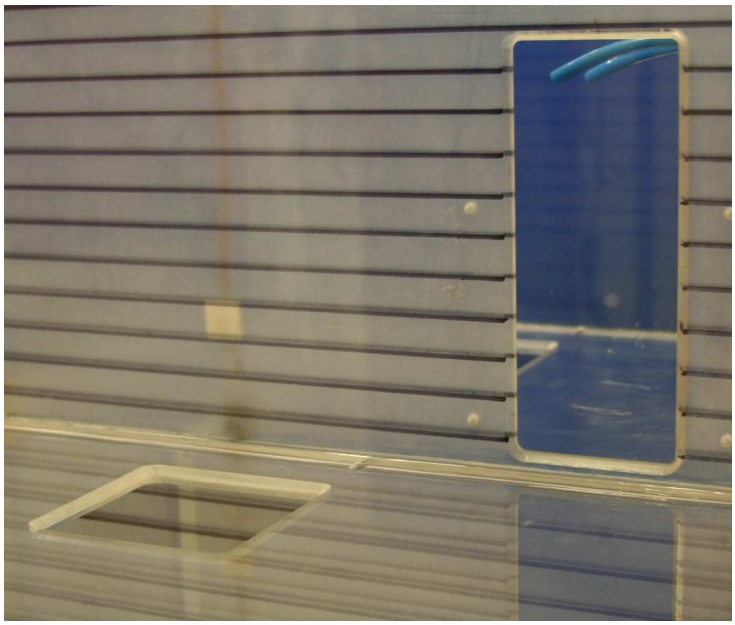

Figure 1.13 Opening in the upper deck and the open WT-door in the transverse bulkhead, view from the aft compartment

1.6 Intact Condition

The intact condition of the model in all performed tests is presented in Table 1.3. The draft of the model in intact condition is 0.500 m and the corresponding volume of displacement is 1.450 m^3.

The model is loaded so that the desired vertical center of gravity is 0.280 m above the base line of the model. The model has a large initial metacentric height $\overline{GM_0}$, and therefore, it will not heel much during the intermediate stages of flooding. The final $\overline{KG}$ value was achieved by performing an inclining test for the fully instrumented and ballasted model, see section 3.2. The final results are given in Table 1.3.

The longitudinal center of gravity is amidships so that the model has no initial trim. The center of gravity of the buoyancy is 0.270 m above the base line when the draft of the model is 0.500 m.

Table 1.3 Initial condition

Draft, T	0.500 m
Heel, ϕ	0.0°
Trim, θ	0.0°
Vertical center of buoyancy, $\overline{KB_0}$	0.270 m
Initial metacentric radius, $\overline{B_0M_0}$	0.118 m
Initial metacentric height, $\overline{GM_0}$	0.110 m
Vertical center of gravity, $\overline{KG}$	0.278 m

2 Instrumentation

2.1 Measurement of Floating Position

The floating position of the model was measured with Krypton Rodym DMM, a camera-based solution for measuring the 6D movements of objects in space. A frame with three LEDs in triangular position was installed on the top of the model (Figure 2.1). The camera system monitors the position of these LEDs and calculates the translational and rotational motions of the center of gravity of the model, COG. The vertical motion of the COG from the sea level Z_G, the heeling angle ϕ and the trim angle θ were recorded. The COG of the intact model is used as a reference. The applied co-ordinate system is presented in Figure 2.2.

The other degrees of freedom (surge, sway and yaw) were not recorded since they do not have any importance in the flooding process in calm water.

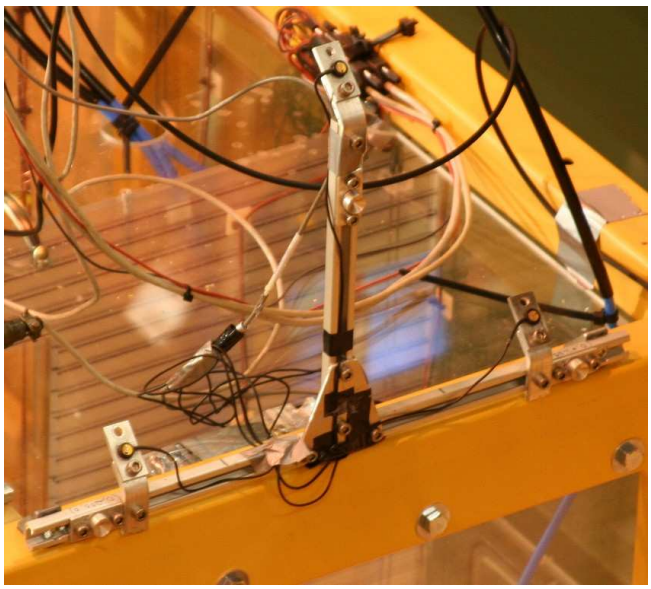

Figure 2.1 The LED frame installed on the top of the model

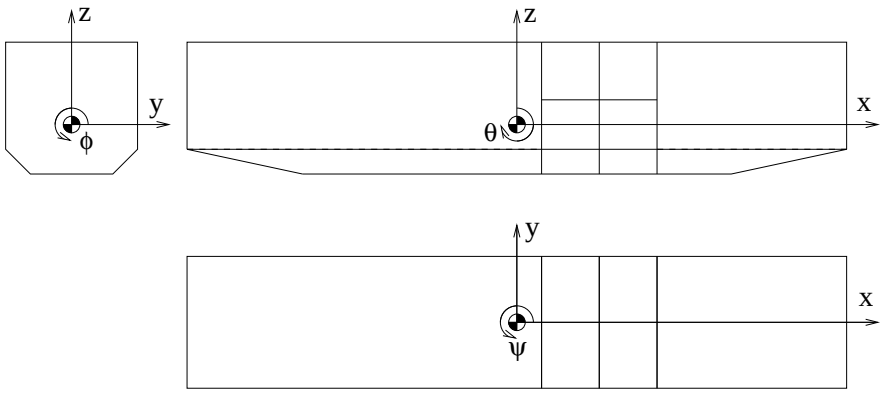

Figure 2.2 Co-ordinate system, fixed to the center of gravity of the intact model

The applied measurement system has limits for the longitudinal and transverse motions of the model during the test. Therefore, soft rubber strings were attached; connecting the model to the carriage, see Figure 2.3. This procedure ensured that the model could not drift too much during the tests; and yet the strings were so loose that they did not affect the measured motions of the model (heel, trim and sinkage), see section 3.3.

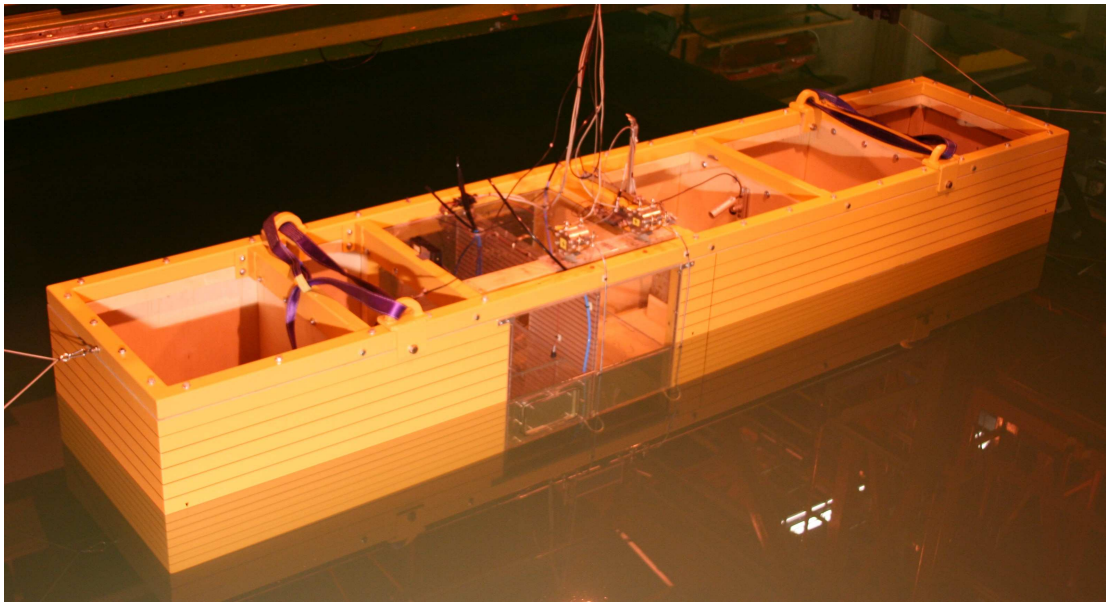

Figure 2.3 The intact model afloat, connected to the carriage with the soft rubber strings

2.2 Measurement of Water Heights

The water level is measured at least at one point in every flooded compartment. The sensor is placed near the corner that will be the lowest one as the model trims and heels due to the flooding. In the forward double bottom compartment another sensor is placed in the opposite corner to ensure that the water level can be measured even if the model is trimming and the compartment is nearly full of water.

The sensors are based on the “hot wire” technique and each sensor consists of two parallel stainless steel wires with a diameter of 2 mm. The distance between the wall and the wires is 5 mm and the distance between the centers of the wires is 7.5 mm. Therefore, the sensor cannot measure the water height precisely in a single point. However, the error is minimal with small heel and trim angles. In general, the accuracy of the sensors is considered to be better than 0.5 mm. However, the surface tension may decrease the accuracy for very small water heights.

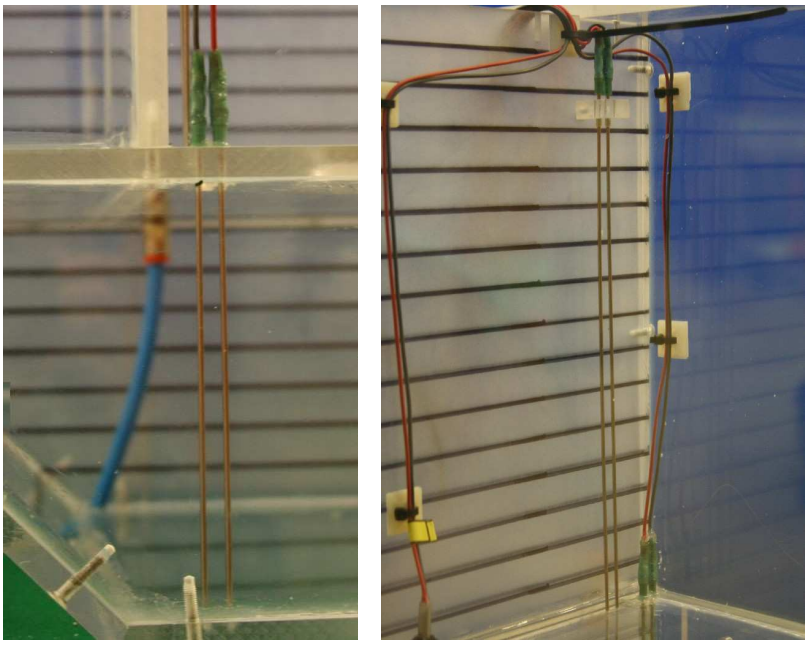

Figure 2.4 Water height sensors in the double bottom (left) and on the upper deck (right)

Location and Identification of the Sensors

The sensors are placed approximately 5 mm from the bulkhead. The identification and location of the sensors are presented in Figure 2.5. The red dots mark the centers of the sensors. Some additional dimensions are also provided.

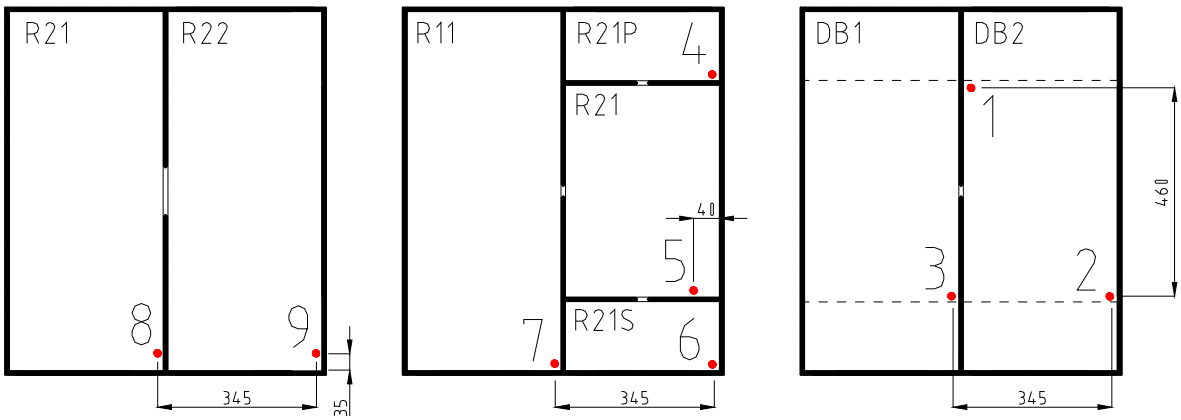

Figure 2.5 The location and identification of the water height sensors (from left: upper deck, lower deck and double bottom)

Calibration of the sensors

Each sensor and the corresponding measurement card (and cables) were calibrated before the flooding tests. Water from the towing tank was used (same conductivity) and the measurement cards were adjusted so that the sensors were linear throughout the measurement

range (from dry to fully submerged). Furthermore, the range of the output voltage was as wide as possible in order to achieve better accuracy. The results are presented in Appendix B.

During the test program, it was observed that the actual calibration factors were smaller than the results of the calibration. Therefore, a systematic post-test calibration was performed. The whole model was fixed to the carriage and the draft was changed by lifting the model, see Figure 2.6 and Figure 2.7. The results correspond very well with the last performed flooding test, but not with all performed tests. Generally, the difference between the flooding tests is less than 5 %.

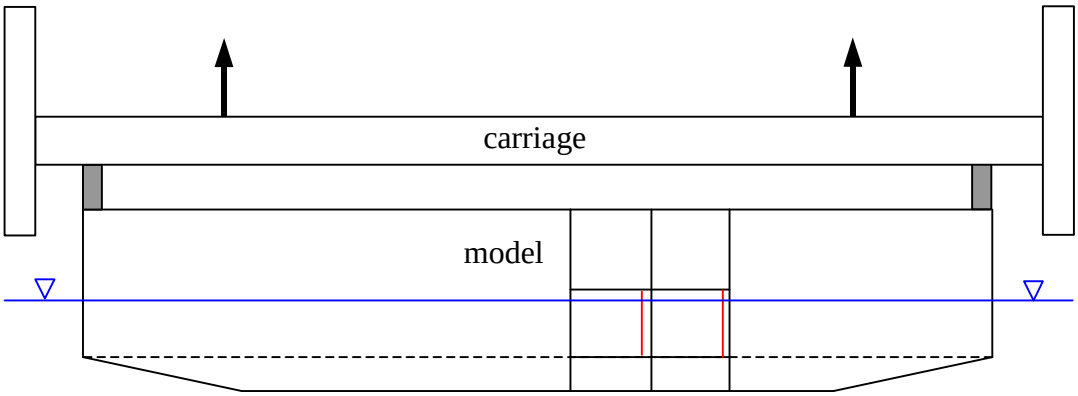

Figure 2.6 Setup for the post-test calibration of the water height sensors (red lines); the blue line is the water level

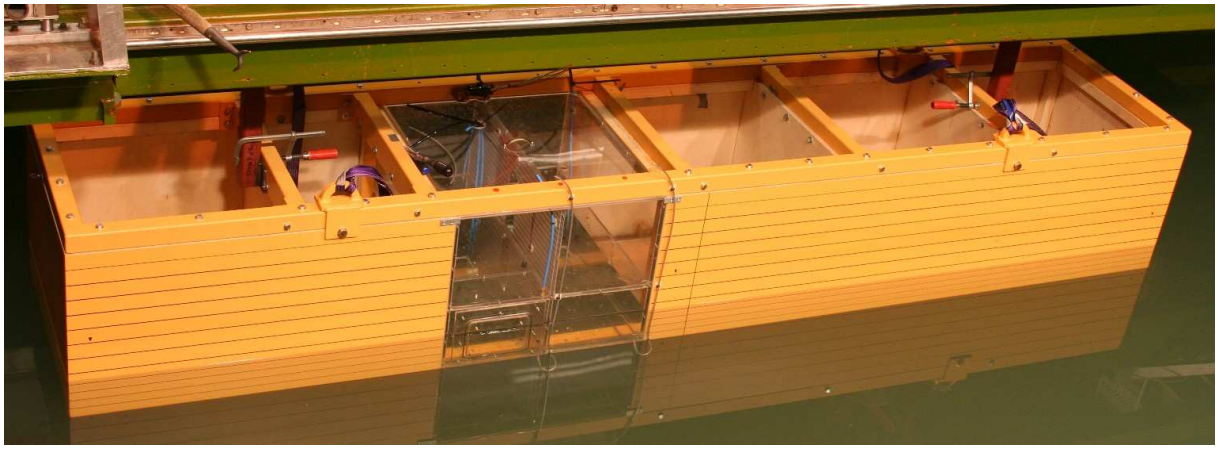

Figure 2.7 The model is lifted with the carriage during the post-test calibration

The changes in the calibration factors were likely caused by the long cables that needed to be plugged in and plugged out between the tests since the compartments had to be emptied from the flooded water. Furthermore, in some cases the input voltage may have varied a little

between the tests. It was found out that the used measurement cards are very sensitive to the input voltage.

At the end of each flooding test, the pipes to the pressure gauges were opened so that the whole double bottom was flooded. Therefore, the output voltage for fully submerged sensors was known for these compartments as well. In the analysis of the results (chapter 4), the applied calibration factors for the water height sensors were obtained by dividing the length of the sensor by the output voltage for the fully submerged sensor. This procedure is considered to be justified since the used sensors and measurement cards are shown to be linear (Appendix B) and the results clearly correspond the visual observations.

2.3 Measurement of Air Pressures

The over-pressures in the double bottom compartments were measured with pressure difference gauges. The applied devices are Sensotec's low range pressure transducers; model A-5. These devices are normally used for measuring the wake of a model ship. The inlets of the sensor pipes are placed in the bilge plate close to the tank top in order to avoid premature flooding to the pipe. The outer diameter of the pipes is 6 mm and the pipes go up to the sensors on the top of the model. The reference pressure was the atmospheric pressure in the laboratory.

The pressure gauges were installed on top of the model so that the volume of air in the pipes would be as minimal as possible. The length of the pipes is approximately 1.00 m and the inner diameter is 5 mm. Hence the volume of one pipe is only 0.0196 liters while the net volume of one double bottom compartment is approximately 31 liters. The pipes were emptied from possible flooded water before each test. The pressure gauges were calibrated with fresh water.

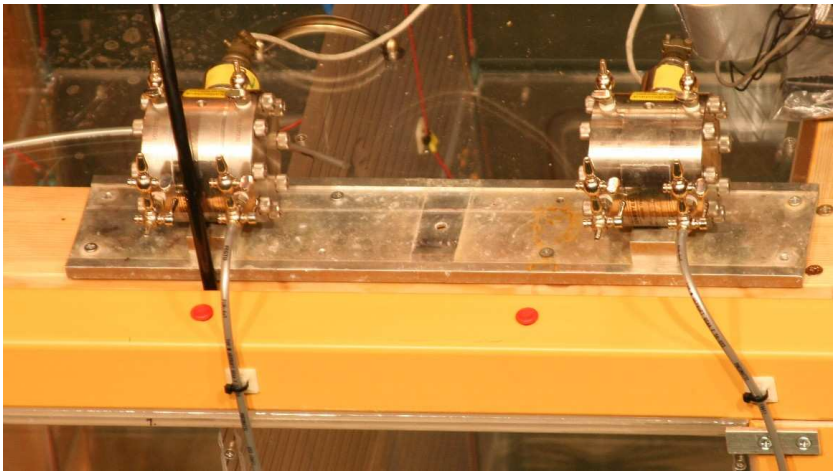

Figure 2.8 The air pressure gauges, installed on the top of the model; the pipes lead to the double bottom compartments

2.4 Discharging Devices

The flooded compartments had to be emptied from the floodwater between the tests. Some auxiliary discharging devices were installed in the model in order to make this process easier and faster.

The lower compartments are equipped with suction pipes, with an outer diameter of 8 mm (Figure 2.10). The inlets of the pipes are close to the bottom of the compartments in order to avoid unwanted ventilation in the flooded conditions.

The double bottom compartments are equipped with additional discharge holes that could be closed tightly with a plug, see Figure 2.9. These small holes proved to be very useful when the model was emptied from the flooded water.

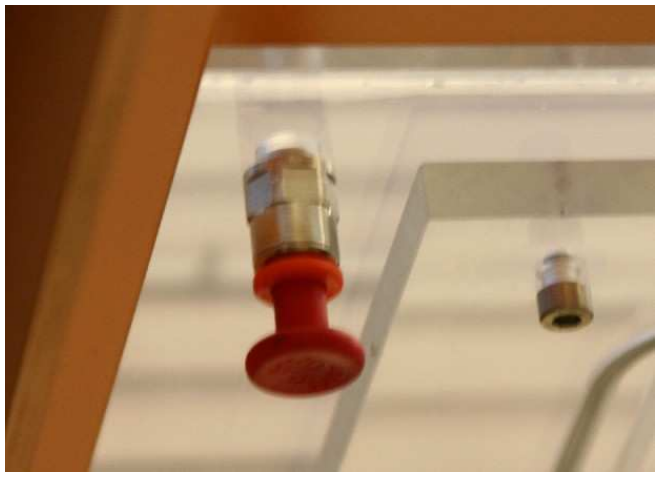

Figure 2.9 Closed discharge hole in the bottom of the model

2.5 Ventilation Pipes

The side compartments are equipped with ventilation pipes in order to model decreased level of ventilation. The inner diameter of the pipes is 5 mm and the length of each pipe is approximately 400 mm. The inlets of these pipes are located near the side of the model and the transverse bulkhead.

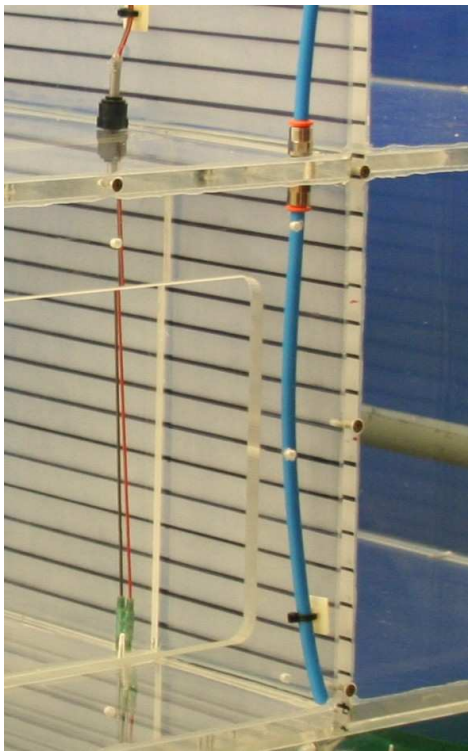

Figure 2.10 Discharging pipe and cables for a water height sensor; the pipe was used for ventilation when the lower part was removed

2.6 Video Recording

Video cameras were installed in the forward and aft end of the flooded compartments. This allowed visual analysis of the flooding process in the compartments on the lower and upper decks. Furthermore, an external video camera was used for filming the changes of the floating position. This camera was fixed to the carriage.

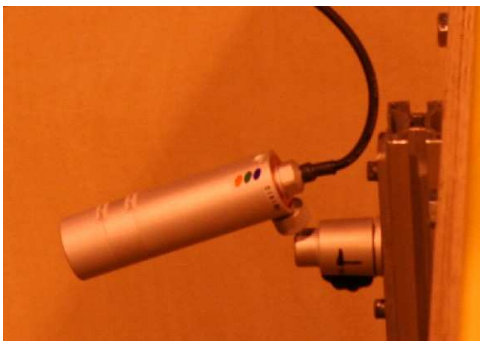

Figure 2.11 Video camera installed in the model

3 Preliminary Tests

3.1 Evaluation of Discharge Coefficients

A simple hydraulic model is generally used for calculation of the water flows in flooding simulations methods (see e.g. *Ruponen, 2006*). The discharge coefficient of an opening describes all the pressure losses that are caused by the opening. This includes jet contraction and viscous drag. The value of the coefficient depends on the size and shape of the opening. Therefore, the discharge coefficients were evaluated experimentally for all the openings in the model.

The volume of water in a discharging tank with perpendicular walls (Figure 3.1) is governed by the following differential equation (Appendix A):

$$\frac{dV_w(t)}{dt} = -C_d A\sqrt{2g\frac{V_w(t)}{S}}, \tag{3.1}$$

where A is the area of the opening (in the bottom) and S is the area of the free surface in the tank (constant). Hence the average discharge coefficient during the test can be calculated from the following equation:

$$C_d = S\frac{\sqrt{2gH_1} - \sqrt{2gH_2}}{TgA}, \tag{3.2}$$

where H_1 is the initial water height from the level of the opening, H_2 is the water height after the test and T is the time period between these two water levels. The equation is derived in Appendix A.

During the test, the rooms on both sides of the tested opening were properly vented in order to avoid air compression.

Each test was performed three times and the measured draining times were verified with video recordings. The calculated average discharge coefficients are given in Table 3.1.

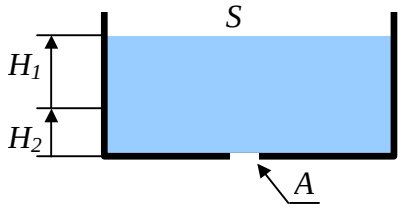

Figure 3.1 Setup for the draining test

Table 3.1 Average discharge coefficients and standard deviation for the openings

Opening	Average C_d	Standard deviation
Large damage (40 mm × 60 mm)	0.78	0.0083
Small damage (25 mm × 25 mm)	0.83	0.0024
Broken pipe (∅ 20 mm)	0.80	0.0328
Partly open door (20 mm × 200 mm)	0.75	0.0096
Staircase (100 mm × 100 mm)	0.72	0.0011

3.2 Inclining Test

In order to evaluate the vertical center of gravity accurately, an inclining test was performed for the fully loaded (instrumentation and ballast included) and intact model (the damage hole was closed with a tight plug). The model was heeled to both sides with four different heeling moments. The weights and levers were selected so that the heel angles did not exceed 3°. The used weights were part of the ballast, and therefore, correction of the results was not needed. A schematic picture of the test setup is presented in Figure 3.2.

The heeling moment, caused by the mass *m* is:

$$M_{heel} = m \cdot g \cdot e \cdot \cos\phi, \tag{3.3}$$

where *e* is the distance between the heeling weight and the center line.

Based on the approximation of initial stability (small heel angle), the static righting moment is:

$$M_{st} = -\Delta \cdot \overline{\mathrm{GM}_0} \cdot \sin\phi, \tag{3.4}$$

where Δ is displacement and $\overline{\mathrm{GM}_0}$ is the initial metacentric height.

In the equilibrium condition $M_{heel} = M_{st}$ and the initial metacentric height can be presented on the basis of the measured heel angle ϕ:

$$\overline{\mathrm{GM}_0} = \frac{m \cdot g \cdot e}{\Delta \cdot \tan\phi}. \tag{3.5}$$

The metacentric radius is the moment of inertia of the entire waterplane about the ship's centerline I_T, divided by the volume of displacement ∇. Since the waterplane is square-shaped:

$$\overline{\mathrm{B_0M_0}} = \frac{I_T}{\nabla} = \frac{1}{\nabla} \cdot \frac{B^3 L}{12}, \tag{3.6}$$

where B is the breadth and L the length of the water plane.

The vertical center of gravity is:

$$\overline{KG} = \overline{KM_0} - \overline{GM_0} = \overline{KB_0} + \overline{B_0M_0} - \overline{GM_0}, \tag{3.7}$$

where $\overline{KB_0}$ is the initial vertical center of buoyancy, measured from the base line.

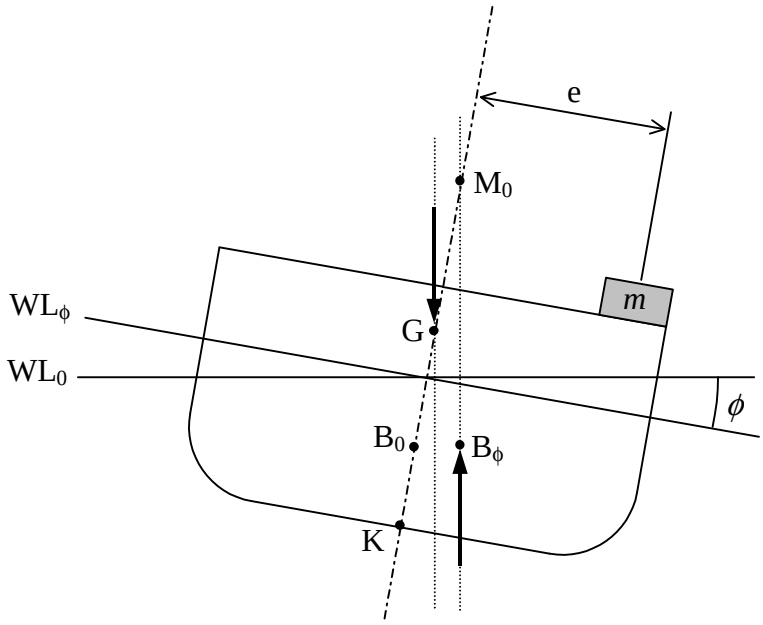

Figure 3.2 Schematic picture of the inclining test

The applied weights (2 × 10 kg and 2 × 5 kg) were placed along the centerline of the model, symmetrically from the midsection. The weights were part of the ballast. For the inclining test, the weights were moved to transverse direction in order to create a heeling moment. The moments and measured heeling angles are presented in Table 3.2. The heeling moment is plotted as a function of $\Delta \cdot \tan(\phi)$ in Figure 3.2. The initial metacentric height, i.e. the slope of the linear fit, is approximately 0.110 m.

Table 3.2 Results of the inclining test

Test	lever [m] for 2×5 kg	lever [m] for 2×10 kg	M_{heel} [Nm]	ϕ [°]	$\Delta\tan(\phi)$ [N]
1	0.200	0.000	-19.62	-0.75	-186.17
2	0.300	0.000	-29.43	-1.10	-273.07
3	0.300	0.150	-58.86	-2.15	-533.91
4	0.300	0.250	-78.48	-2.85	-707.99
5	-0.300	-0.250	78.48	2.85	707.99
6	-0.300	-0.150	58.86	2.15	533.91
7	-0.300	0.000	29.43	1.10	273.07
8	-0.200	0.000	19.62	0.70	173.76

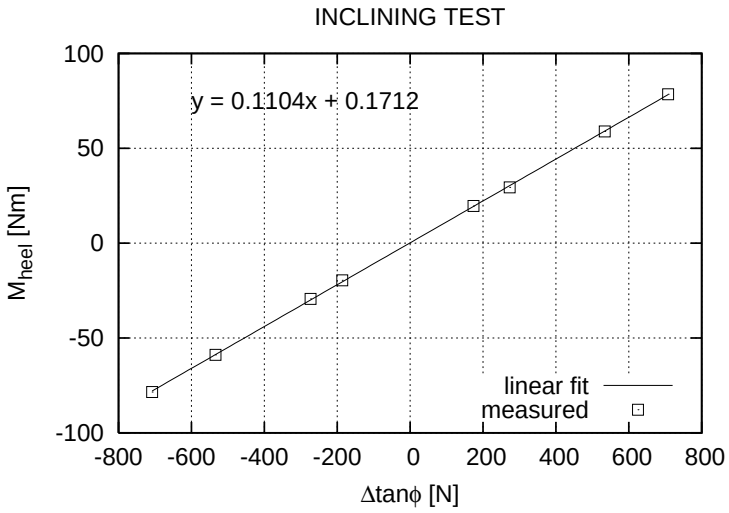

Figure 3.3 Results of the inclining test and the linear fit

3.3 Roll Decaying Test

As described in section 2.1, the model had to be connected to the carriage with soft rubber strings in order to ensure that the floating position could be measured during the whole test. Therefore, a roll decaying test was performed for the model with and without the soft rubber strings. The results for both tests in non-dimensional form are presented in Figure 3.4. The curves are almost identical. Therefore, it seems likely that the strings do not have a significant effect on the roll motion of the model.

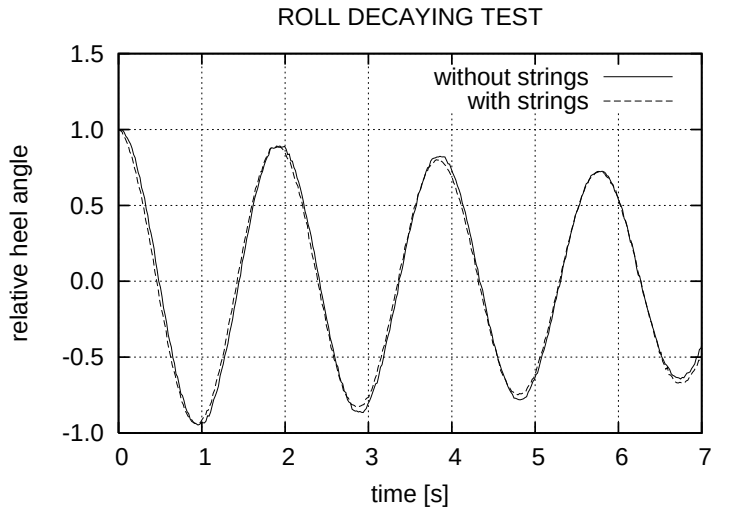

Figure 3.4 Results of the roll decaying tests (initial heel angle is 2.1° without the strings and 2.8° with the strings)

The measured time history for the roll decaying test (with the soft rubber strings) is fitted to the theoretical equation, (see e.g. *Matusiak, 1996*):

$$\phi(t) = \phi_0 \, \mathrm{e}^{-\xi\omega_\phi t} \cos\left[\omega_\phi \left(1-\xi^2\right)t\right], \tag{3.8}$$

where ϕ_0 is the initial heel angle, ω_ϕ is the natural frequency of roll motion and ξ is the critical roll damping ratio. The natural period of the roll motion is:

$$T_\phi = \frac{2\pi}{\omega_\phi}. \tag{3.9}$$

The measured and calculated theoretical roll decaying with the strings are presented in Figure 3.5. The natural period of roll motion is 3.26 s. and the critical roll damping ratio is 0.019.

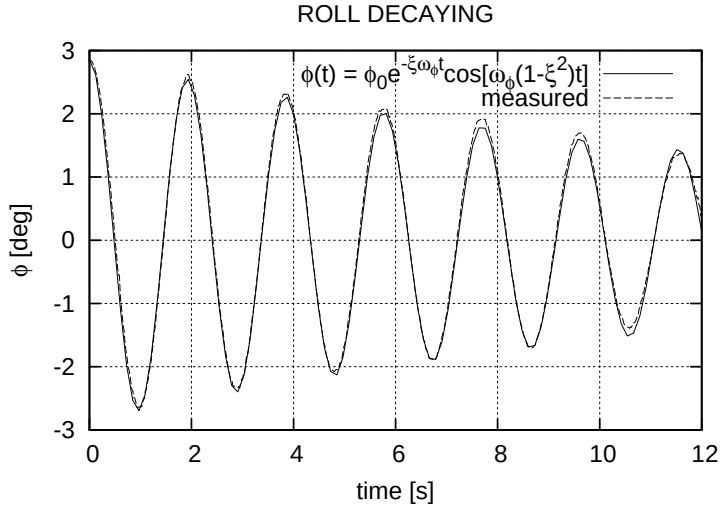

Figure 3.5 Measured roll decaying with the strings and a fitted theoretical curve

4 Flooding Tests

4.1 Performed Tests

A list of the performed tests is given in Table 4.1. In the basic intact condition (see section 1.6), all internal openings, except the WT-door on the upper deck, are open.

The model was raised from water between the tests. The compartments were emptied from the flooded water and dried as carefully as possible. However, in some cases a very small volume of water was left inside some compartments but this did not have a significant effect on the flooding process.

Table 4.1 Performed tests, Comp1 is the aft compartment and Comp2 is the forward one

Name:	Damage Case:	WT-door:	Special:
Test01	Bottom Comp2 small	closed	Fixed floating pos.
Test02	Bottom Comp2 small	closed	
Test03	Bottom Comp2 small	open	
Test04	Bottom Comp2 large	closed	
Test05	Bottom Comp1 large	closed	
Test06	Side Comp2 large	closed	Double bottom dry

4.2 Bottom Damage

4.2.1 Flooding with Fixed Floating Position (Test01)

The motions of the model were prevented by fixing the model to the carriage, see Figure 4.1. The investigated damage case is the small damage hole (25 mm × 25 mm) in the bottom of the forward compartment (DB2). In this test, the floating position was not measured since it was kept fixed. Visual observations confirmed that the floating position did not change during the test.

Even through the damage hole is rather small, the start of the flooding is dramatic: water sprays from the hole to the bottom of the tank top (Figure 4.2). When water in DB2 reaches the opening to DB1, an air pocket is formed in DB1 since there is no direct route for the air to escape the inflow of water. As a result, the air pressure builds fast (Figure 4.13). The high-pressure air slowly escapes in bubbles to DB2 and further up to R21 through the manhole. This bubbling causes high local waves near the water height sensor in the room R21 (Figure 4.8). The bubbling and the waves are clearly visible in the video captures that are presented in Figure 4.3.

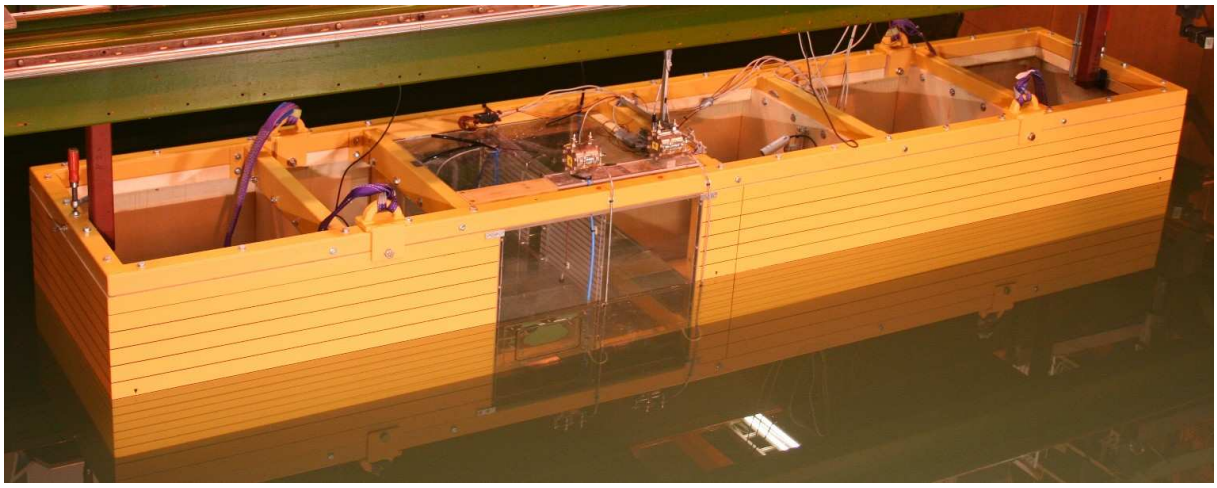

Figure 4.1 Test01 – model is fixed to the carriage, status after the flooding

Figure 4.2 Test01 – video captures from the start of the flooding

Figure 4.3 Test01 – video captures from the air bubbling (pointed by the arrows)

There was a small amount of water left from a previously performed test in the rooms R11 and R22. This can be seen from the measurement results for the sensors number 7 and number 9 (Figure 4.10 and Figure 4.12). The volumes of these additional waters are so small that they do not affect the flooding process and the floating position of the model.

In DB2 air starts to compress 20 s after the flooding started (Figure 4.14). At this time the room is already full of water (Figure 4.5). Thus in this damage case the opening from DB2 to R21 provides sufficient level of ventilation for the double bottom.

In DB1 the air pressure starts to build when the water level in DB2 reaches the opening that connects the double bottom compartments. There are sudden increases in the air pressure when the compartments DB2 (t = 20 s) and R21 (t = 240 s) become full of water (Figure 4.13 and Figure 4.14). This may, at least partially, result from the decreased escape of air through bubbling, as the bubbles have to flow through more openings and compartments that are full of water.

There are small waves on the upper deck in the rooms R12 and R22 after the flooding has stopped (Figure 4.11 and Figure 4.12). The period of the waves is long (approximately 33 s) and the amplitude is small (less than 2 mm). The waves are in the same phase in both compartments but the amplitude is larger in R22.

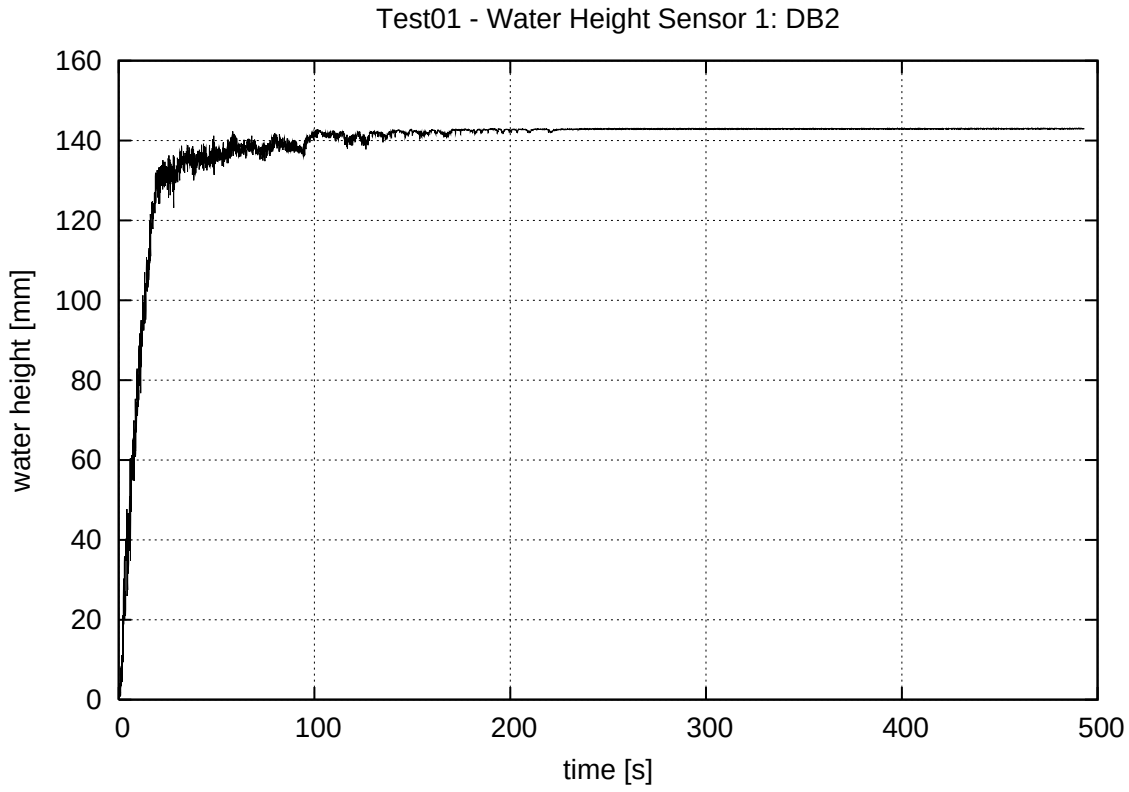

Figure 4.4 Test01 – water height in the room DB2, sensor 1

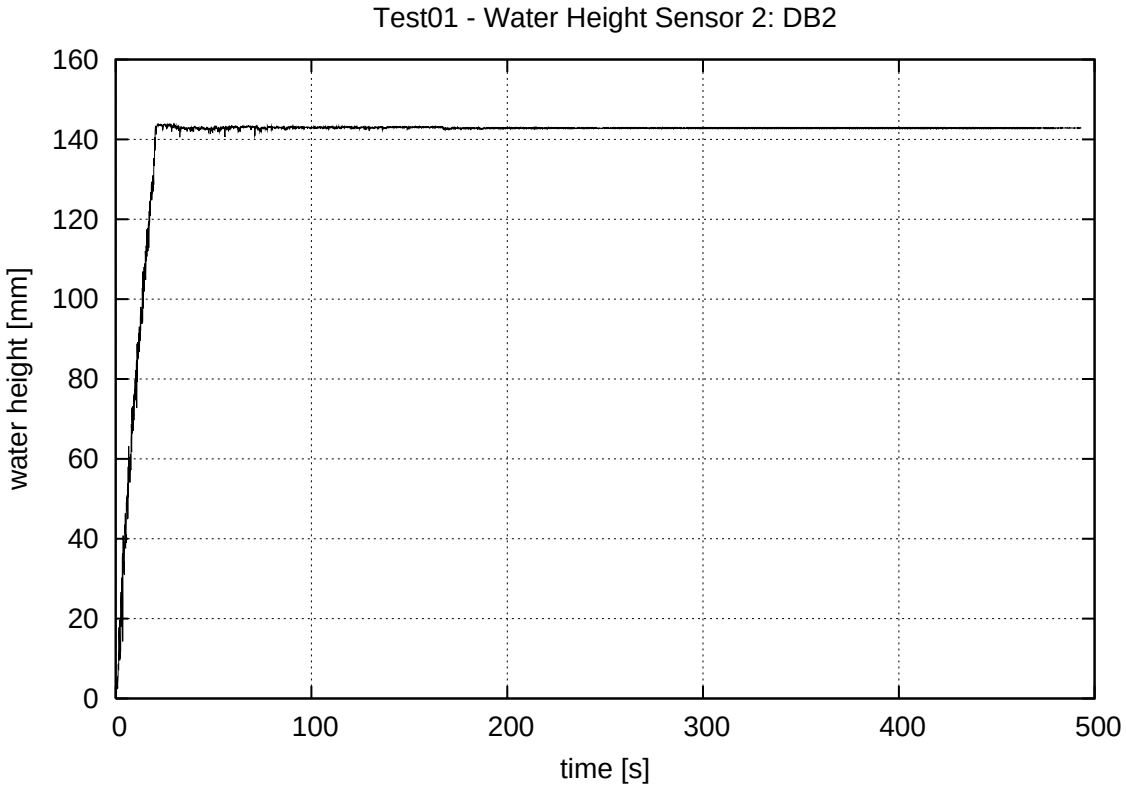

Figure 4.5 Test01 – water height in the room DB2, sensor 2

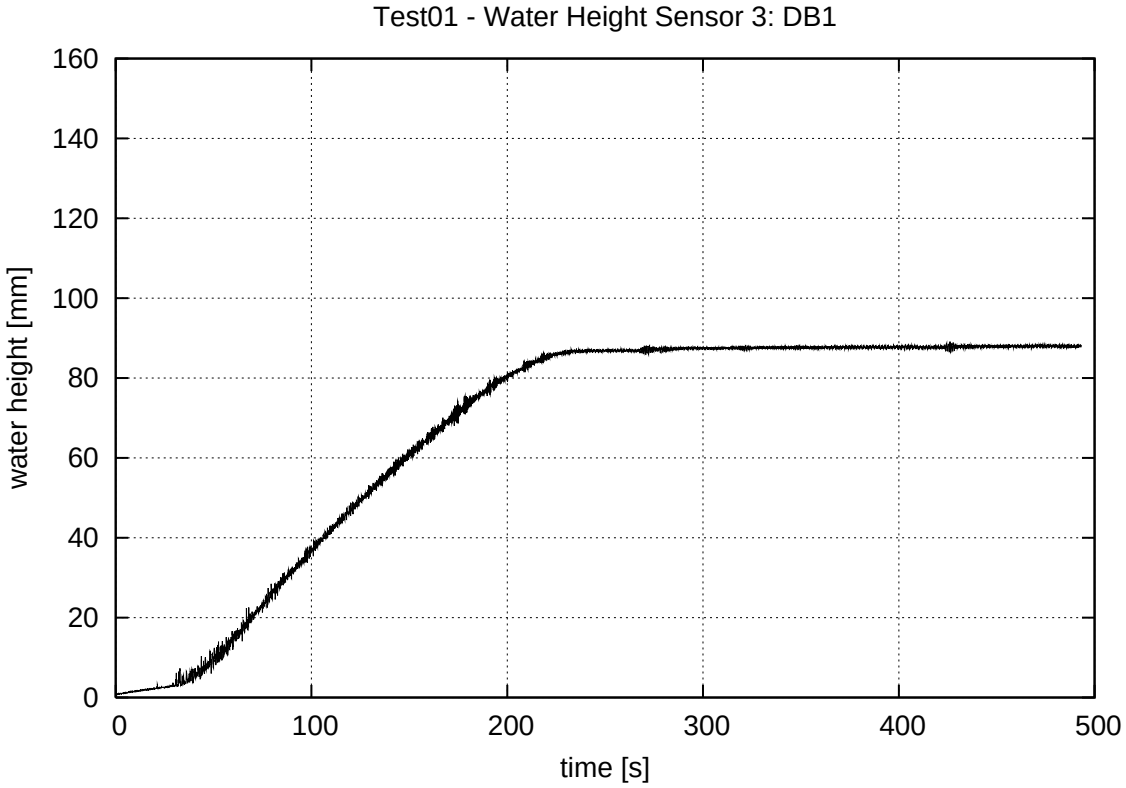

Figure 4.6 Test01 – water height in the room DB1

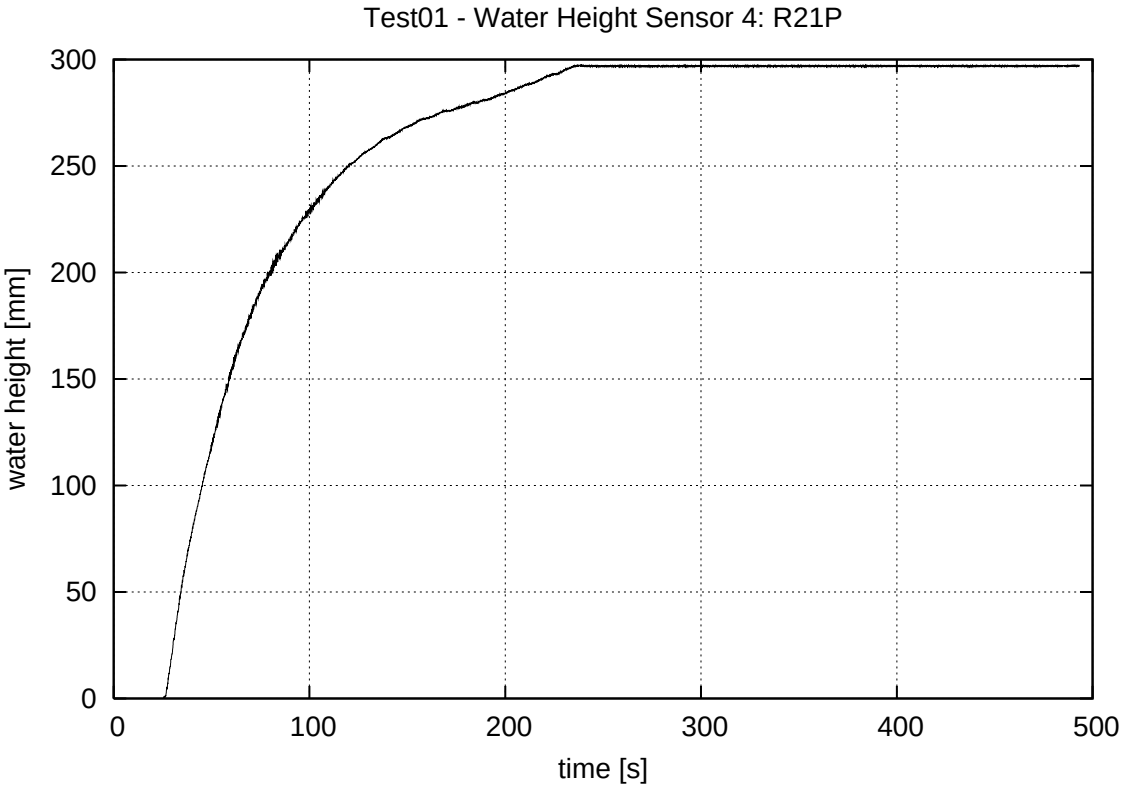

Figure 4.7 Test01 – water height in the room R21P

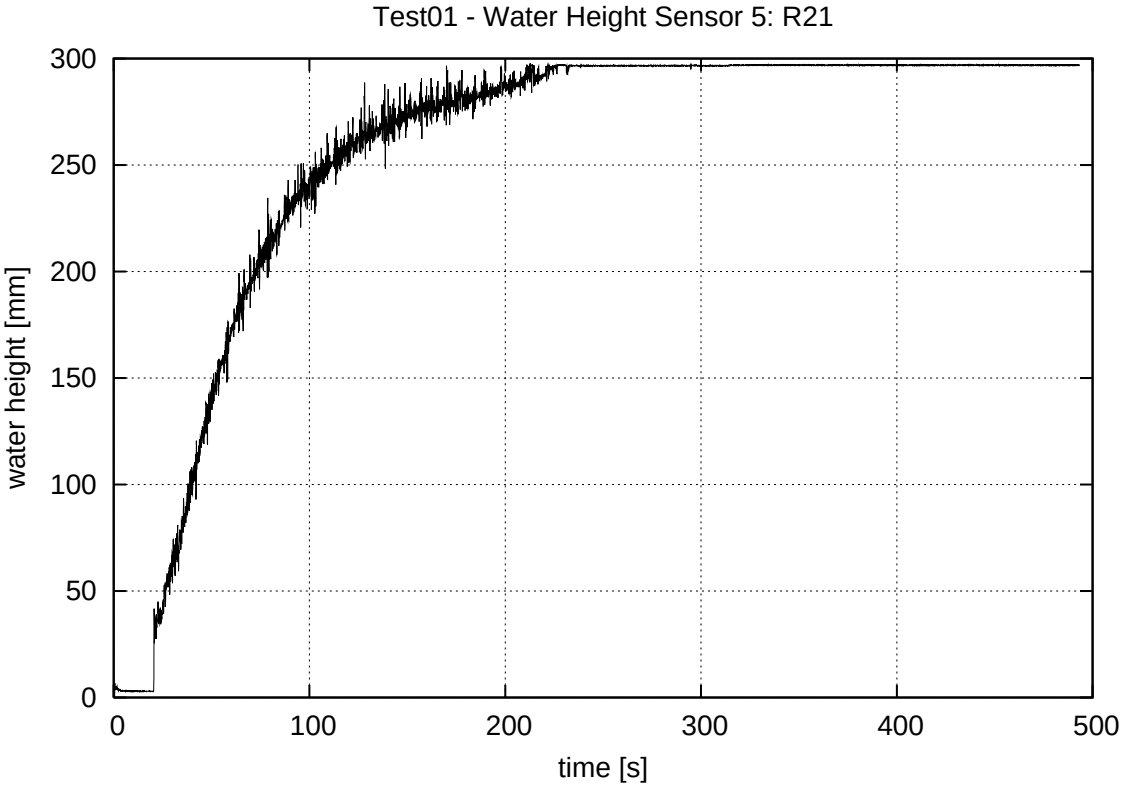

Figure 4.8 Test01 – water height in the room R21

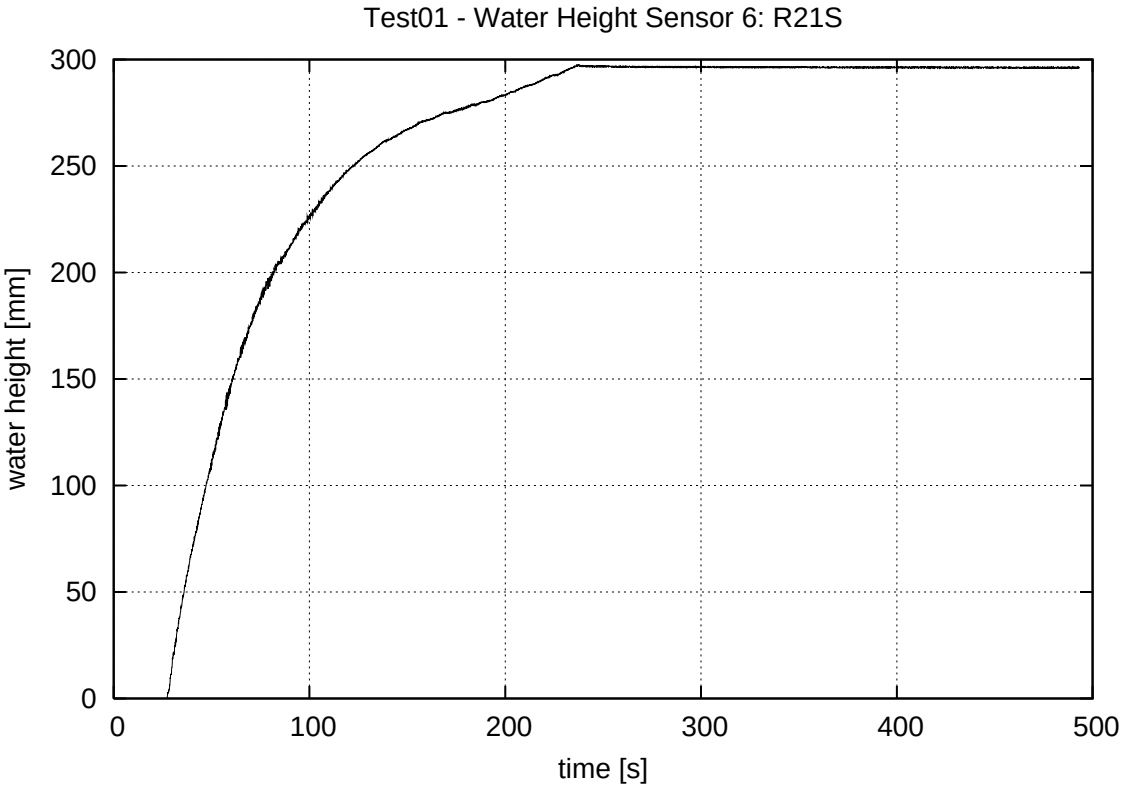

Figure 4.9 Test01 – water height in the room R21S

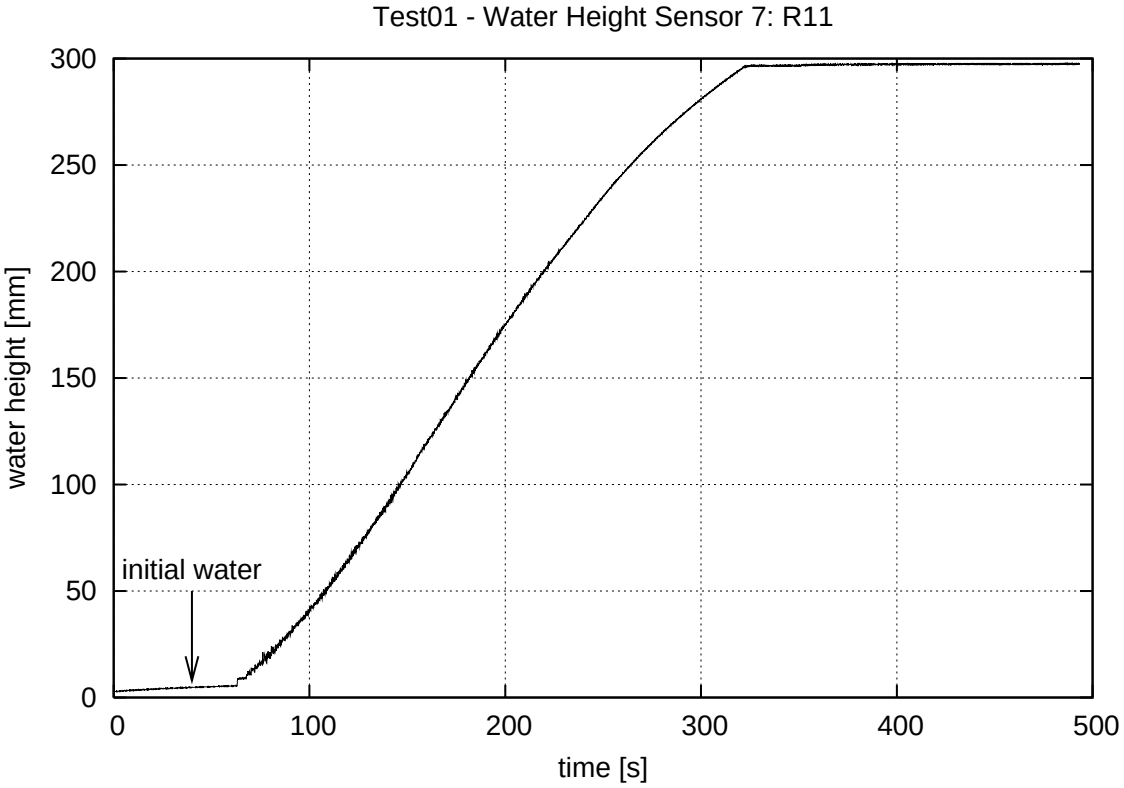

Figure 4.10 Test01 – water height in the room R11

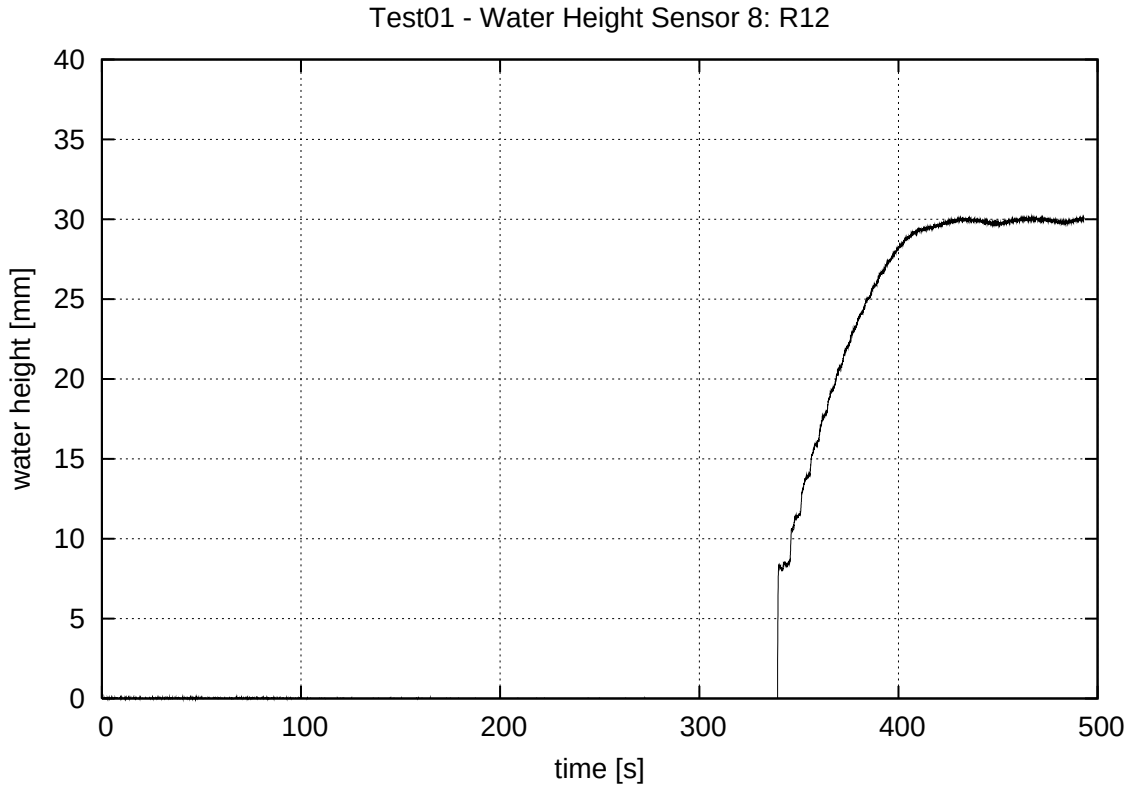

Figure 4.11 Test01 – water height in the room R12

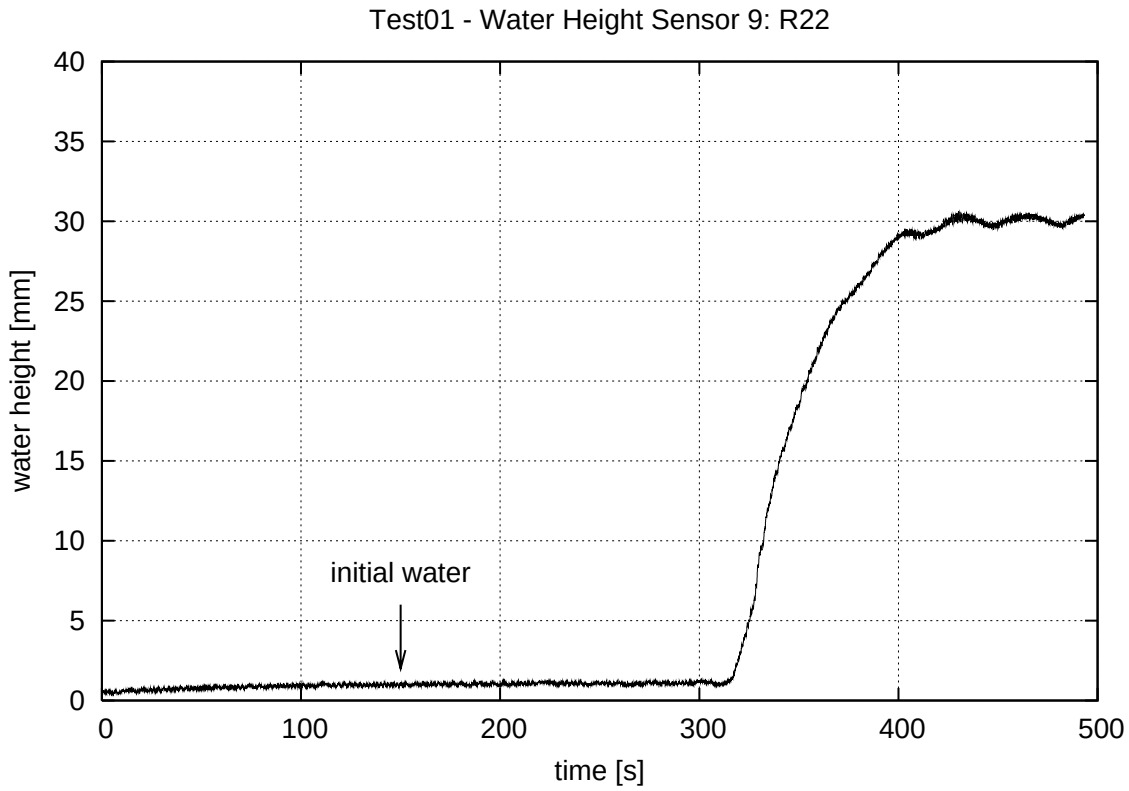

Figure 4.12 Test01 – water height in the room R22

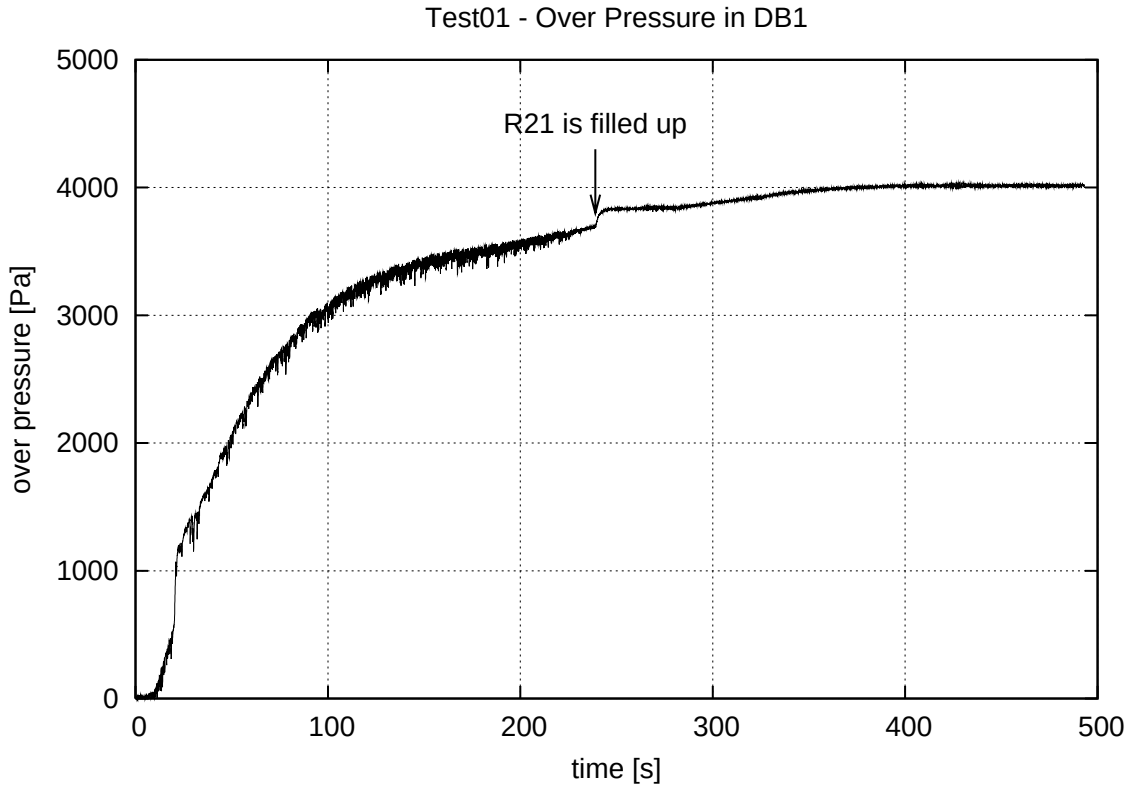

Figure 4.13 Test01 – air pressure in the room DB1

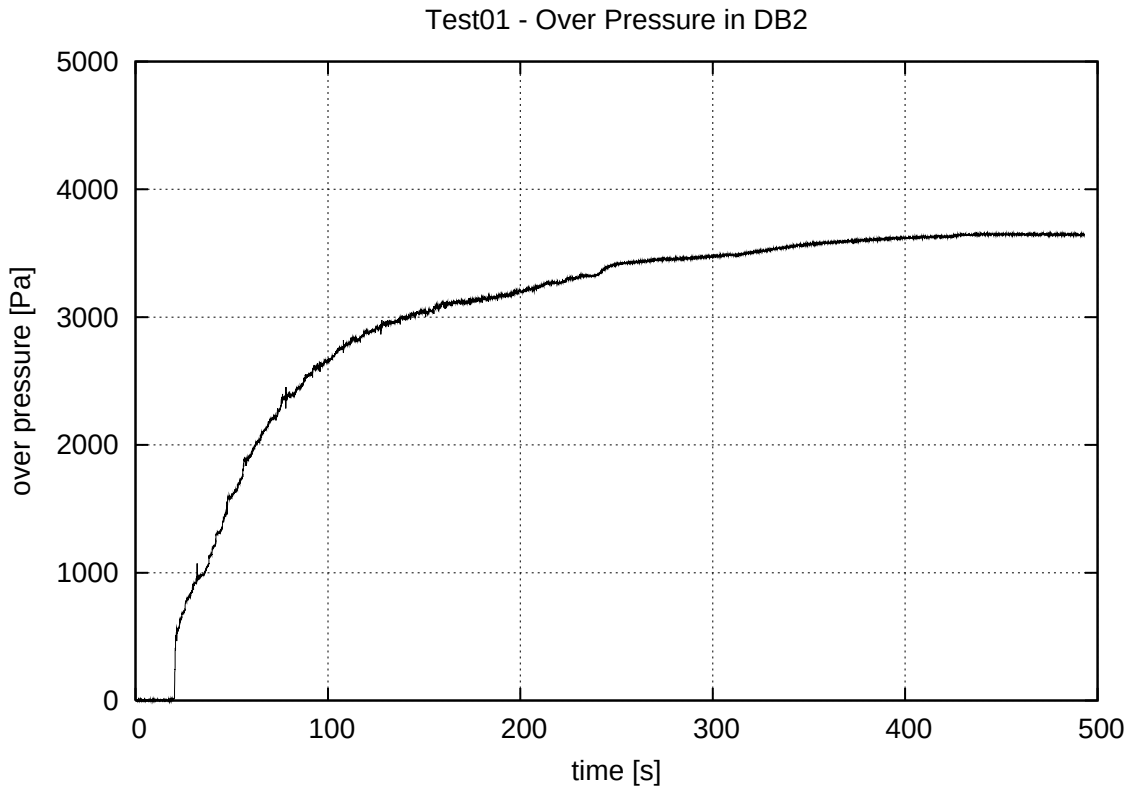

Figure 4.14 Test01 – air pressure in the room DB2

4.2.2 Small Damage in the Forward Compartment (Test02)

The investigated damage case is the small damage opening (25 mm × 25 mm) in the bottom of the forward compartment (DB2). The WT-door on the upper deck is closed with a plate. Therefore, the damage scenario is exactly the same as in Test01 but now the model floats freely.

The time-to-flood is longer than in Test01 since more water can enter the compartments due to the increasing draft and trim of the model. Some video captures from the equilibrium condition are presented in Figure 4.15.

The model heels very slightly (less than 0.1°) for a short time (Figure 4.17) but generally the flooding process seems to be symmetrical as expected.

Similarly to Test01, the measured air pressure in DB2 (Figure 4.29) starts to build only after this compartment is practically full of water (Figure 4.19). Therefore, this compartment was practically fully vented during the flooding and the measured compression occurred only in the pipe to the pressure gauge.

Also in this test, significant bubbling of air from the air pocket in DB1 was observed. This bubbling caused high waves in R21 (Figure 4.23) and in DB2 near the sensor that is close to the opening to R21 (Figure 4.20).

Similarly to the Test01, there is a sudden increase in the air pressure in DB1 (Figure 4.28) when room R21 is filled up with water at time 150 s.

The measured water height in DB1 in the equilibrium condition is 75 mm (Figure 4.21). This indicates that the whole opening between DB1 and DB2 is not fully submerged on both sides. In Test01 the corresponding value is 88 mm (Figure 4.6). However, the final equilibrium floating position is practically the same as in Test03, as expected. In Test03 the final water height in DB1 is 86 mm. This indicates that the applied calibration factor for the water height sensor in DB1 (sensor number 3) may not be very accurate in this particular case (Test02).

Figure 4.15 Test02 – video captures from the equilibrium condition (on left the aft compartment and on right the forward compartment

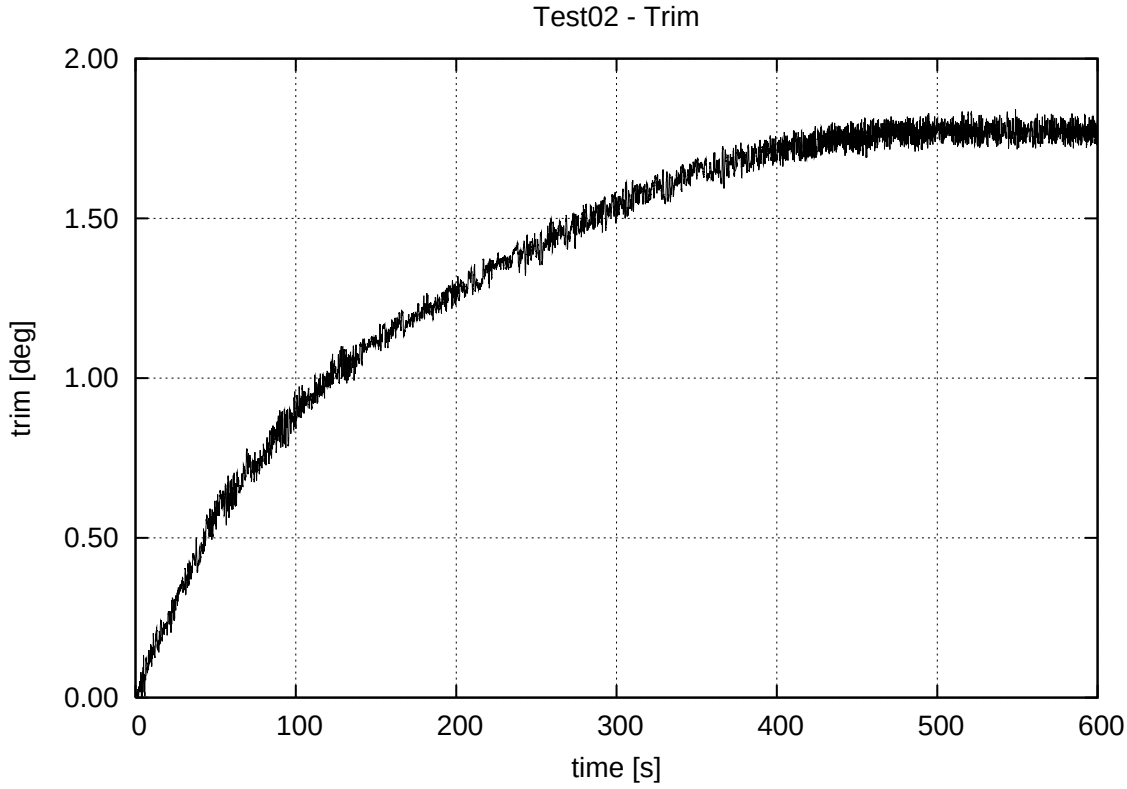

Figure 4.16 Test02 – measured trim angle

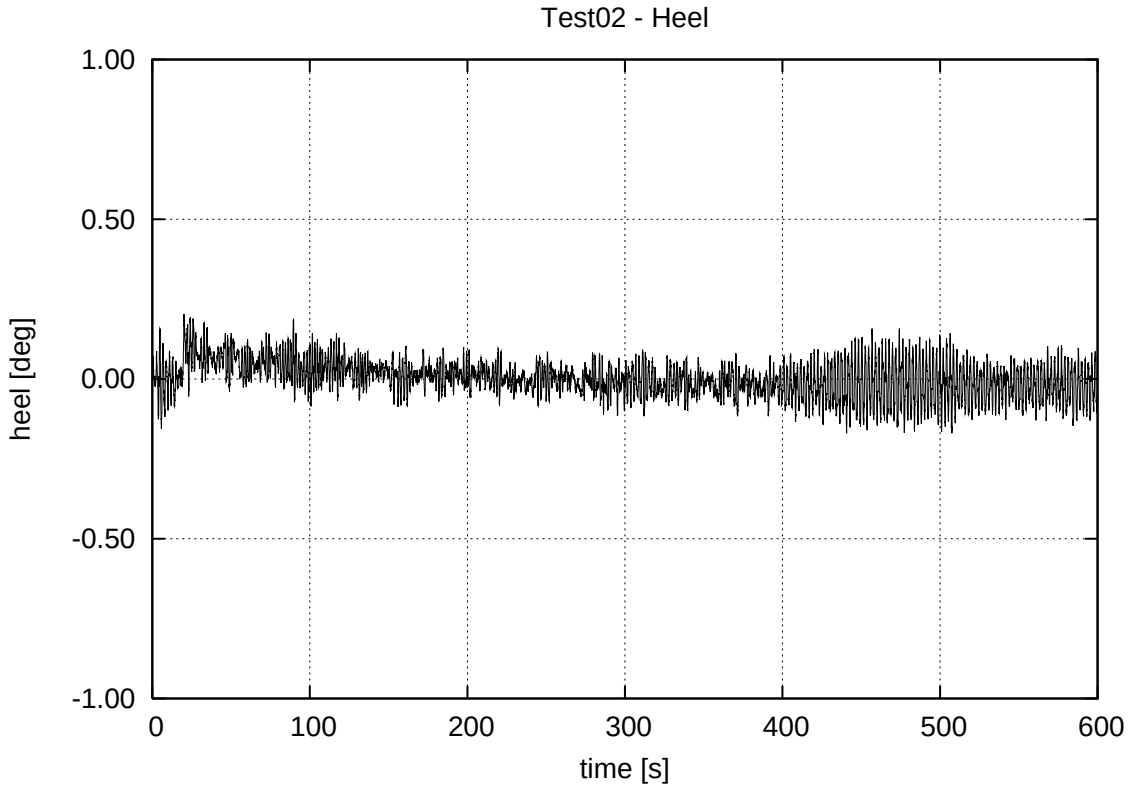

Figure 4.17 Test02 – measured heel angle

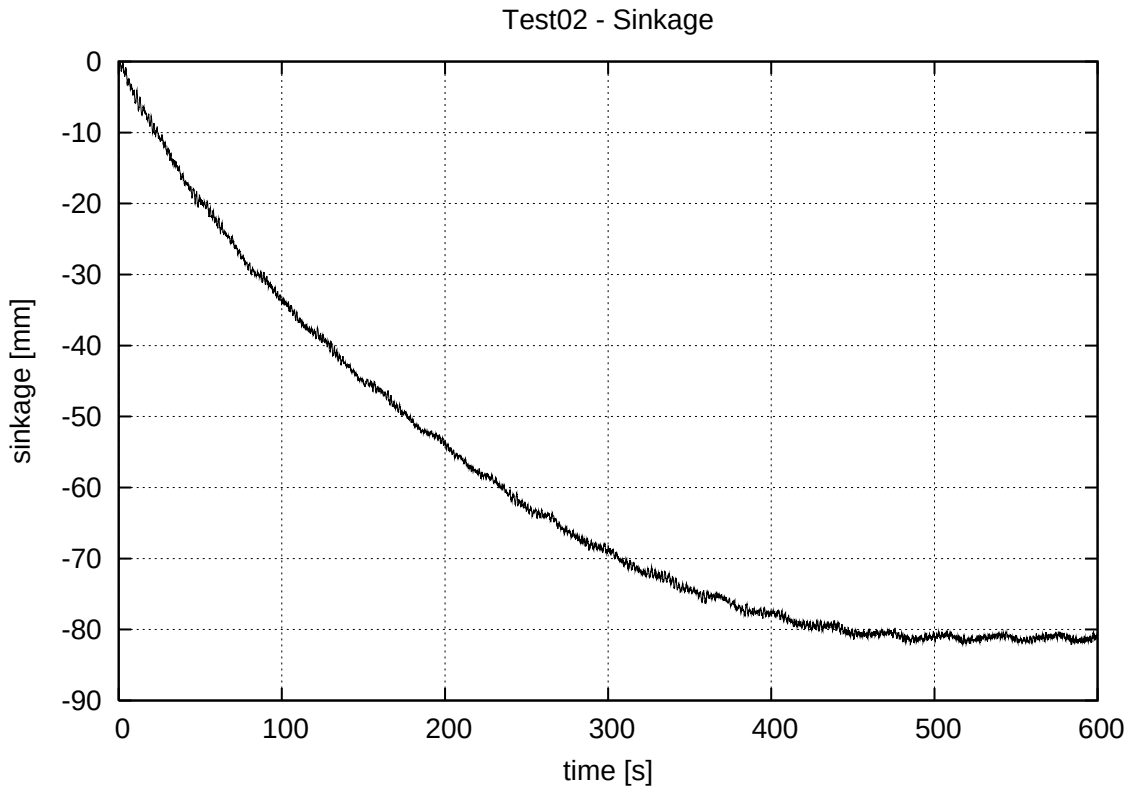

Figure 4.18 Test02 – measured sinkage of the c.o.g.

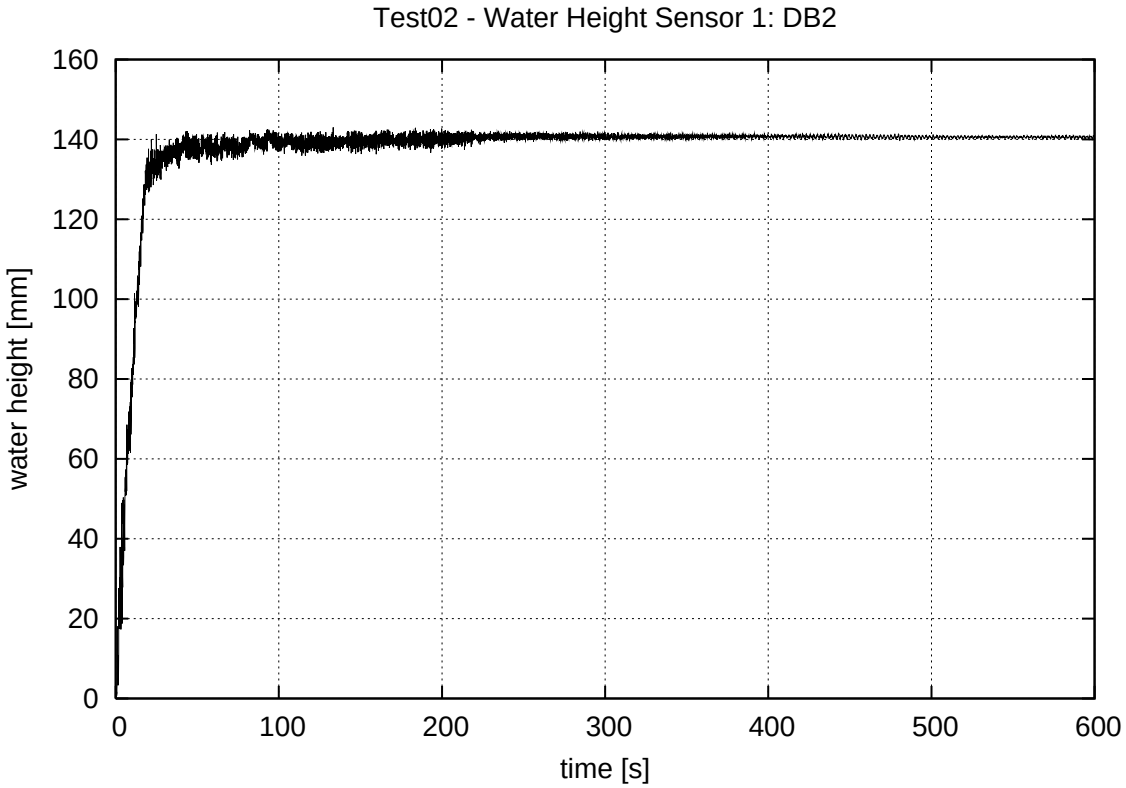

Figure 4.19 Test02 – water height in the room DB2, sensor 1

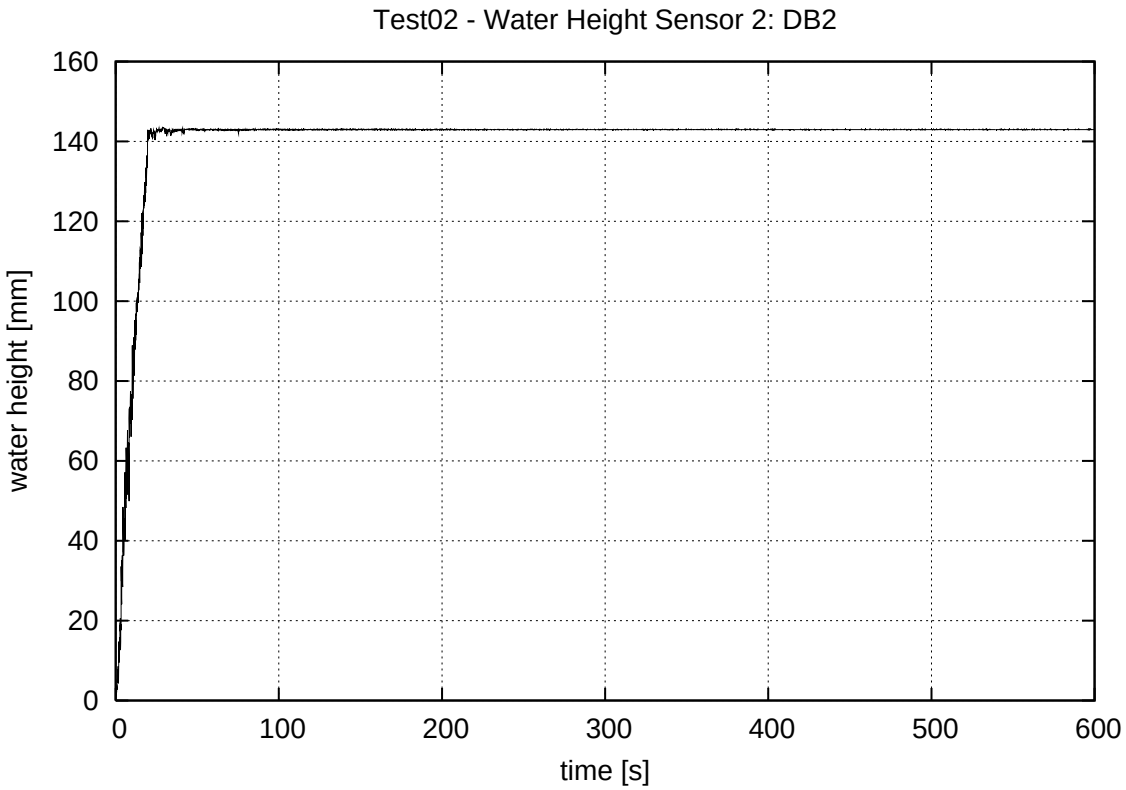

Figure 4.20 Test02 – water height in the room DB2, sensor 2

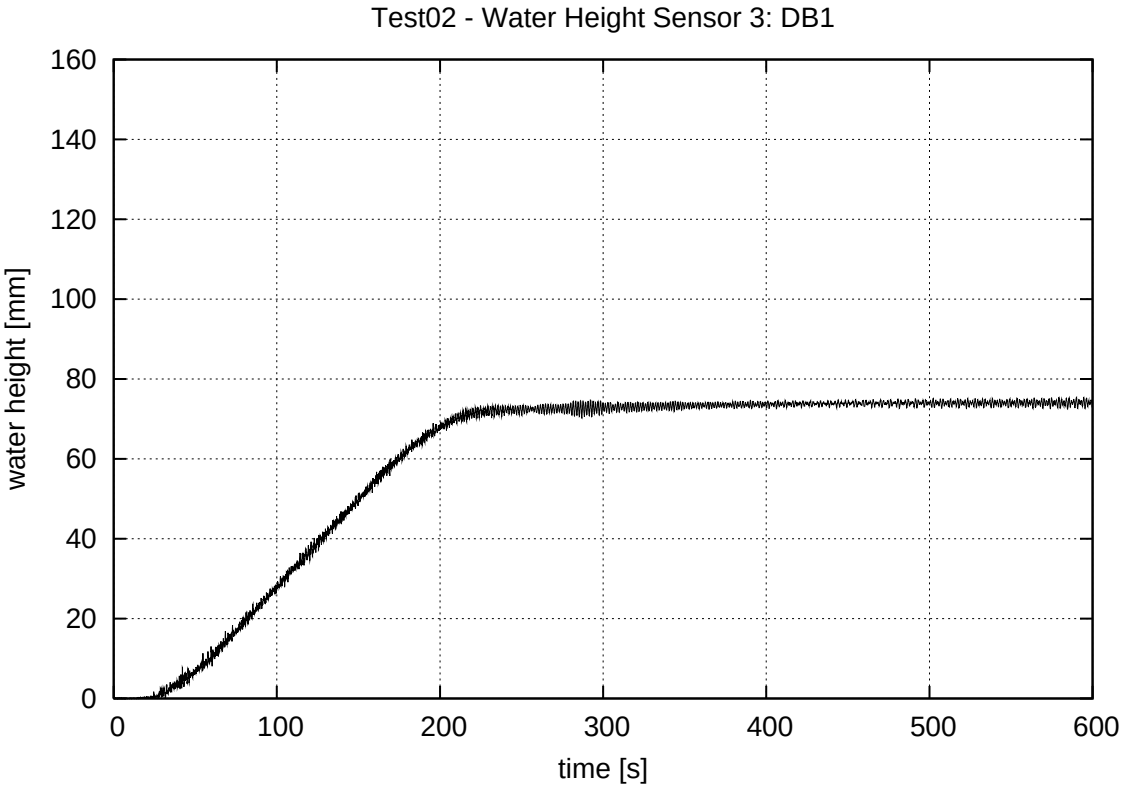

Figure 4.21 Test02 – water height in the room DB1

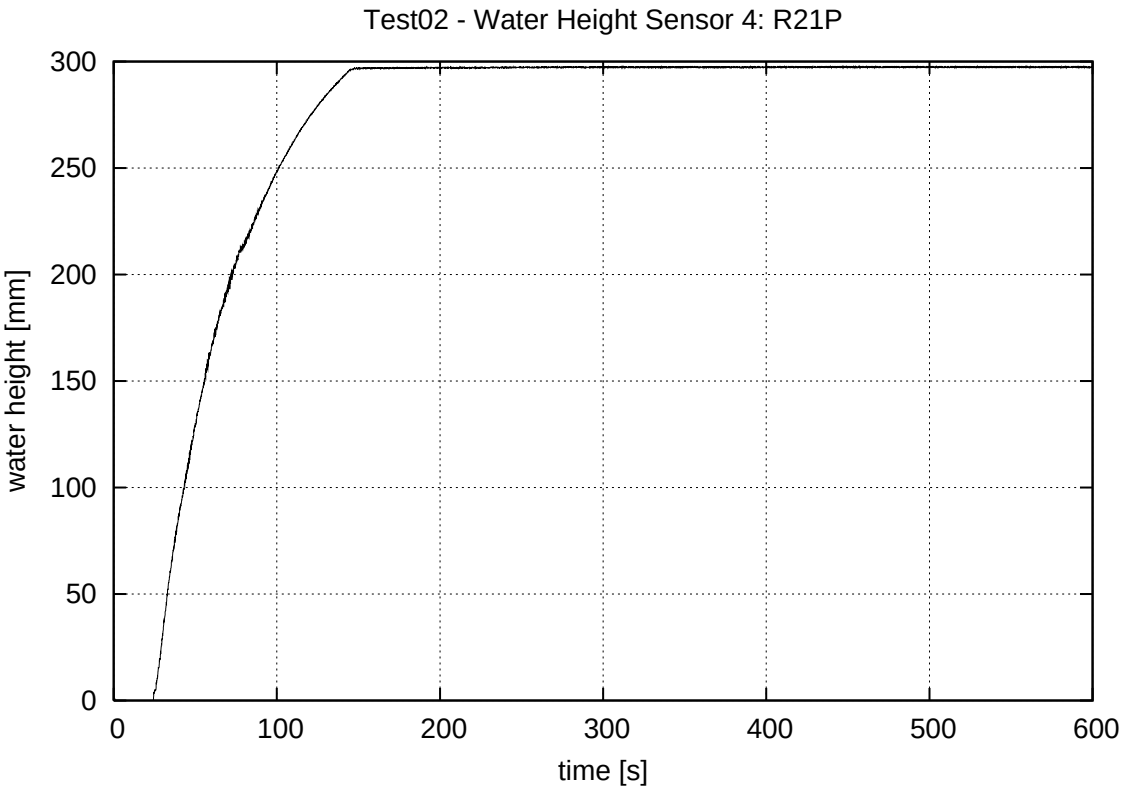

Figure 4.22 Test02 – water height in the room R21P

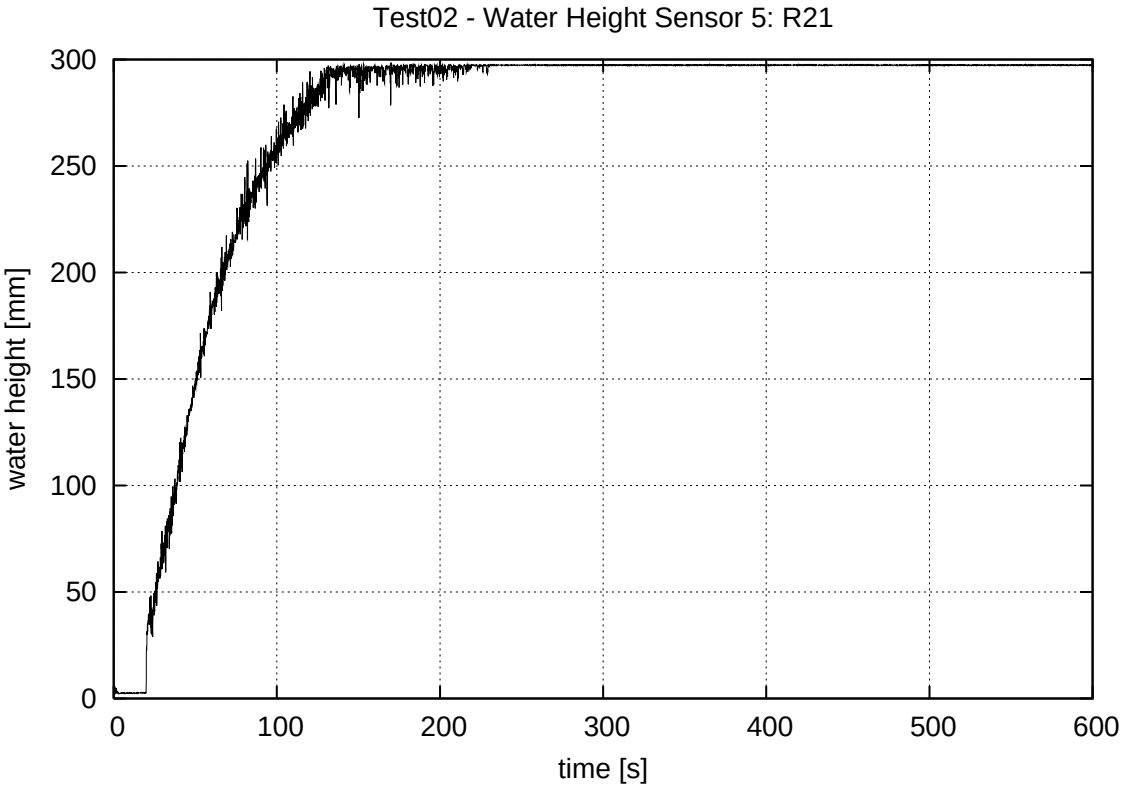

Figure 4.23 Test02 – water height in the room R21

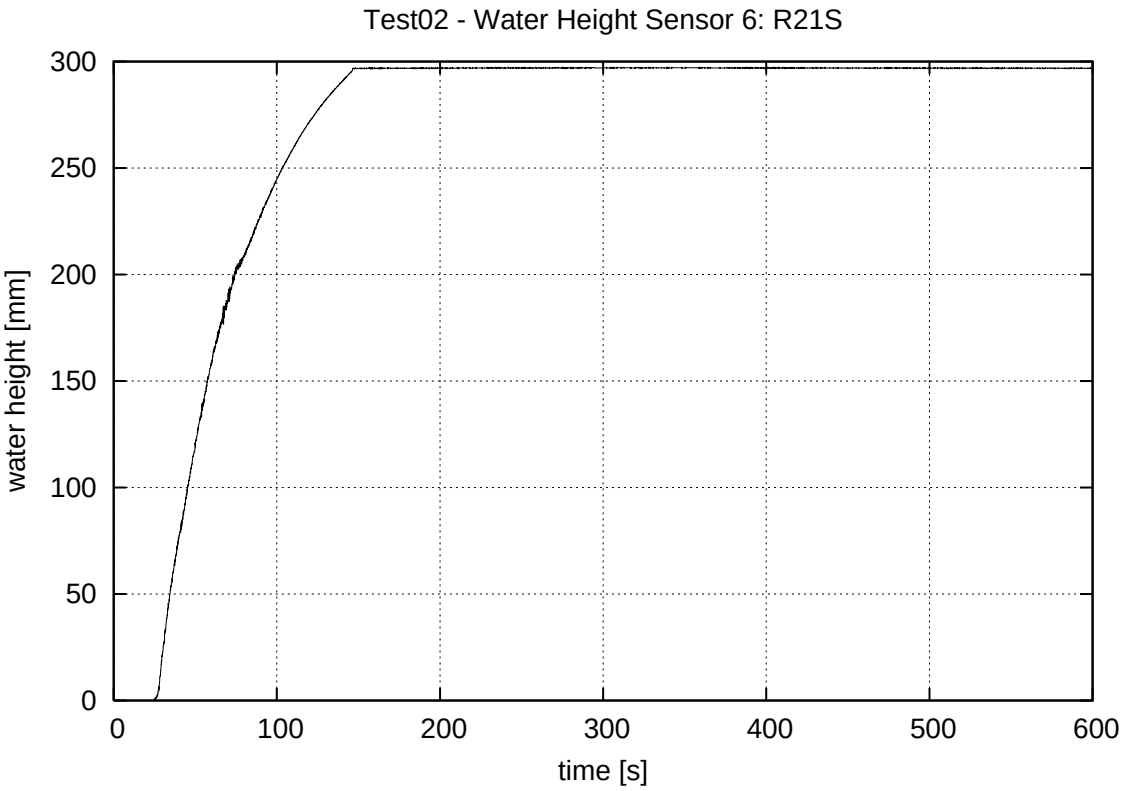

Figure 4.24 Test02 – water height in the room R21S

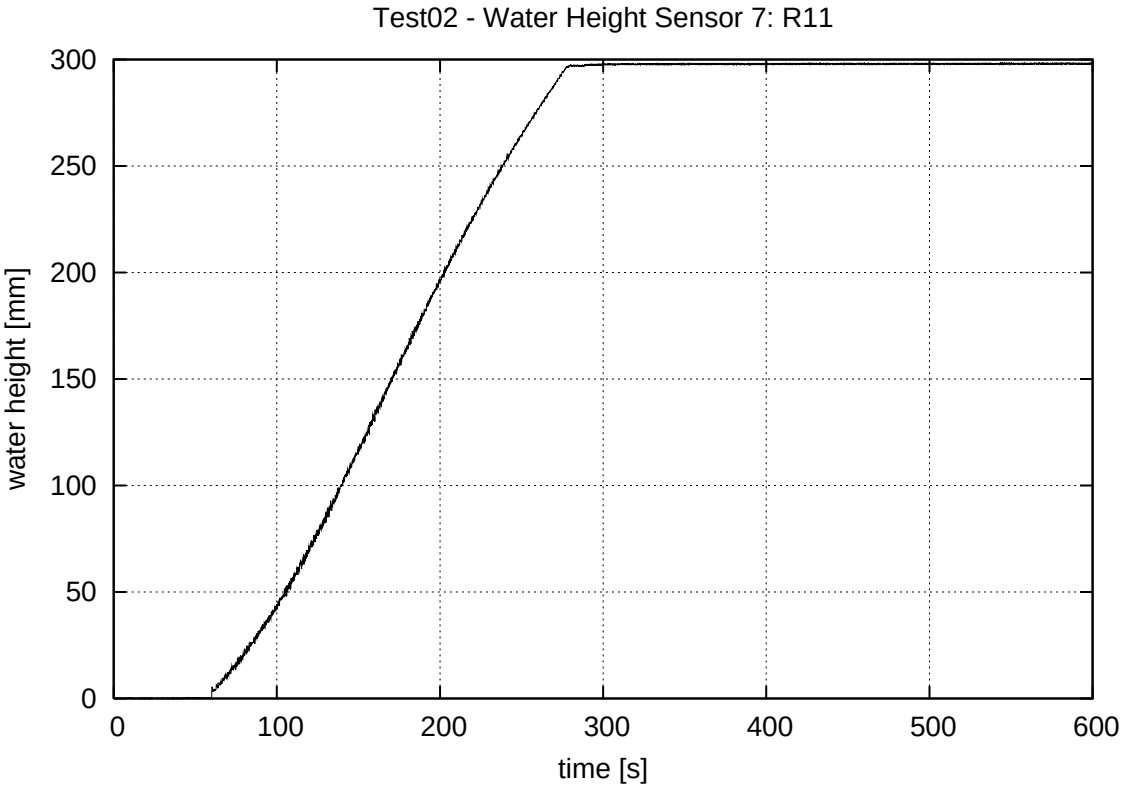

Figure 4.25 Test02 – water height in the room R11

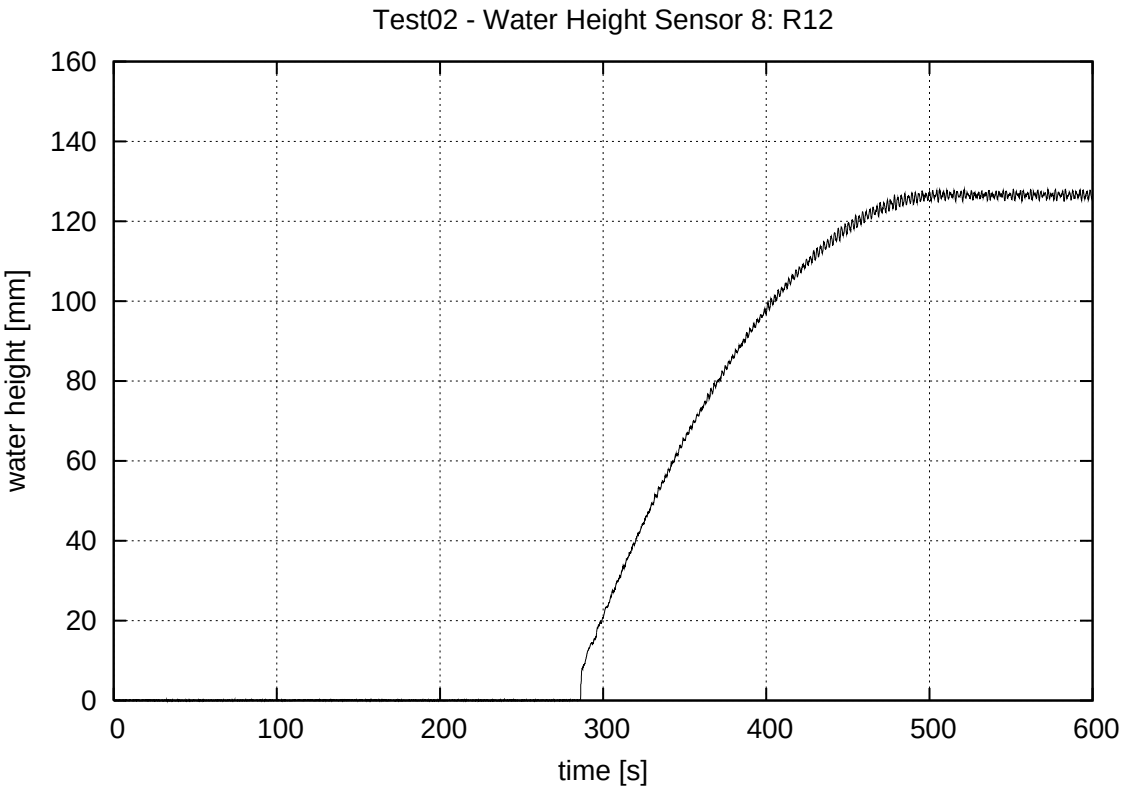

Figure 4.26 Test02 – water height in the room R12

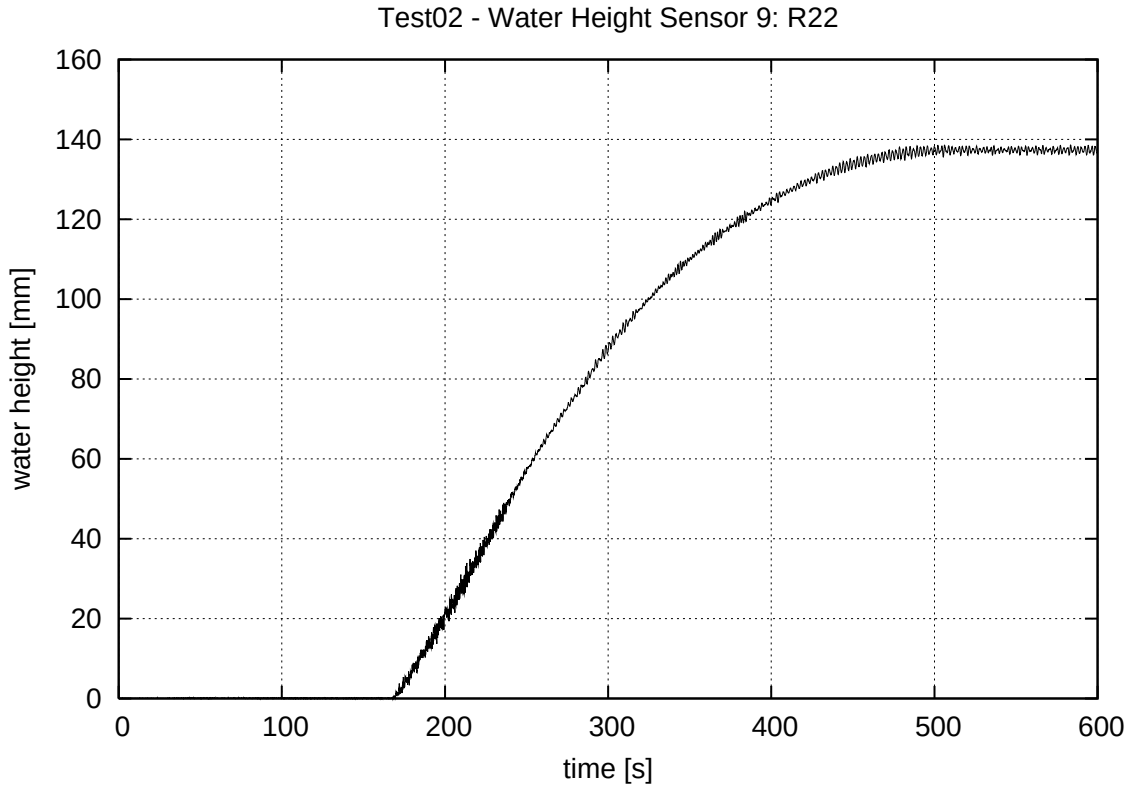

Figure 4.27 Test02 – water height in the room R22

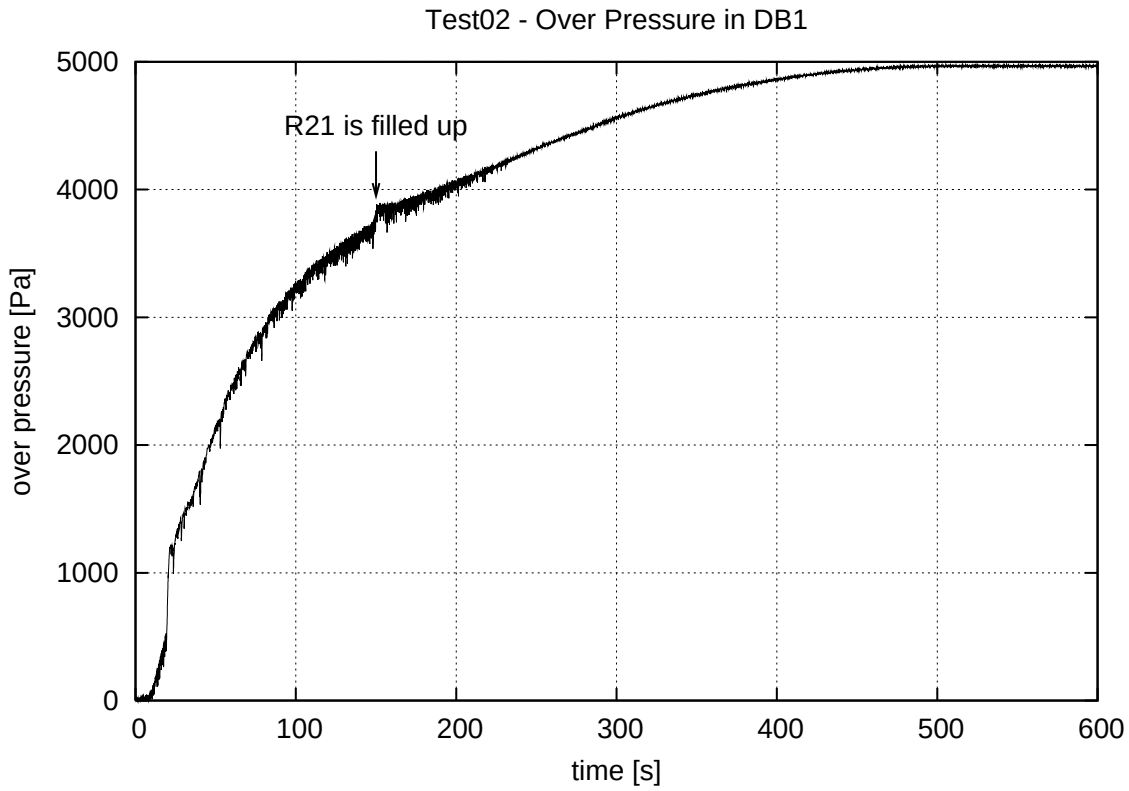

Figure 4.28 Test02 – air pressure in the room DB1

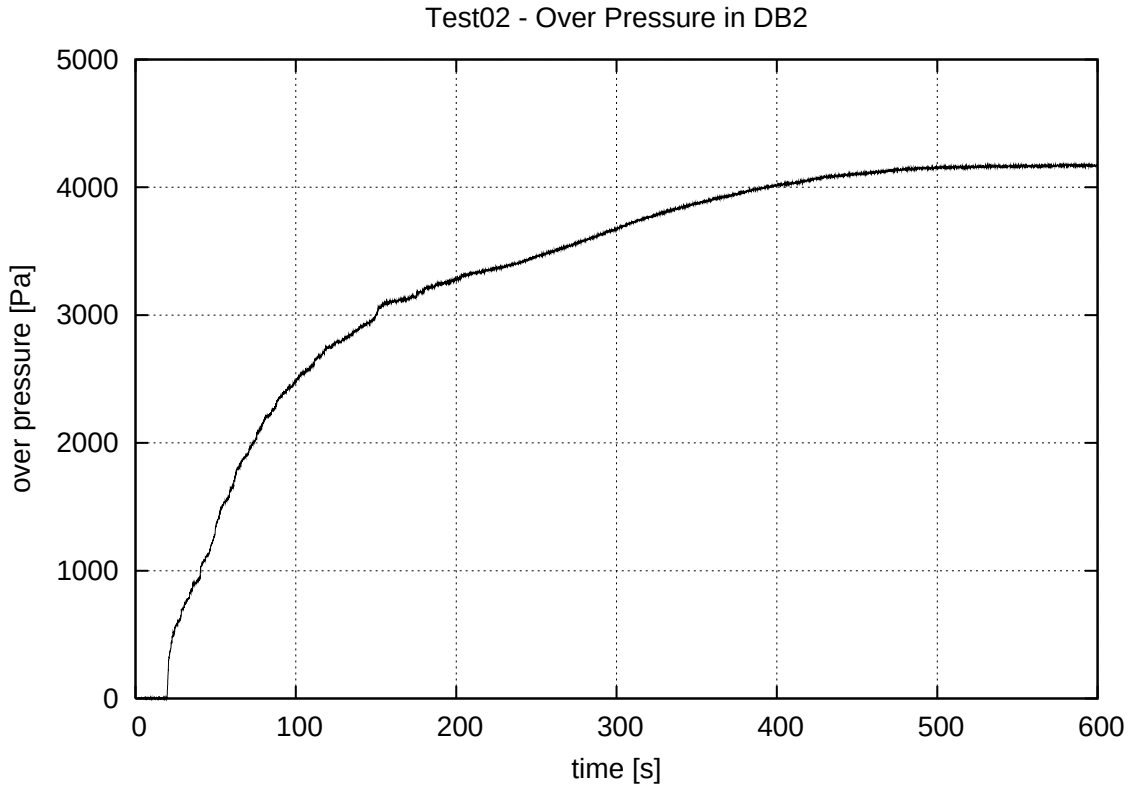

Figure 4.29 Test02 – air pressure in the room DB2

4.2.3 Small Damage in the Forward Compartment – WT-Door Open (Test03)

The investigated damage case is the small damage hole (25 mm × 25 mm) in the bottom of the forward compartment (DB2). Contrary to the Test02, the WT-door that connects the WT-compartments on the upper deck (rooms R21 and R22) is now open.

The forward compartment is flooded faster than the aft compartment since the damage hole is in the bottom of DB2 and there is a direct connection between the lower deck (R21) and the damaged room. Therefore, the open WT-door on the upper deck allows water to flow from R22 to R12 when the lower room in the aft compartment (R11) is not yet full of water. As a result, there is down-flooding from R12 to R11 (Figure 4.30).

Similarly to the Test01 and Test02, the measured air pressure in DB2 (Figure 4.45) starts to build only after this compartment is practically full of water (Figure 4.35). Therefore, this compartment was practically fully vented during the flooding and the measured compression of air occurred only in the pipe to the pressure gauge.

As in the previous tests, air escapes in bubbles from the air pocket in DB1. The bubble flow causes high waves in R21 (Figure 4.39). The bubbling stops when the water level in DB1 has

risen to the top of the opening to DB2, i.e. the measured water height is 86 mm (Figure 4.37) and the opening is fully submerged on both sides.

Flooding on the upper deck from R22 to R12 through the open WT-door starts at t = 193 s and the down-flooding from R12 to R11 starts about 5 s later. The room R12 is filled up at t = 258 s and the flow direction in the opening between R12 and R11 is changed. As a result, the net inflow to the compartments on the upper deck (R12 and R22) is significantly increased (Figure 4.42 and Figure 4.43). As a result, the time derivative of the trim angle is also increased when the room R12 is filled up (Figure 4.32).

Regardless of the down-flooding, the compartment R11 is probably rather well-vented since the opening to R12 is large (100 mm × 100 mm) and the water height in R12 is small (less than 20 mm) during the down-flooding phase. Hence air could escape fairly well through the center of the opening (see Figure 4.30).

The pressures of the air pockets in the double bottom start to increase faster when the room R11 is filled up with water and the flow direction in the opening between R11 and R12 is changed (Figure 4.44 and Figure 4.45). This is likely caused by the fact that the hydrostatic pressure in DB2 is dependent on the water level in R22 (Figure 4.43) and this starts to rise much faster when the down-flooding in the aft compartment has stopped.

Figure 4.30 Test03 – down-flooding from R12 to R11 (left: R12 is flooded through the open WT-door; right: the down-flooding starts)

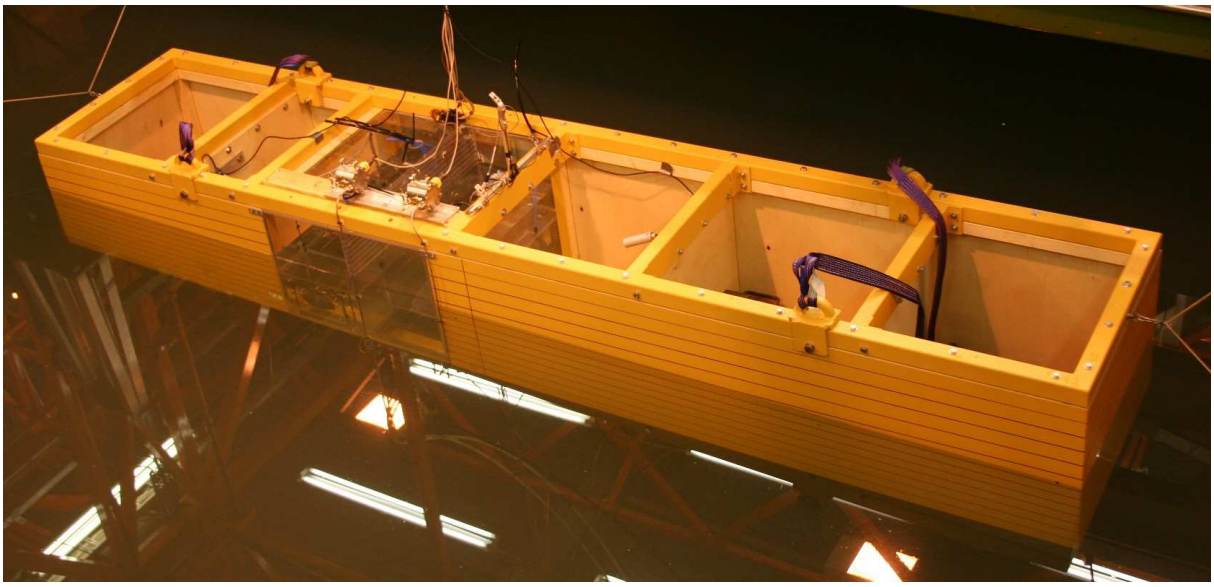

Figure 4.31 Test03 – the final equilibrium floating position

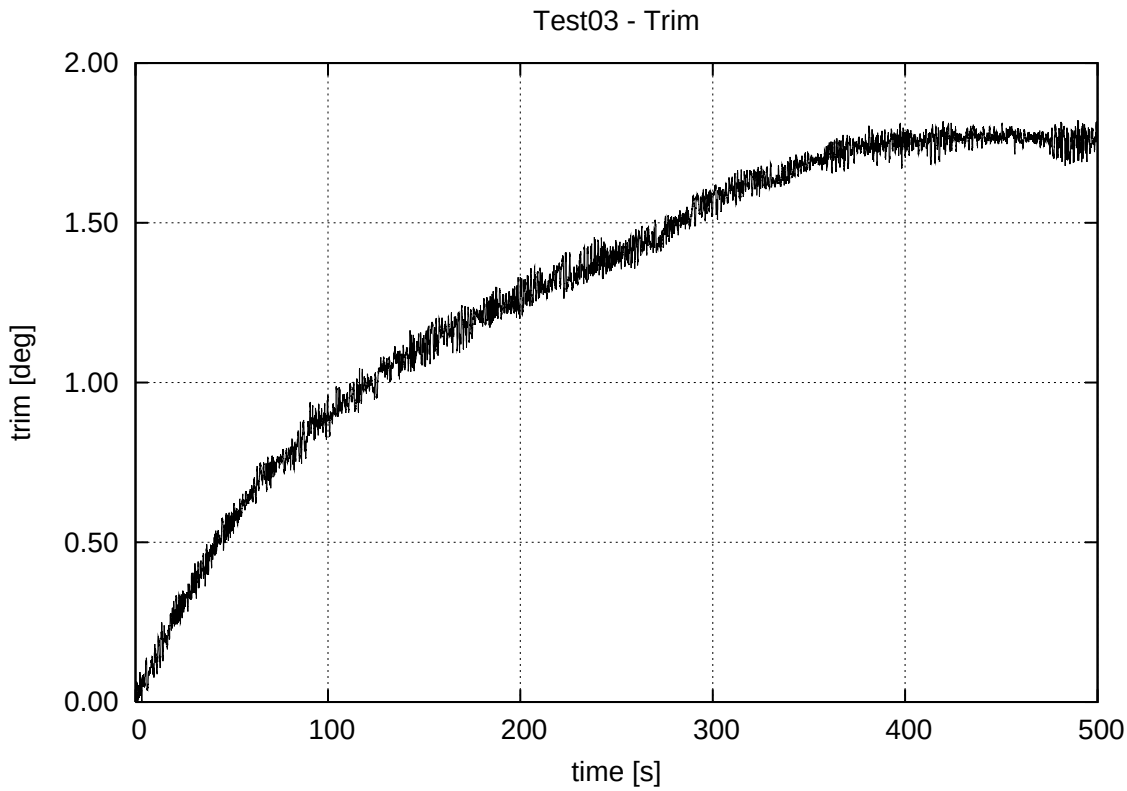

Figure 4.32 Test03 – measured trim angle

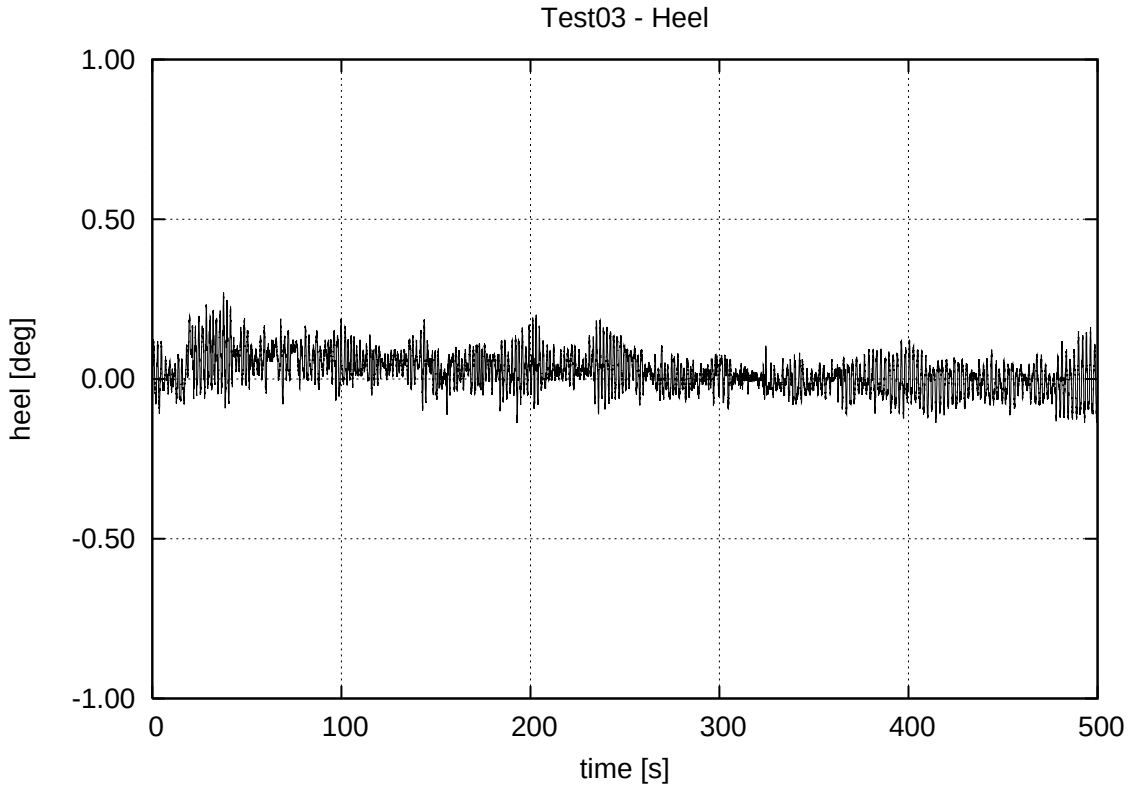

Figure 4.33 Test03 – measured heel angle

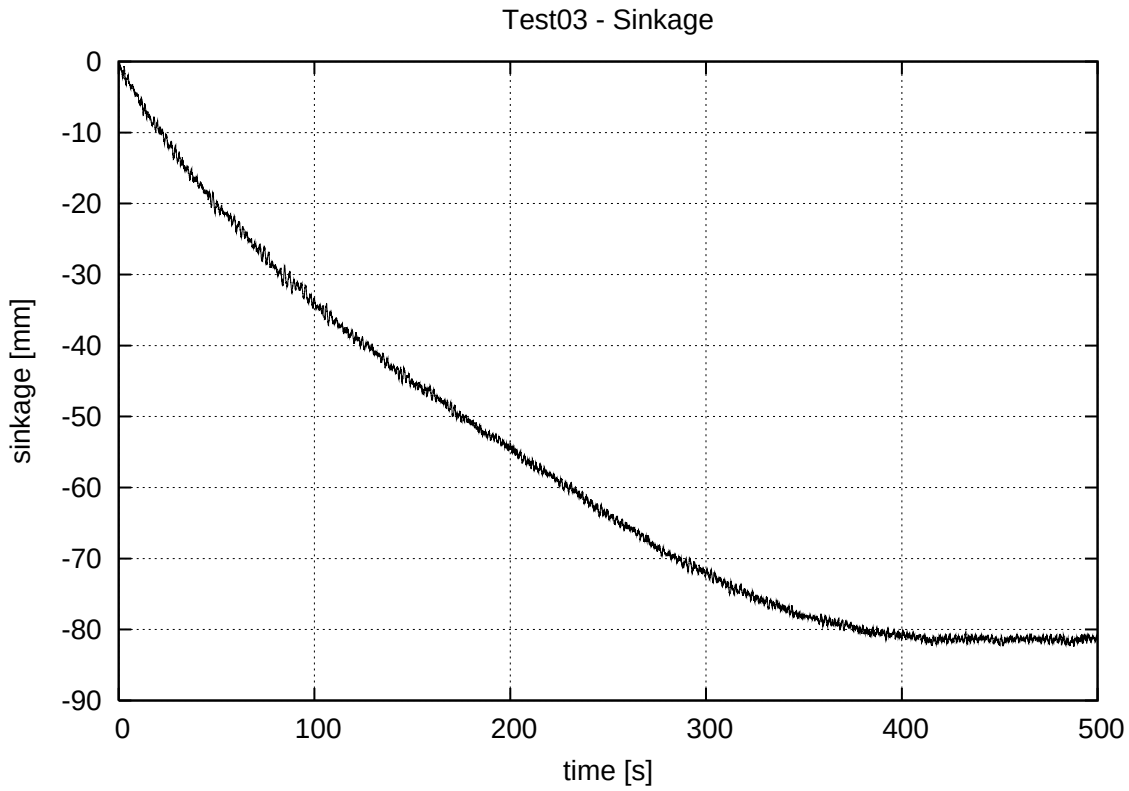

Figure 4.34 Test03 – measured sinkage

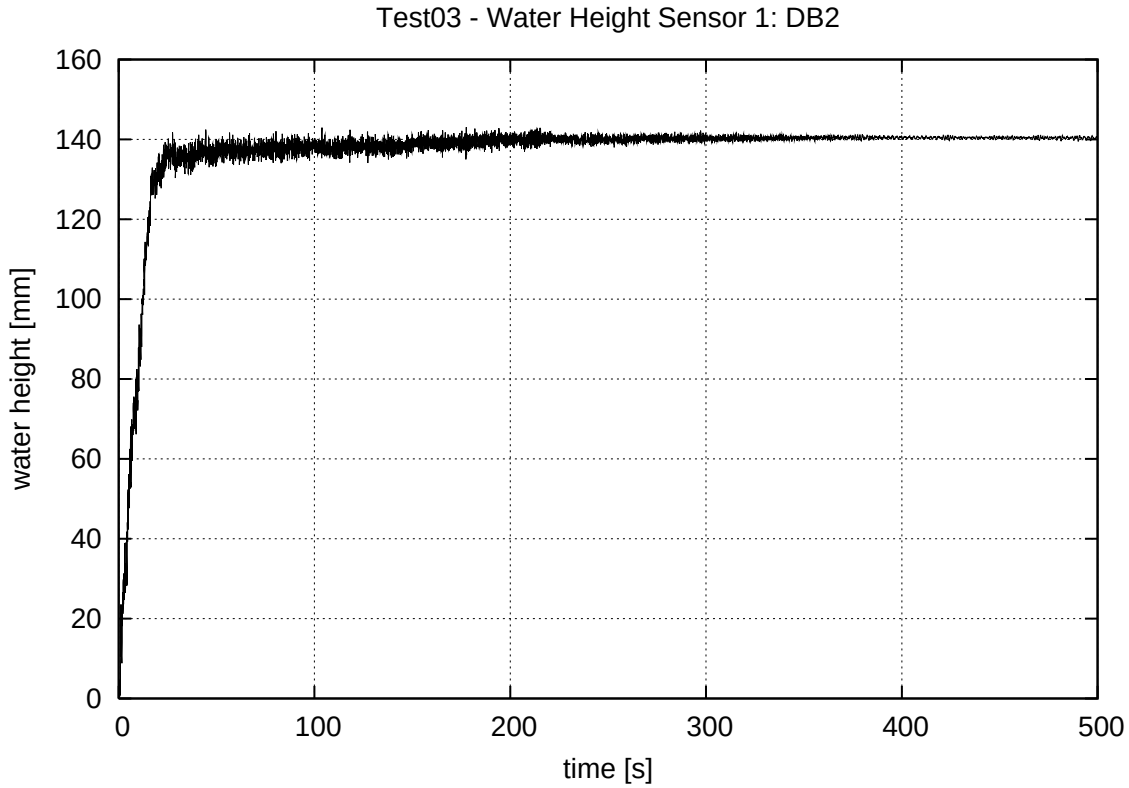

Figure 4.35 Test03 – water height in the room DB2, sensor 1

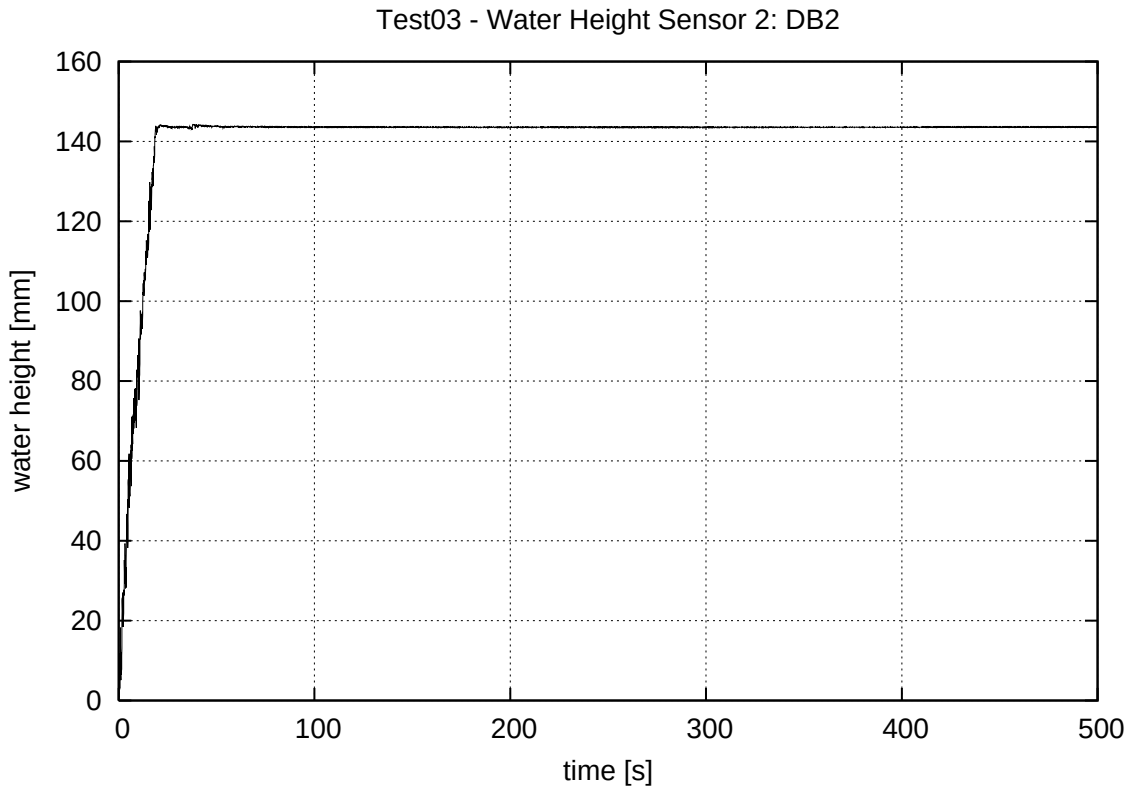

Figure 4.36 Test03 – water height in the room DB2, sensor 2

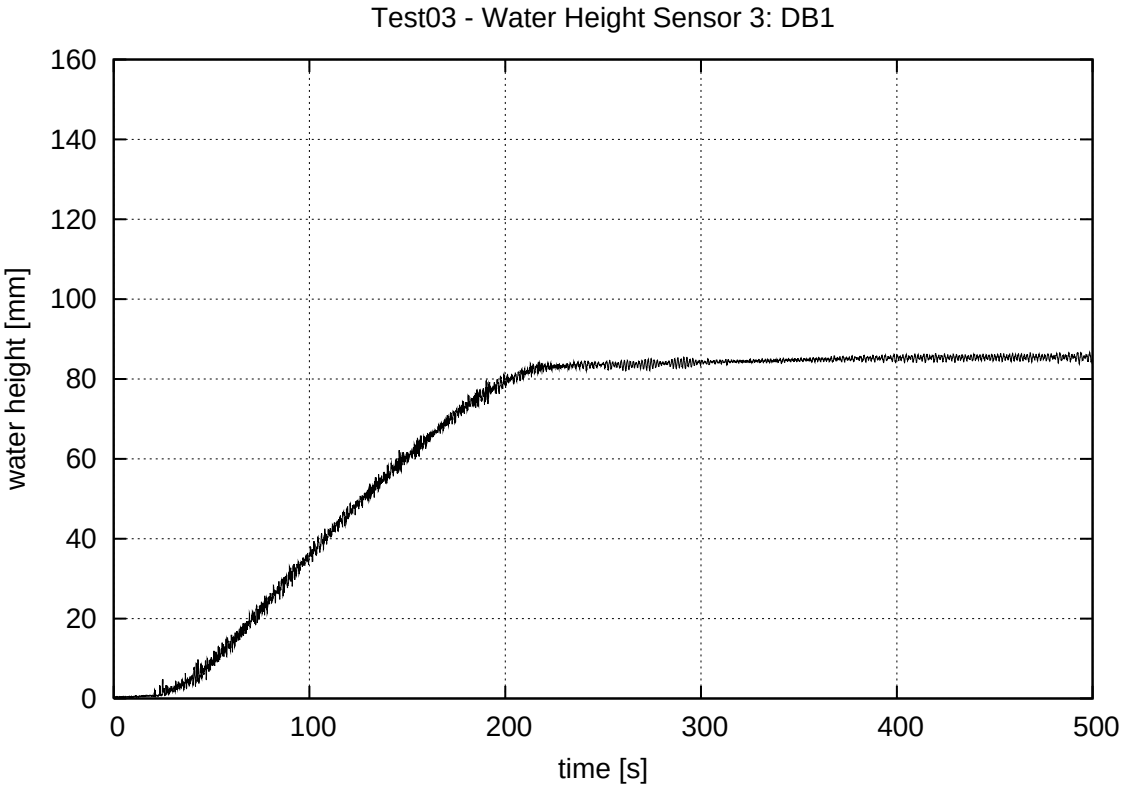

Figure 4.37 Test03 – water height in the room DB1

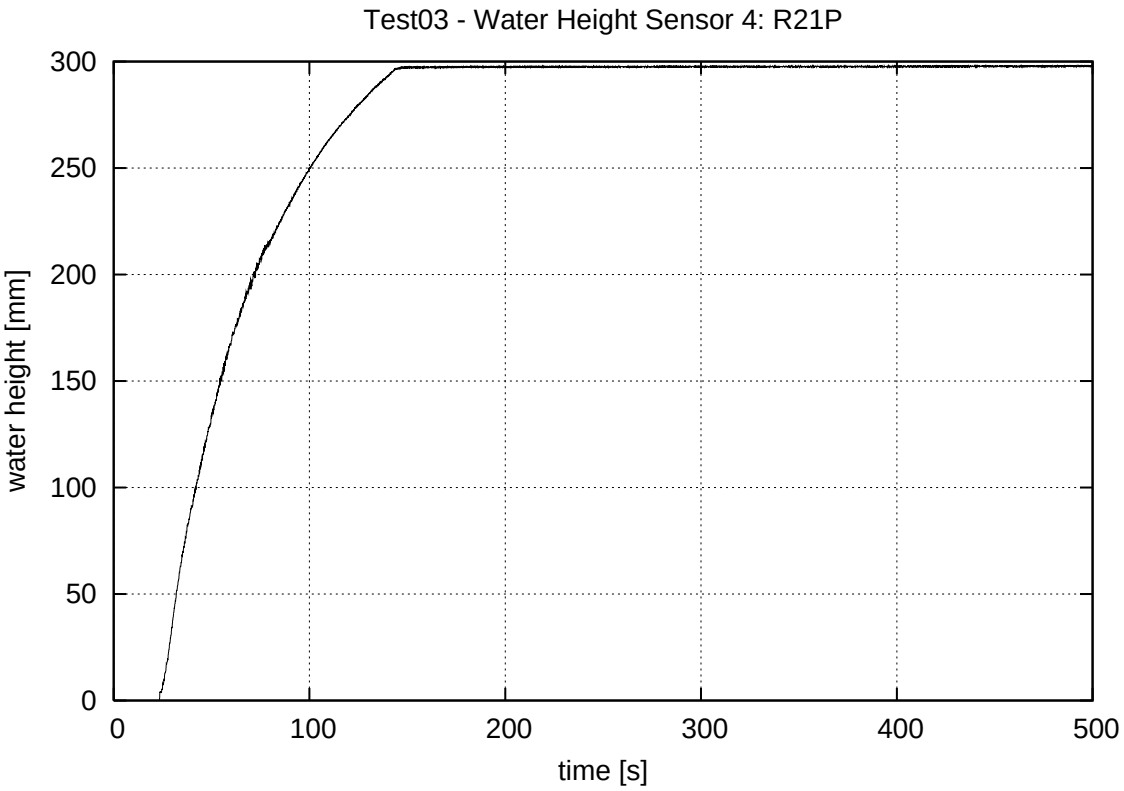

Figure 4.38 Test03 – water height in the room R21P

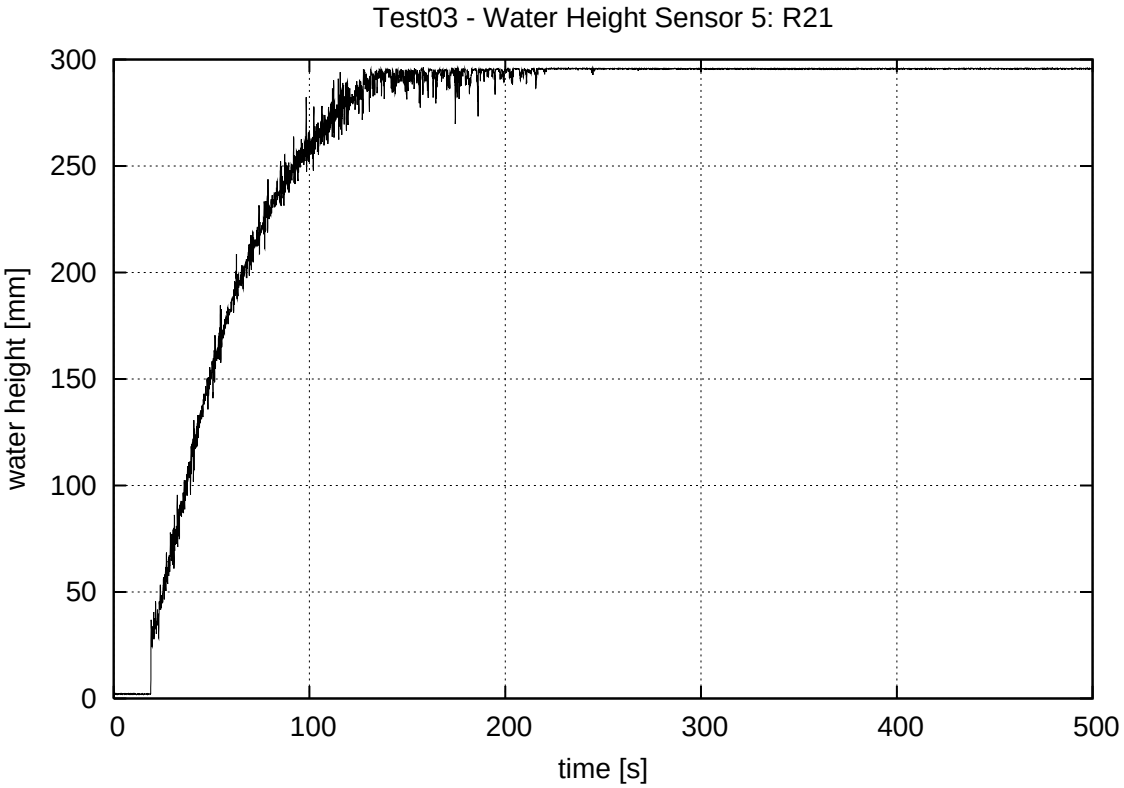

Figure 4.39 Test03 – water height in the room R21

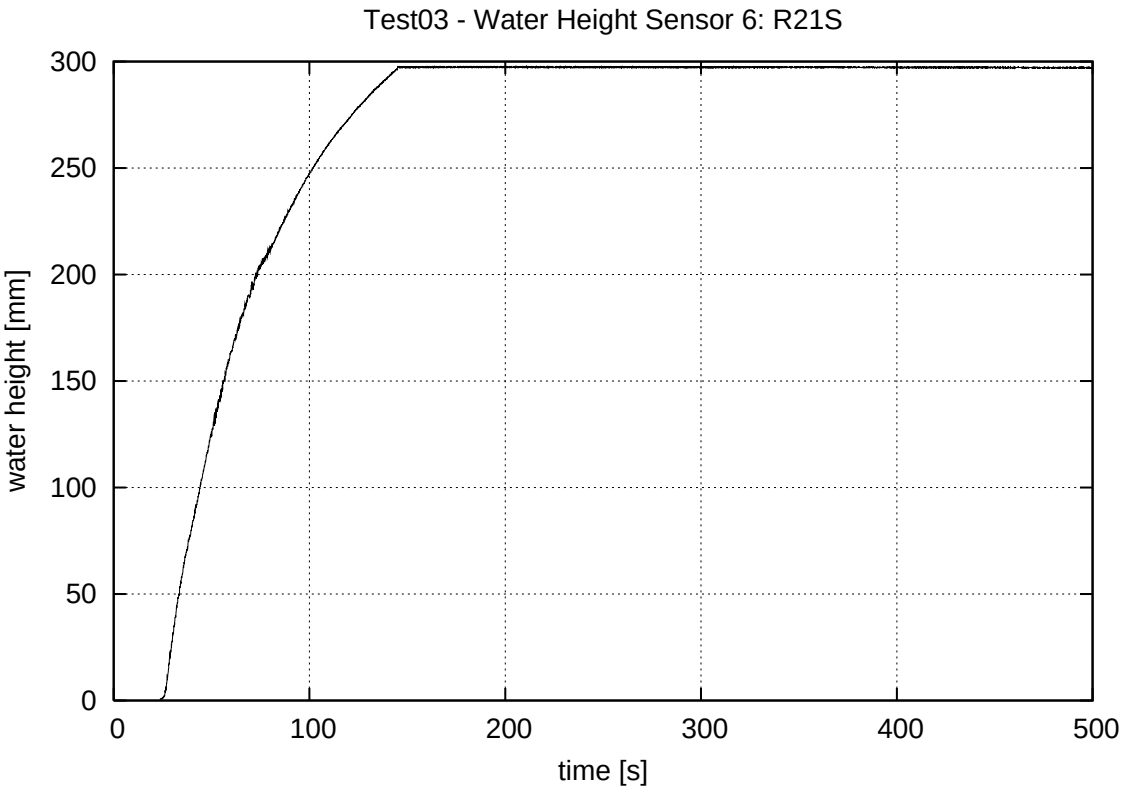

Figure 4.40 Test03 – water height in the room R21S

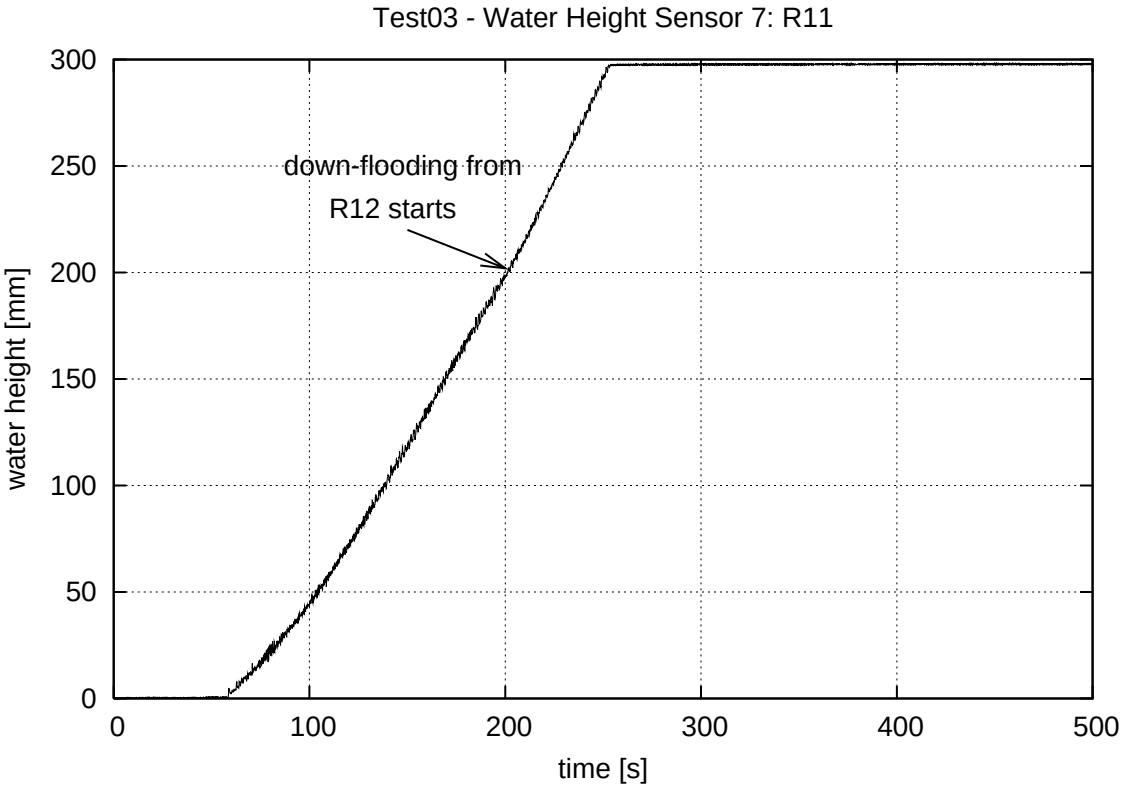

Figure 4.41 Test03 – water height in the room R11

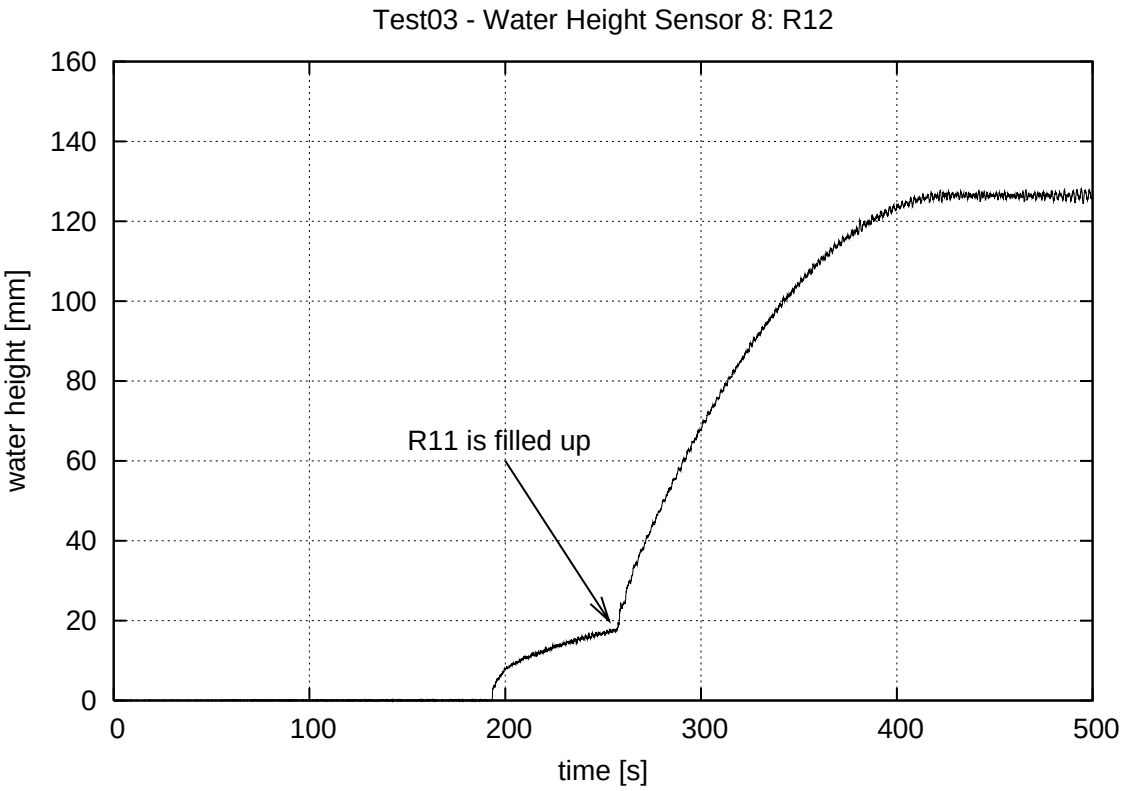

Figure 4.42 Test03 – water height in the room R12

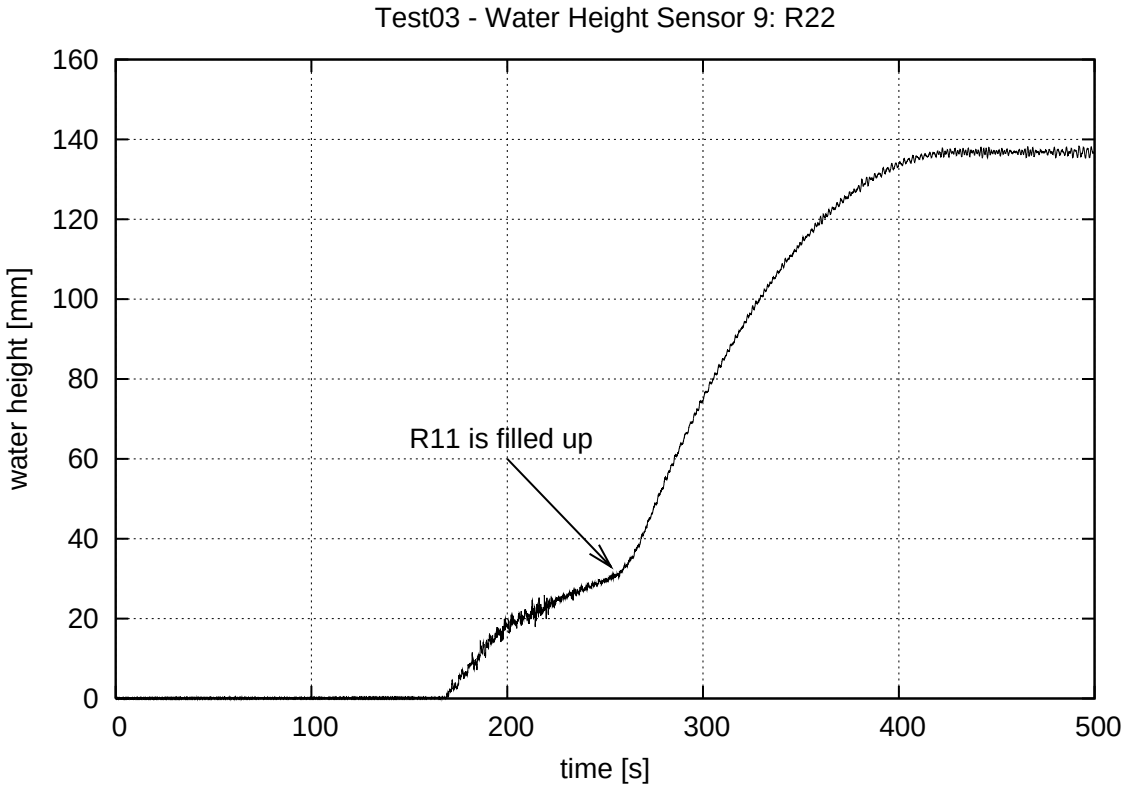

Figure 4.43 Test03 – water height in the room R22

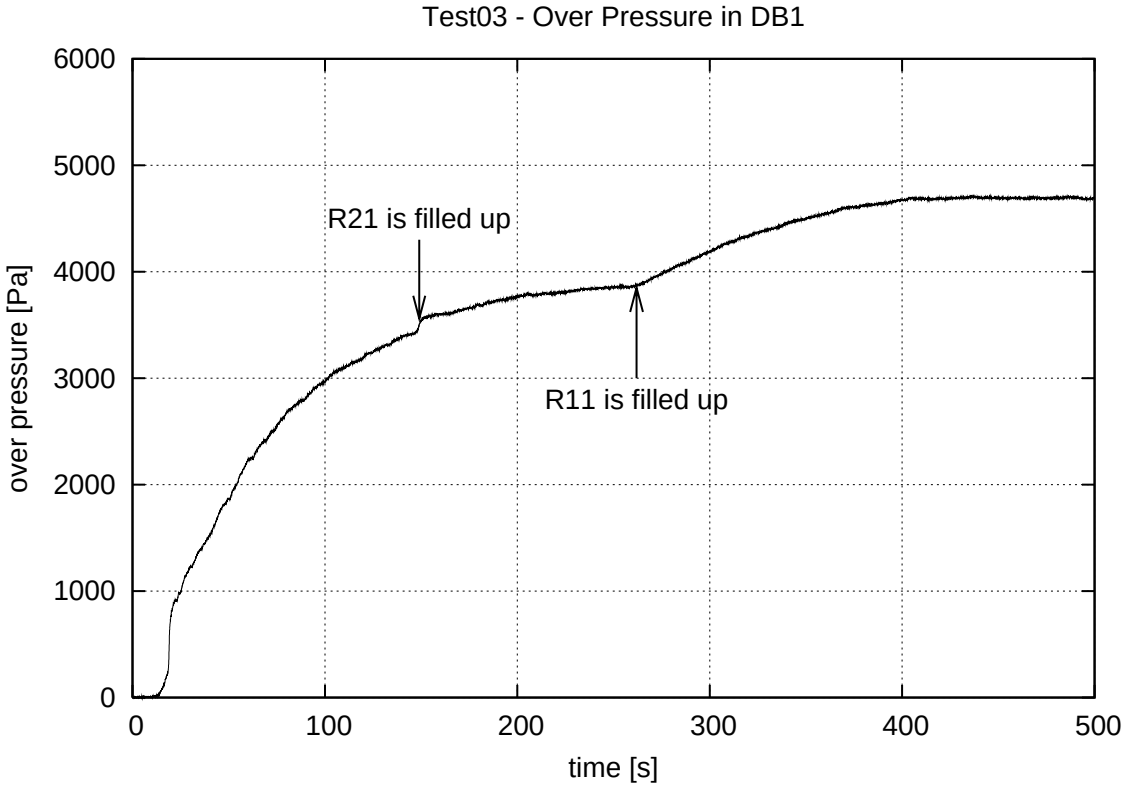

Figure 4.44 Test03 – air pressure in DB1

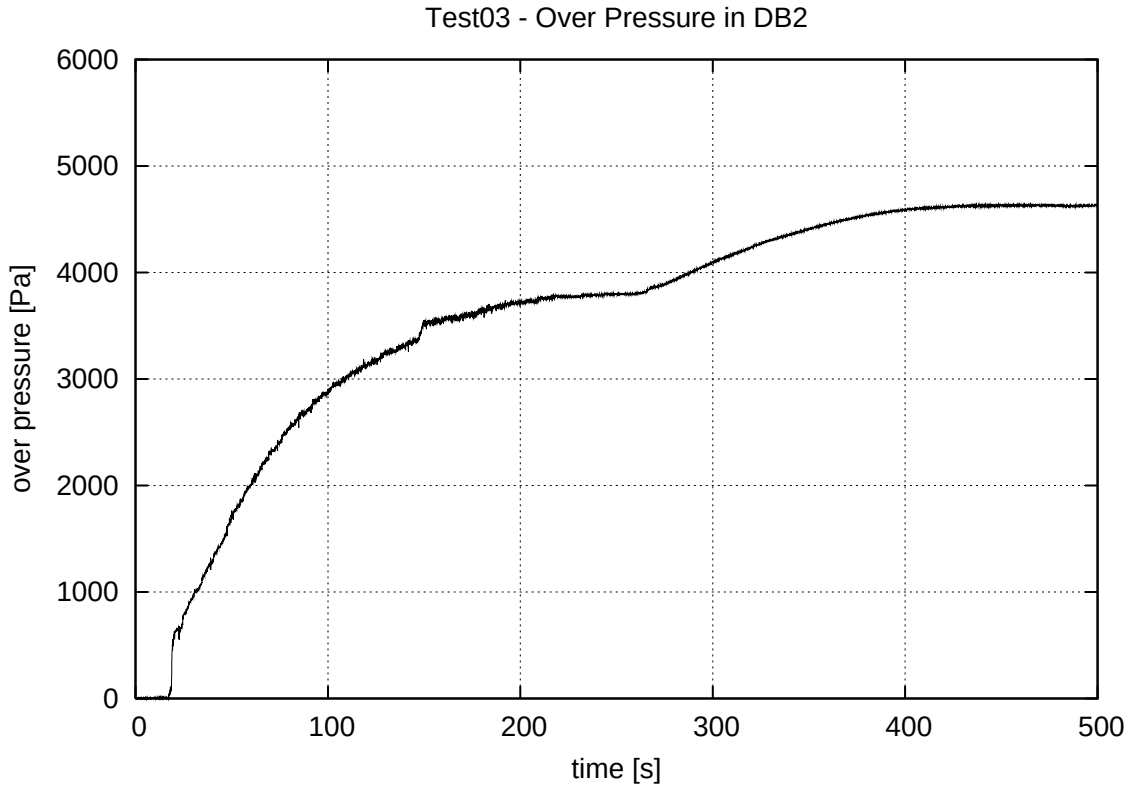

Figure 4.45 Test03 – air pressure in DB2

4.2.4 Large Damage in the Forward Compartment (Test04)

The investigated damage case is the large damage hole (40 mm × 60 mm) in the bottom of the forward compartment (DB2). The WT-door on the upper deck is closed. The size of the damage hole is larger but otherwise this test is identical to Test02.

There was a small volume of water left from a previously performed test in the room R12. As the model started to trim this water was collected near the water height sensor number 8. This is clearly visible in the video captures (Figure 4.46) and in the measured water height (Figure 4.57). However, the volume of this additional water is so small that it does not affect the flooding process and the floating position of the model.

The damaged room DB2 is filled up in just 5 s (Figure 4.51). The corresponding time in Test02 is 20 s, i.e. four times longer. The area of the large damage is 3.84-times larger than the area of the small damage hole. Therefore, in this respect, the results for the Test02 and Tes04 seem to be in good agreement.

The up-flooding to R21 causes high waves (Figure 4.54), mainly due to the air bubbling from the air pocket in DB1.

Air compression in DB2 starts only after the room is already filled up with water. Therefore, the measured compression occurs only in the pipe that leads to the pressure gauge.

The time-to-flood is 135 s shorter than in the case of the small damage hole in the same location (Test02). This is logical as the aft compartment is flooded faster due to the open WT-door in the transverse bulkhead.

In the equilibrium condition the measured water heights and the floating position are practically the same as in Test02. This is how it was expected to be since the damage size should not affect the final equilibrium state if the model did not capsize during the test and if an air pocket was not formed in the damaged room, or in any other room that is flooded rapidly.

Similarly to the previously described tests, there is a sudden increase in the air pressure in DB1 (Figure 4.59) when R21 is filled up with water. However, contrary to the other tests, in this case the increase is much smaller and hardly notable.

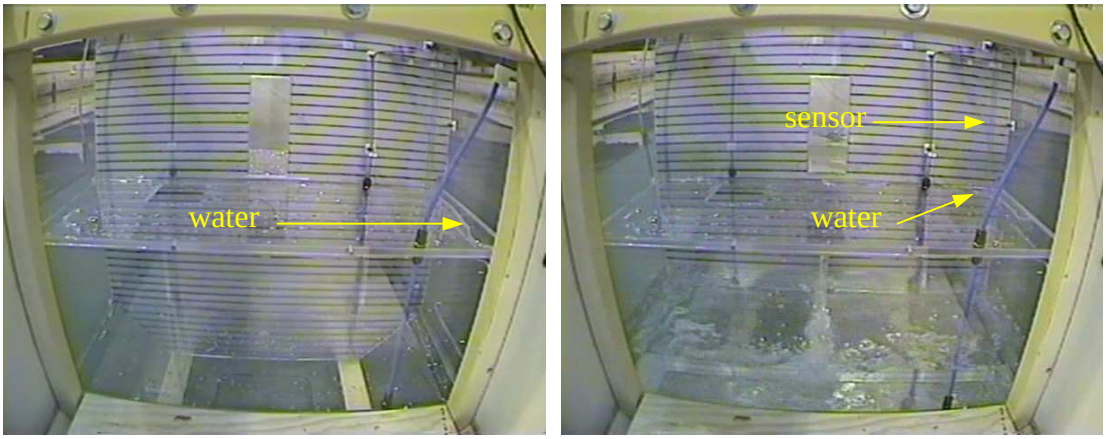

Figure 4.46 Test04 – small initial volume of water in the room R12 (left) is collected around the water height sensor (right) as the model trims

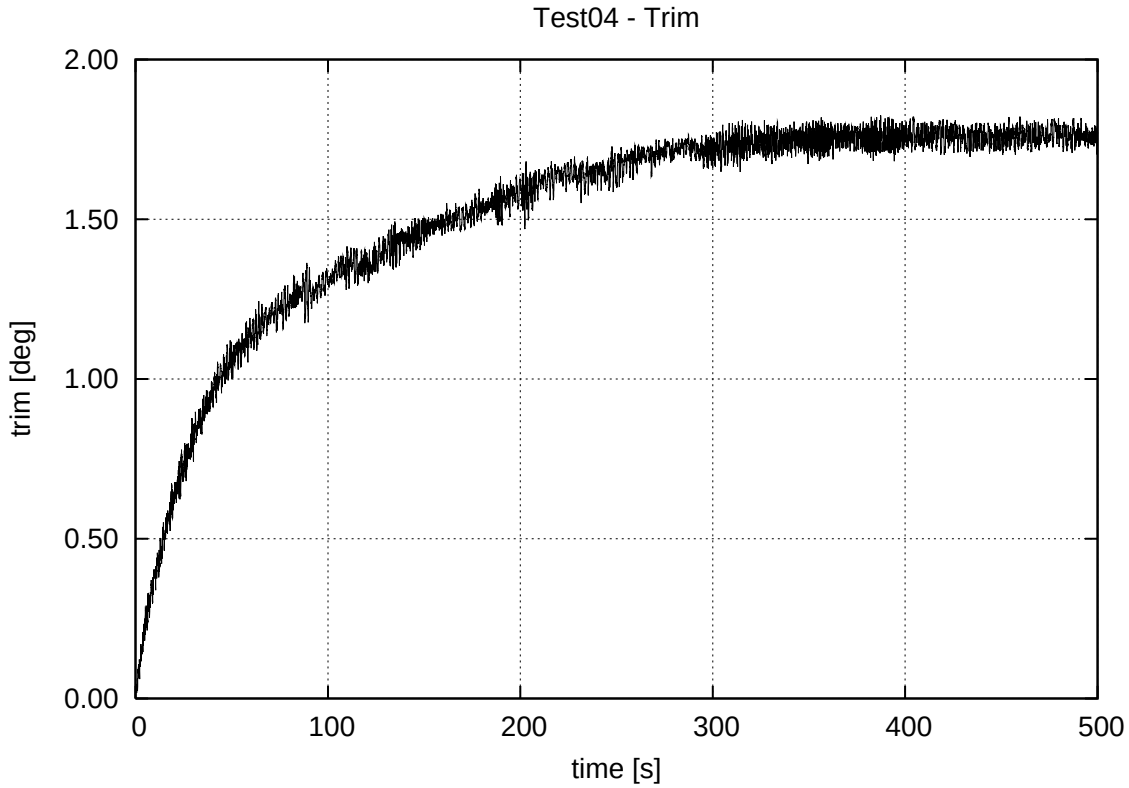

Figure 4.47 Test04 – measured trim angle

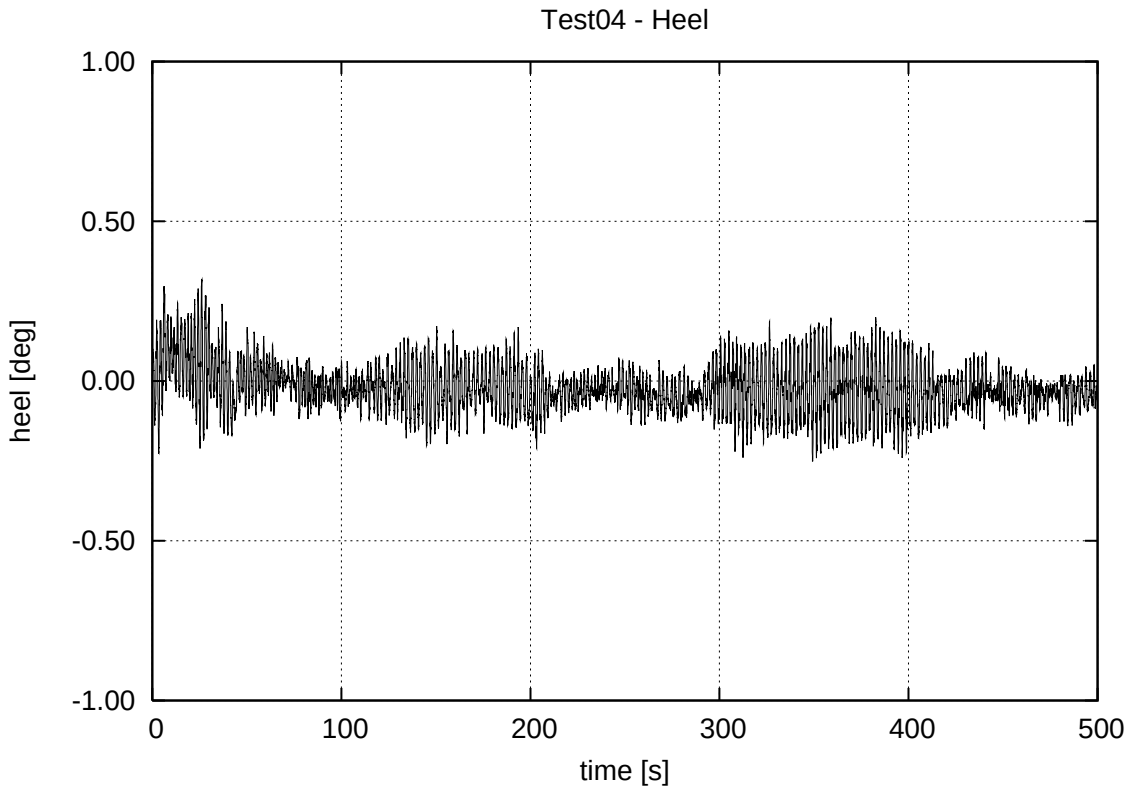

Figure 4.48 Test04 – measured heel angle

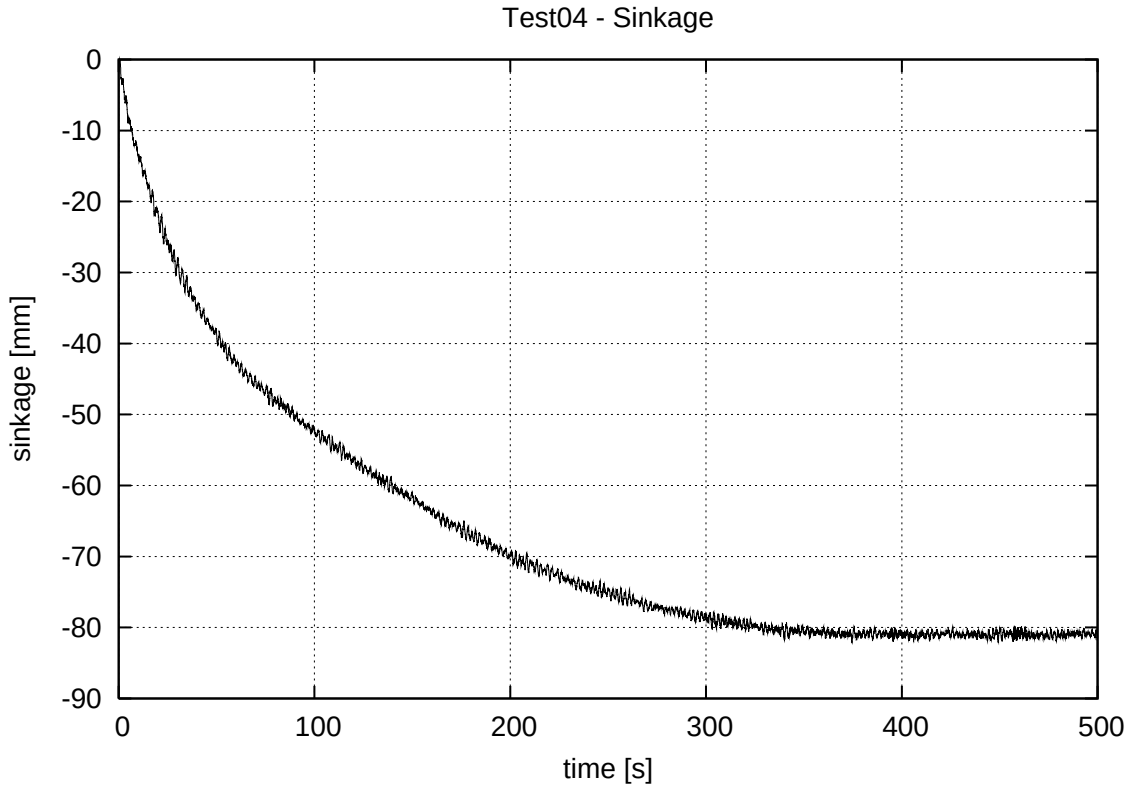

Figure 4.49 Test04 – measured vertical sinkage

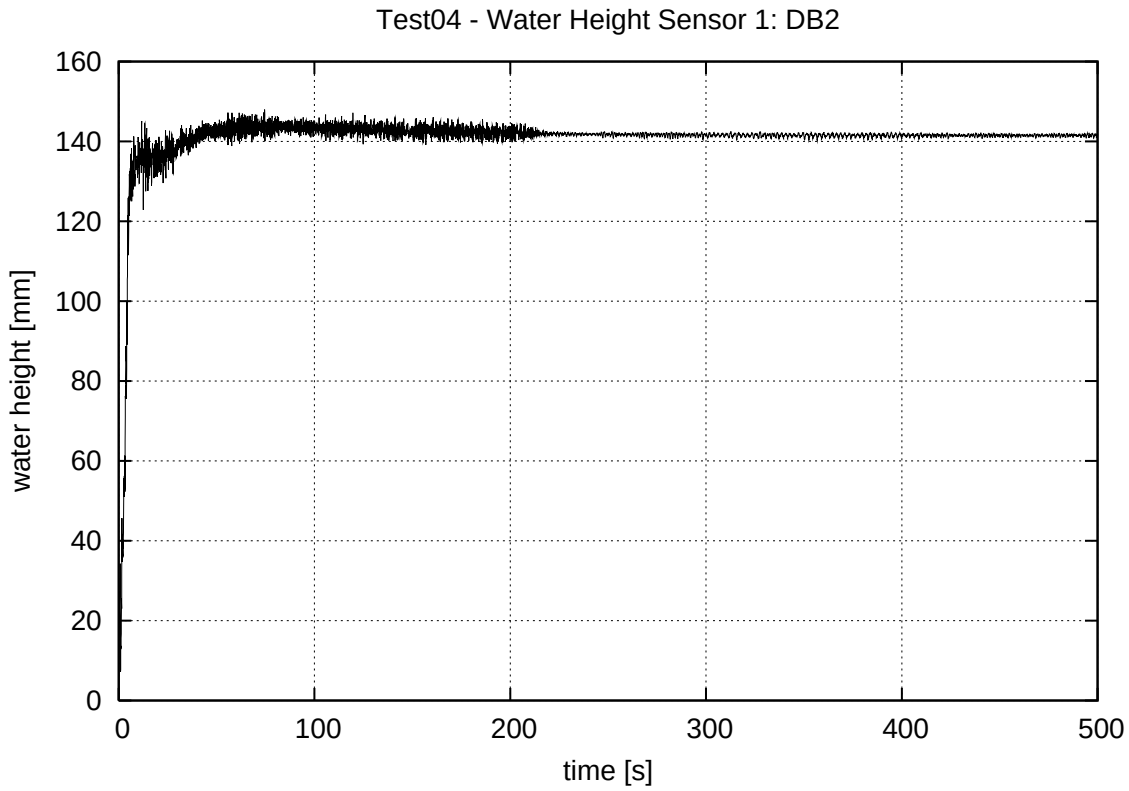

Figure 4.50 Test04 – water height in the room DB2, sensor 1

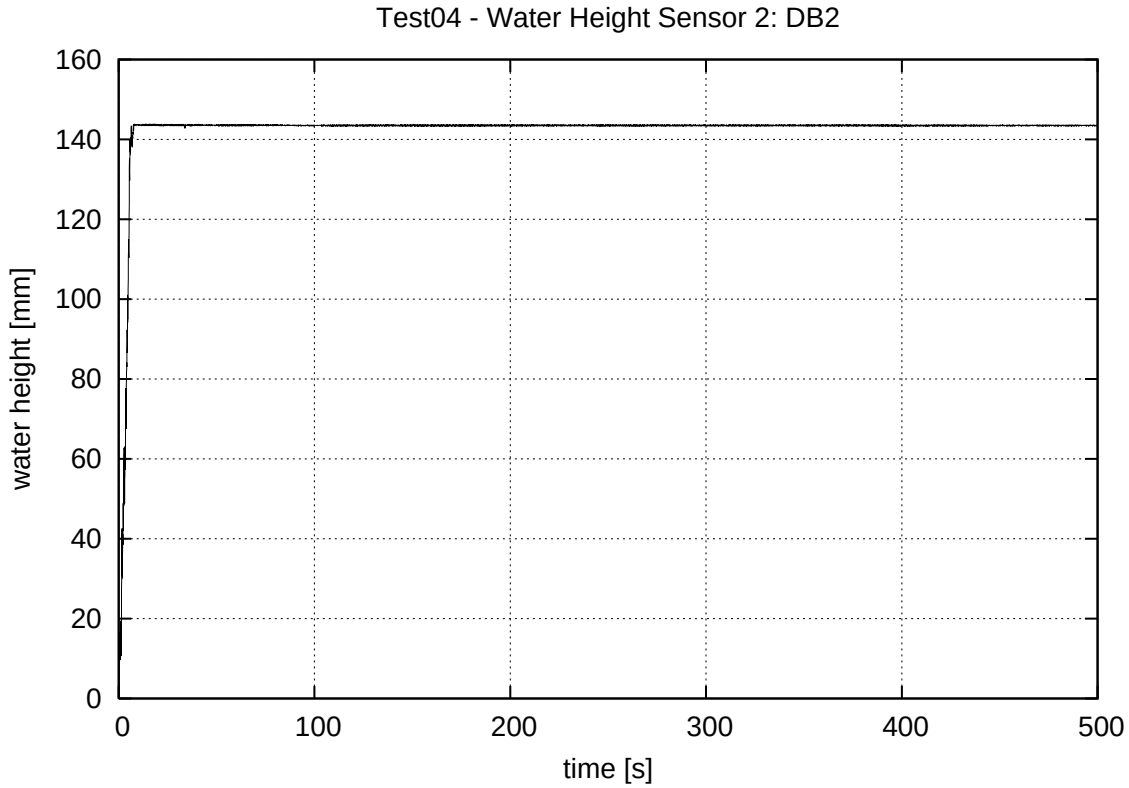

Figure 4.51 Test04 – water height in the room DB2, sensor 2

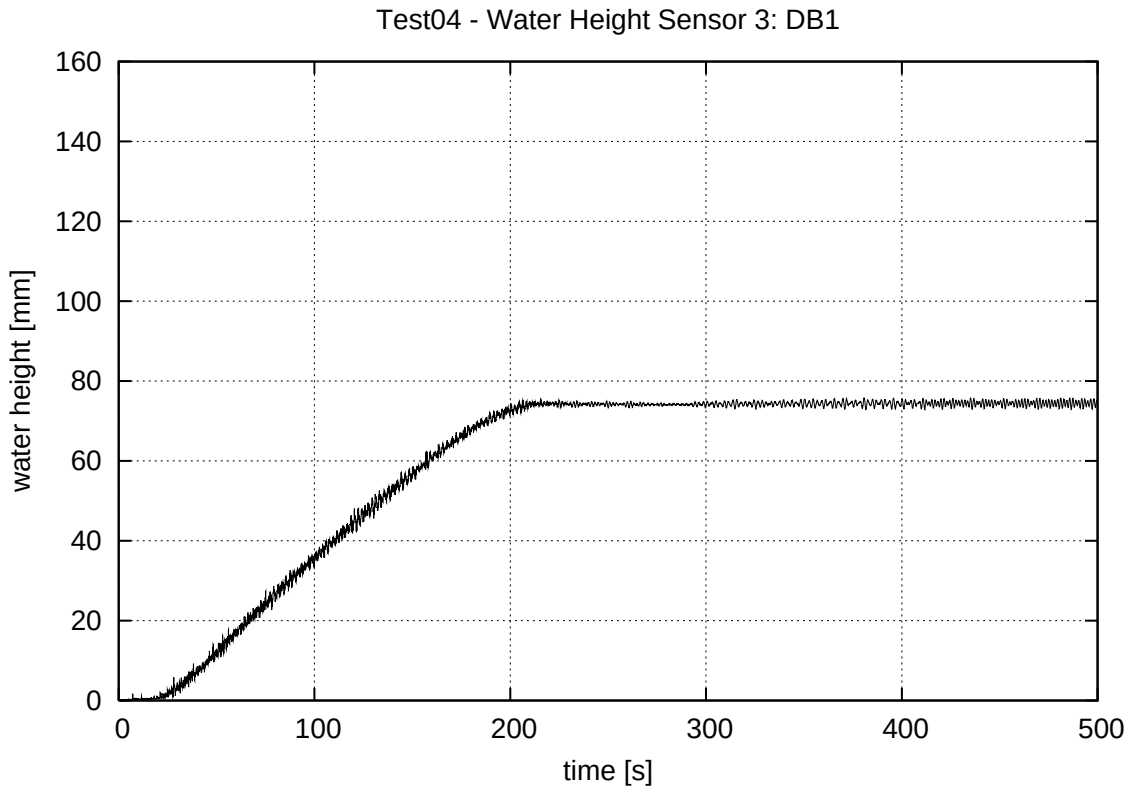

Figure 4.52 Test04 – water height in the room DB1

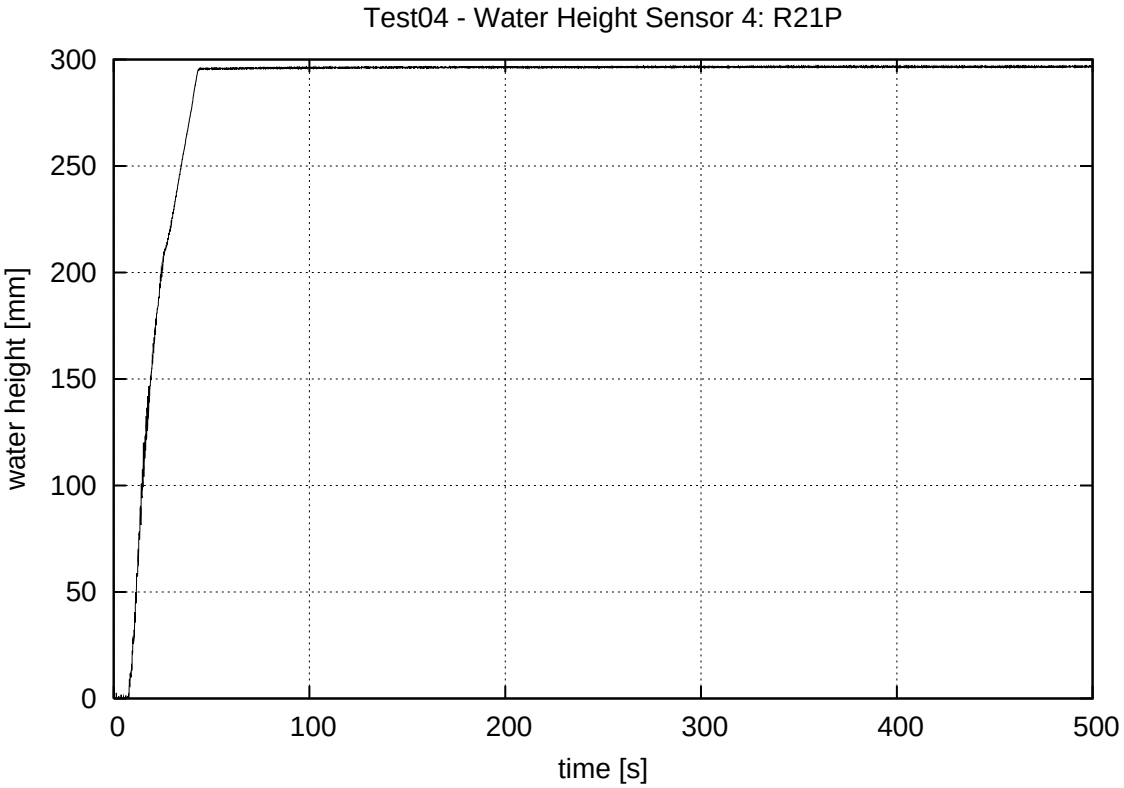

Figure 4.53 Test04 – water height in the room R21P

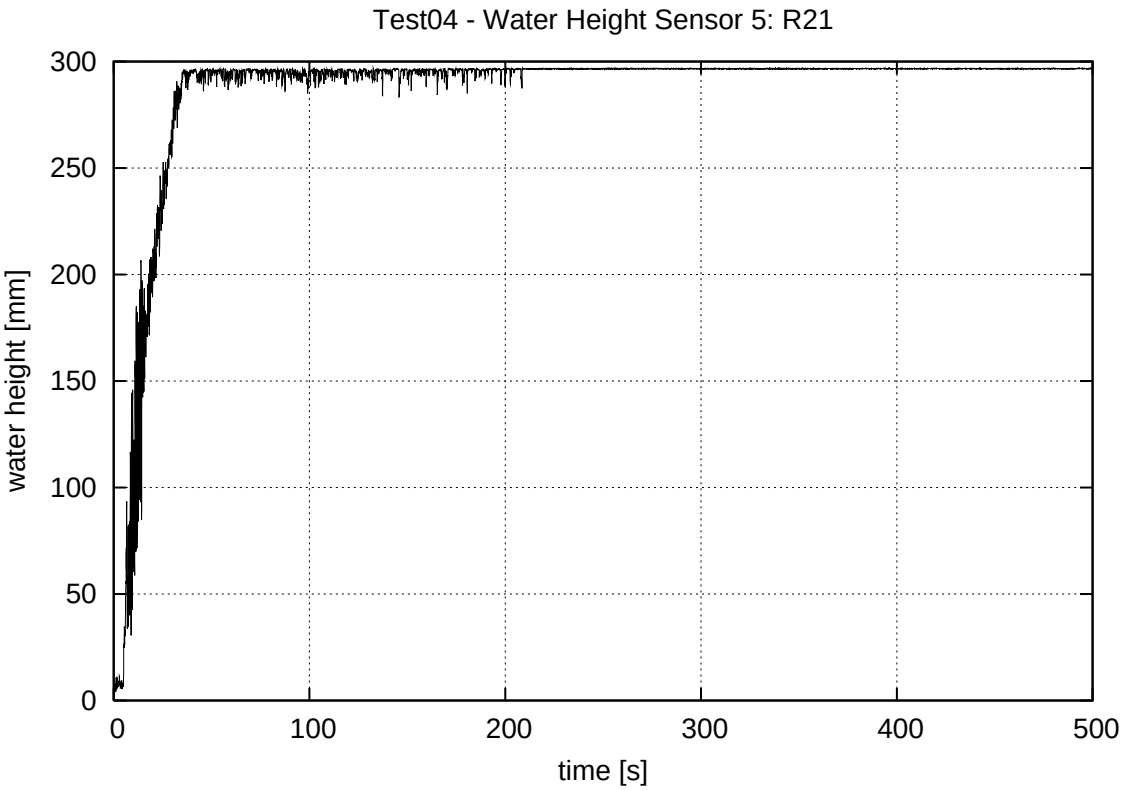

Figure 4.54 Test04 – water height in the room R21

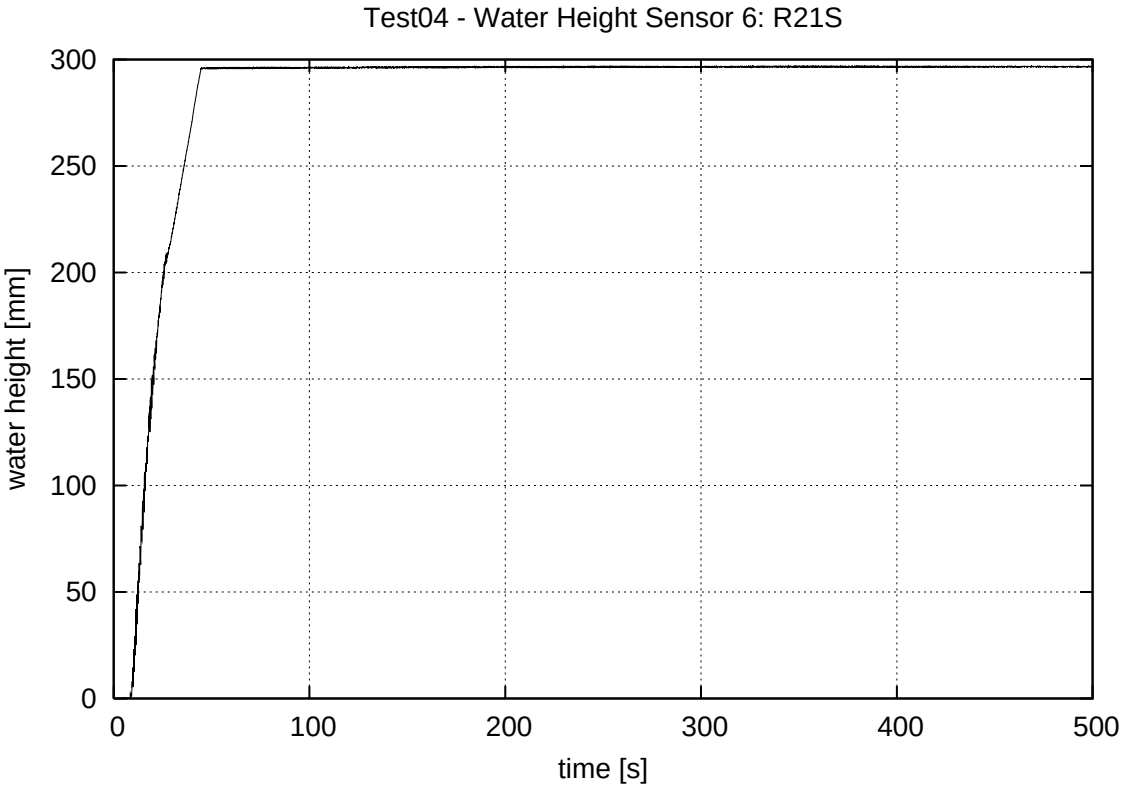

Figure 4.55 Test04 – water height in the room R21S

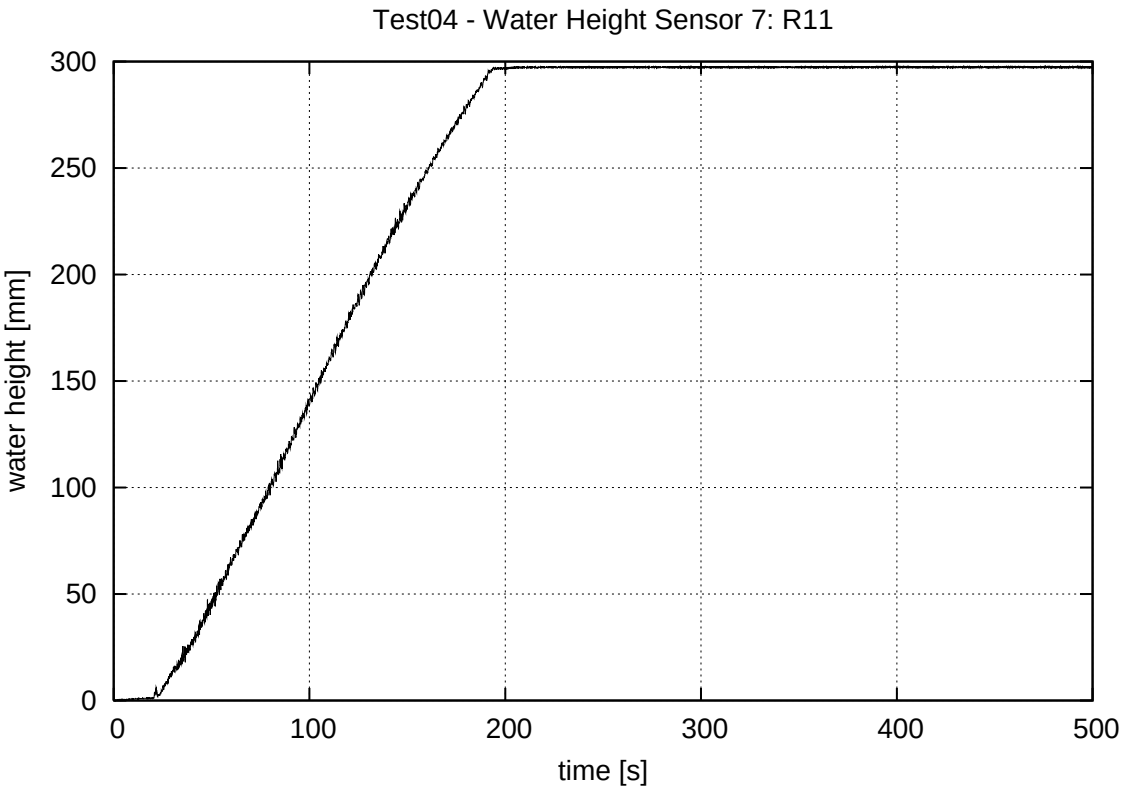

Figure 4.56 Test04 – water height in the room R11

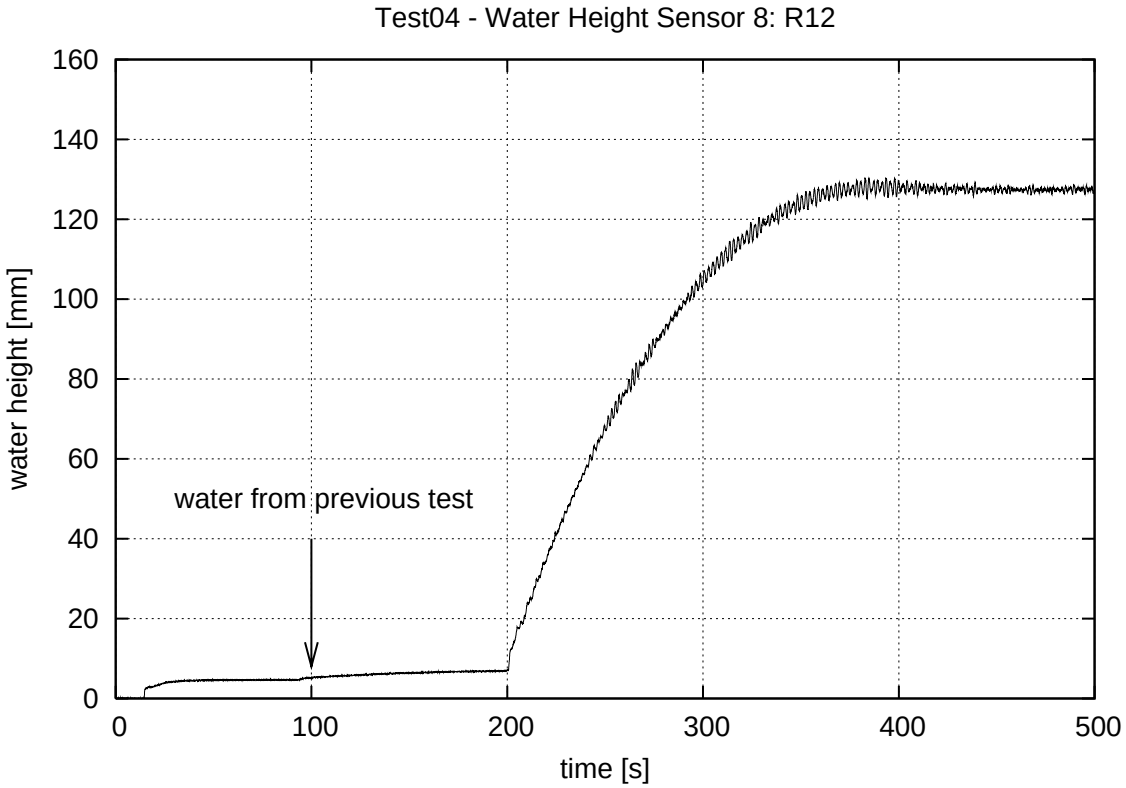

Figure 4.57 Test04 – water height in the room R12

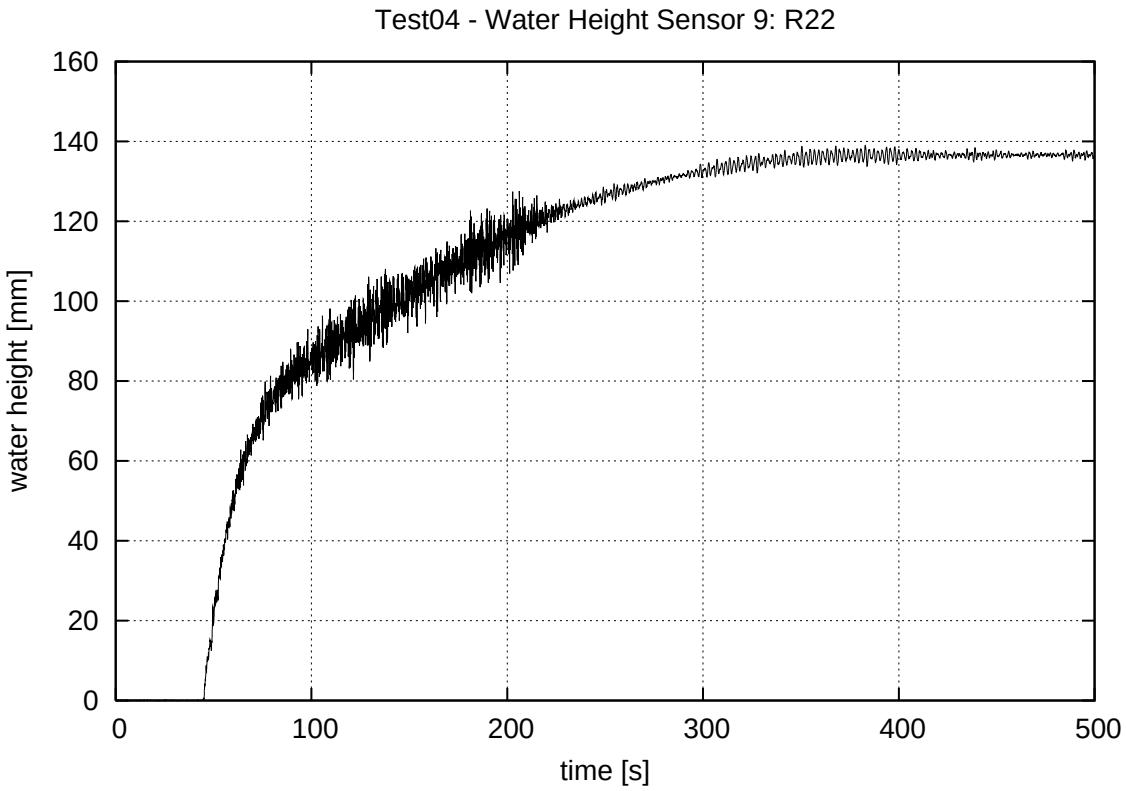

Figure 4.58 Test04 – water height in the room R22

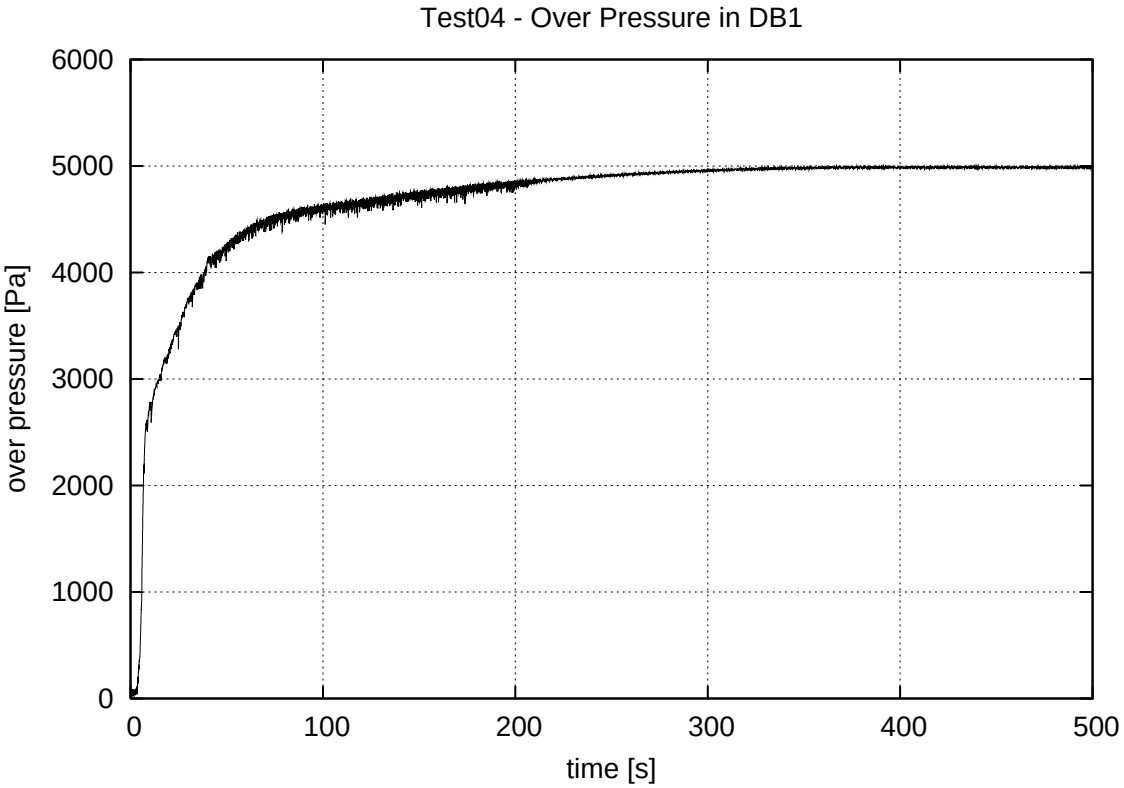

Figure 4.59 Test04 – air pressure in the room DB1

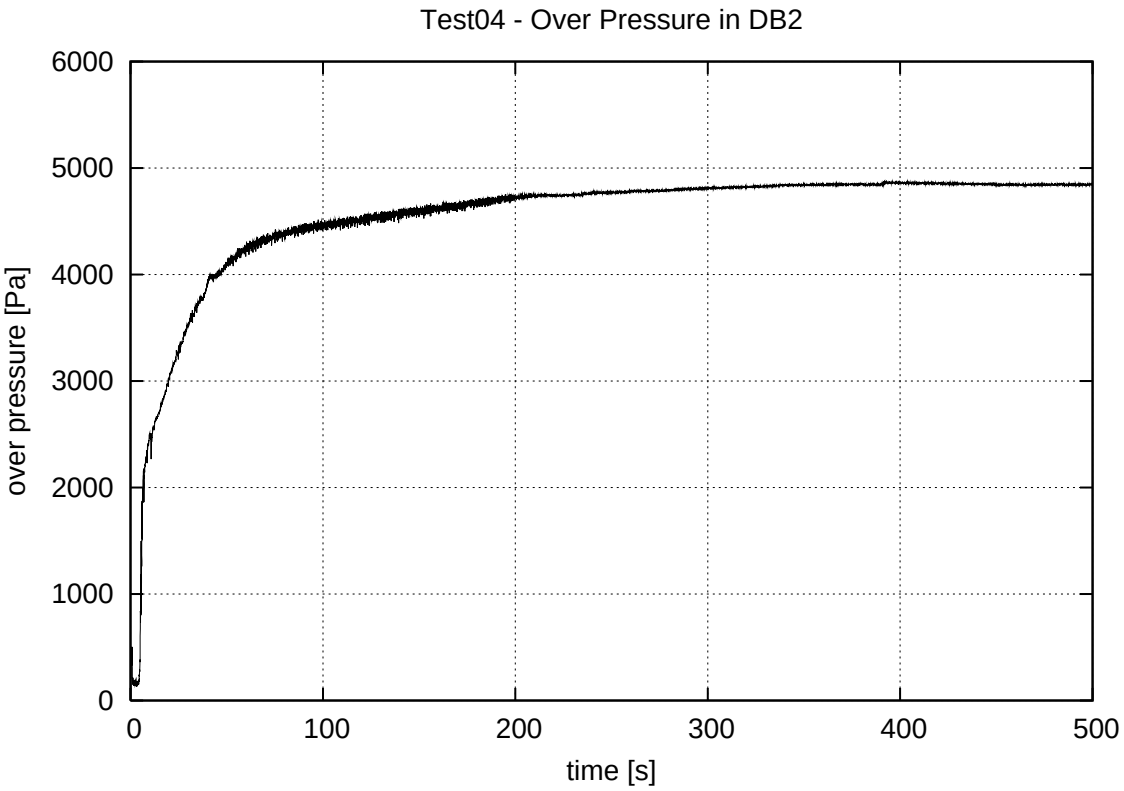

Figure 4.60 Test04 – air pressure in the room DB2

4.2.5 Large Damage in the Aft Compartment (Test05)

The large damage opening (40 mm × 60 mm) is located on the bottom of the aft compartment (DB1). The WT-door on the upper deck is closed.

First, floodwater flows to the forward double bottom compartment (DB2) through the small hole in the transverse bulkhead and then up to the room R21, from where it spreads to the side compartments and back to the aft compartment (R11) through a small hole in the transverse bulkhead. The last room that is flooded is R12 and it is the fifth flooded room in the chain of the flooded compartments from the "sea". The openings in the transverse bulkhead are small and hence the flooding process is very slow.

Some video captures from the start and progress of the flooding are presented in Figure 4.61, Figure 4.62 and Figure 4.63. The final floating position is shown in Figure 4.64.

The damaged room DB1 is flooded almost immediately (Figure 4.70). When the water reaches the top of the opening to DB2, the increase of the water level is stopped since air cannot anymore escape from DB1 and an air pocket is formed. However, the flooding from the "sea" to DB1 is so fast that there are significant waves in DB1 when the water reaches the opening to DB2 (see Figure 4.70). As a result, the water level rises slightly above the top of the opening as air can escape from this compartment when a hollow of a wave is near the opening to DB2. Thereafter, the slow increase in water height is due to the increased sinkage and trim of the model. Also the other double bottom compartment DB2 is flooded rather fast as it is full of water only 40 s after the release of the damage opening (Figure 4.68 and Figure 4.69).

After DB2 is filled up with water, the flooding becomes slower as the water needs to flow through relatively small openings from the "sea" through the double bottom compartments (DB1 and DB2) to the lower deck. The curves of the measured water heights are rather smooth due to the slow flooding that did not cause significant waves in any of the compartments (Figure 4.71 – Figure 4.76).

The air pressure in the damaged room (DB1) rises rapidly during the first seconds of the flooding as the volume of air is decreased due to the rise of the water level (Figure 4.77). The trend changes when water reaches the top of the opening to DB2 and an air pocket is formed in DB1. Similarly to the water height in this room (Figure 4.70), the air pressure is slowly increased as the draft of the model increases.

The air pressure in DB2 starts to rise after 50 s (Figure 4.78). At this time the compartment is already practically full of water (Figure 4.68 and Figure 4.69). The opening between DB2 and R21 (40 mm × 60 mm) apparently ensures sufficient level of ventilation in DB2, at least in this damage case. This means that the measured compression of air occurred only in the pipe to the pressure gauge. No air bubbling was observed in this test.

Figure 4.61 Test05 – start of the flooding

Figure 4.62 Test05 – highly turbulent flooding in DB1 (left) and the start of flooding to DB2 (right)

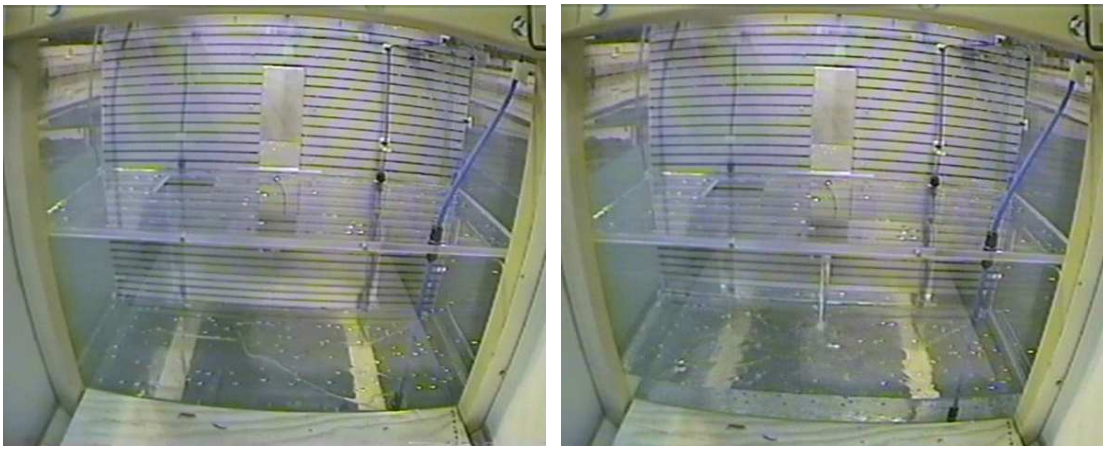

Figure 4.63 Test05 – air pocket in DB1 is visible (left) before the flooding from R21 to R11 (right)

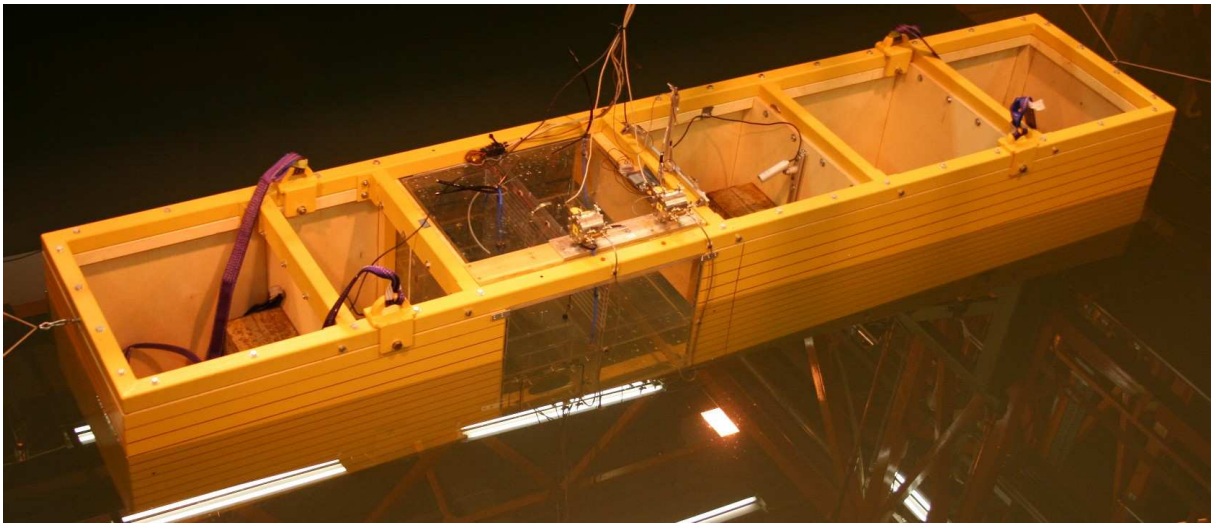

Figure 4.64 Test05 – the final equilibrium floating position after the flooding

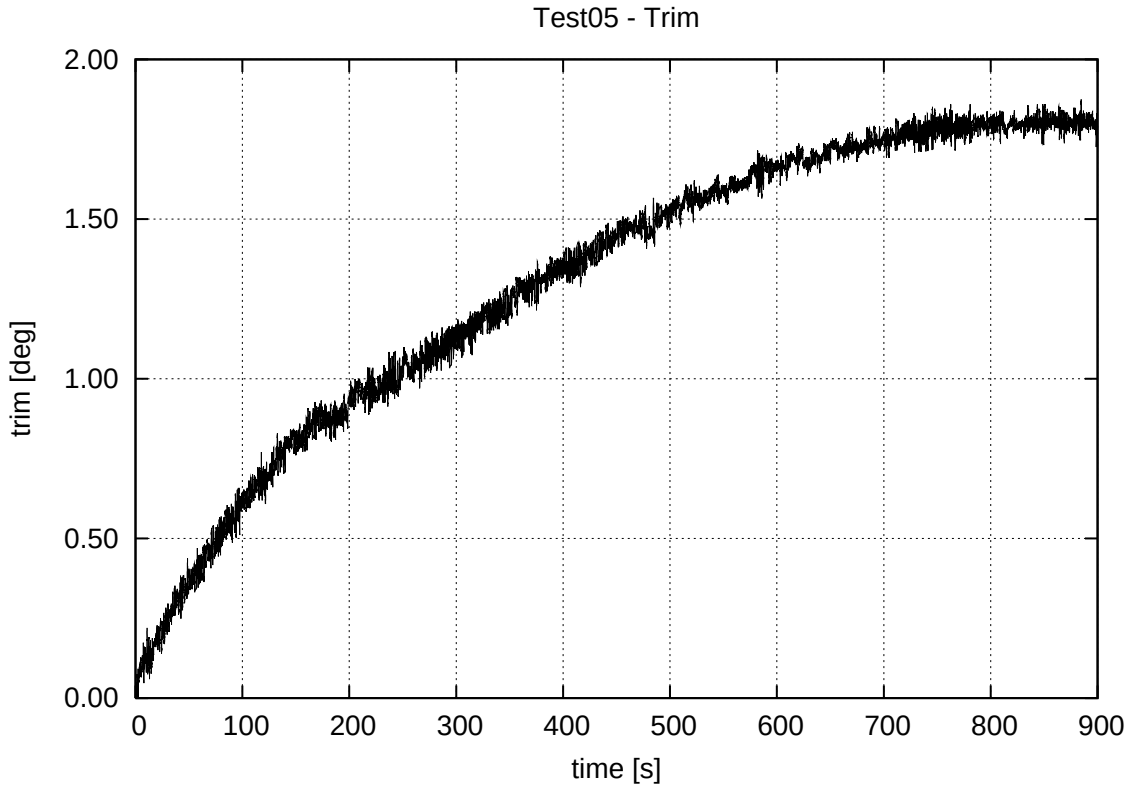

Figure 4.65 Test05 – measured trim angle

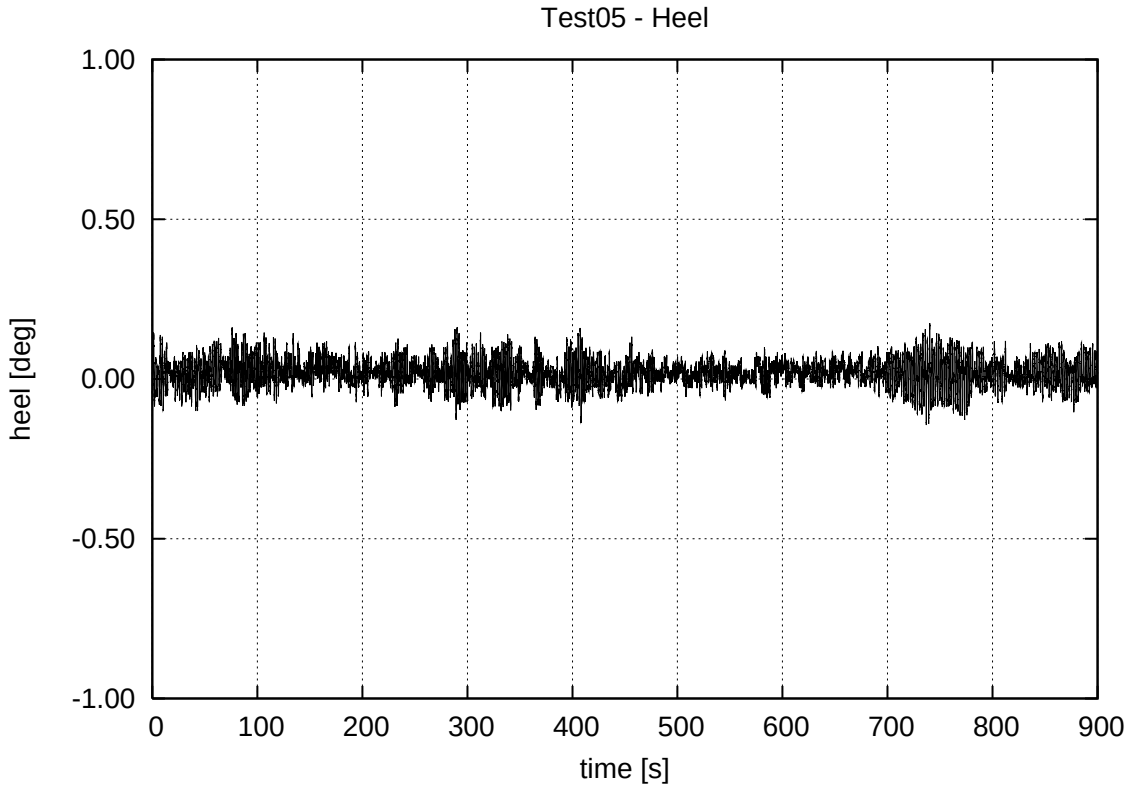

Figure 4.66 Test05 – measured heel angle

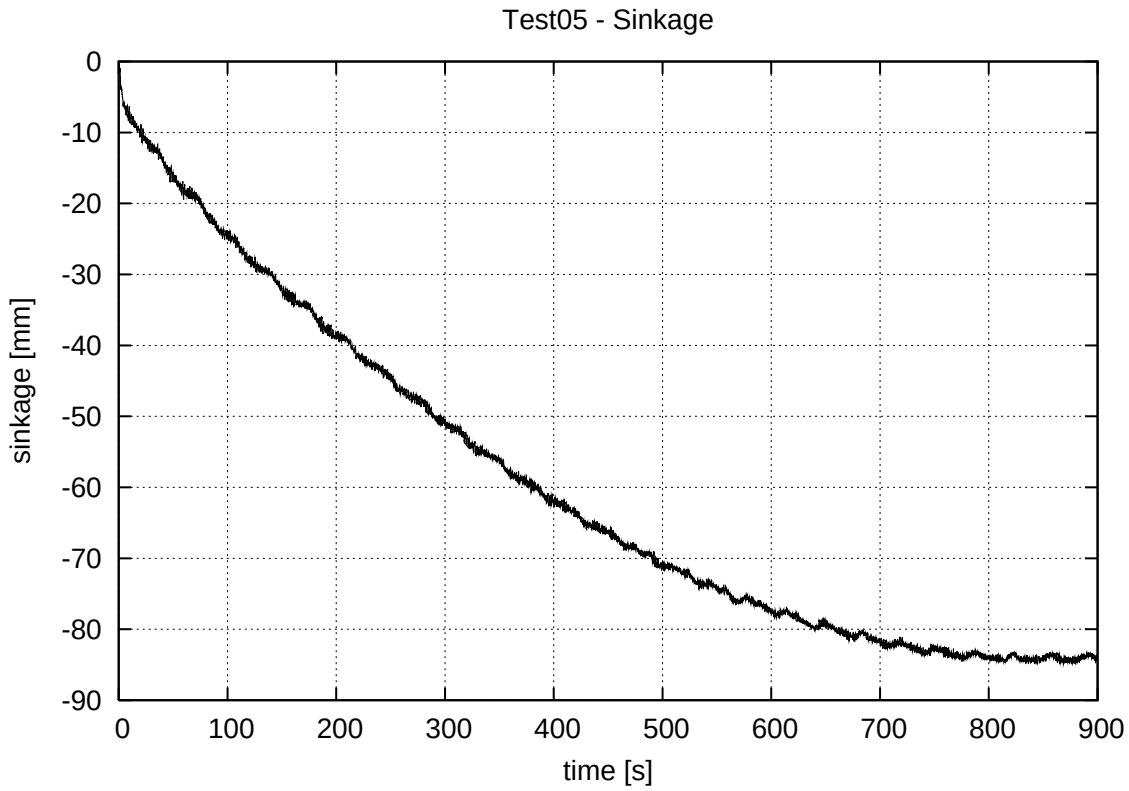

Figure 4.67 Test05 – measured sinkage of the c.o.g.

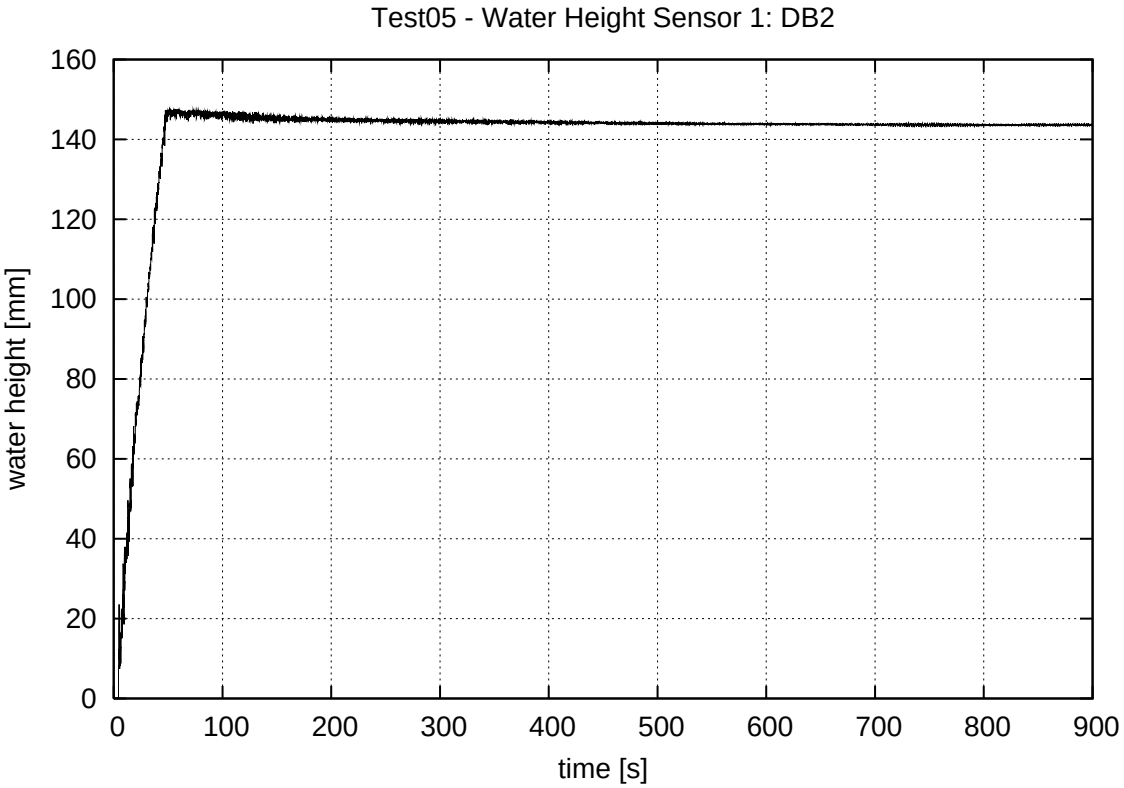

Figure 4.68 Test05 – water height in the room DB2, sensor 1

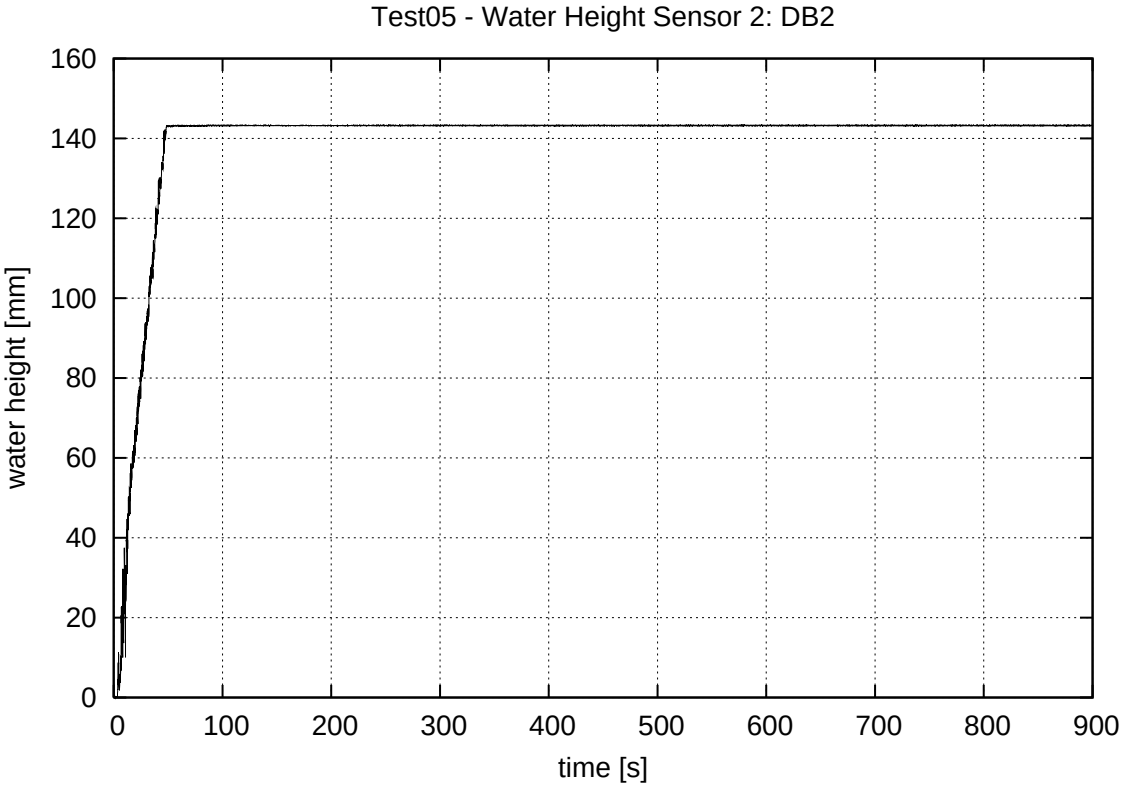

Figure 4.69 Test05 – water height in the room DB2, sensor 2

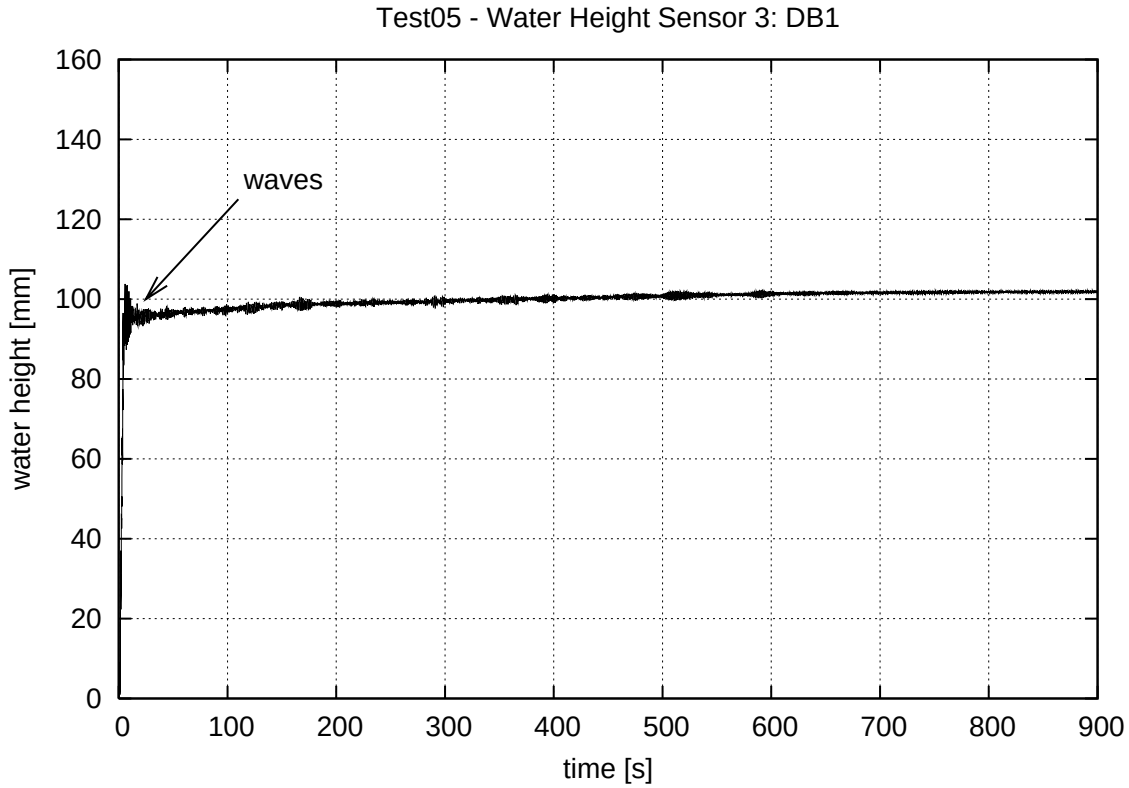

Figure 4.70 Test05 – water height in the room DB1 (damaged room), the arrow points at the relatively high waves when the air pocket is formed

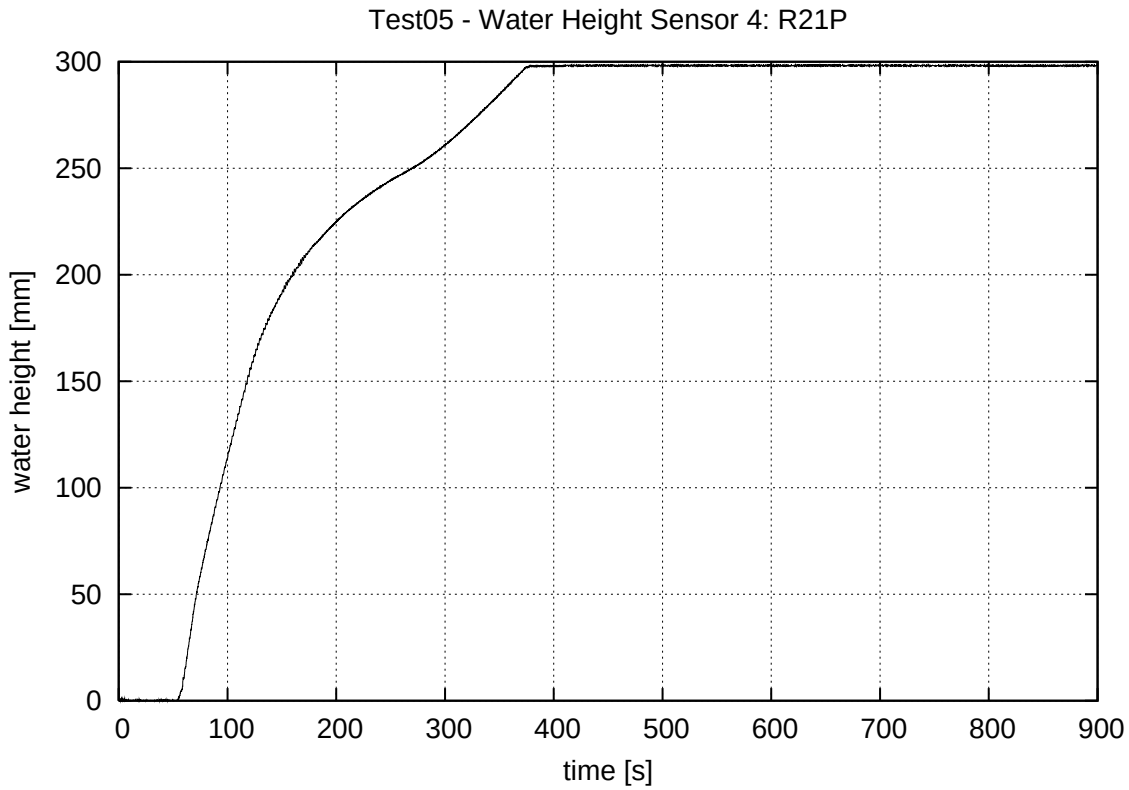

Figure 4.71 Test05 – water height in the room R21P

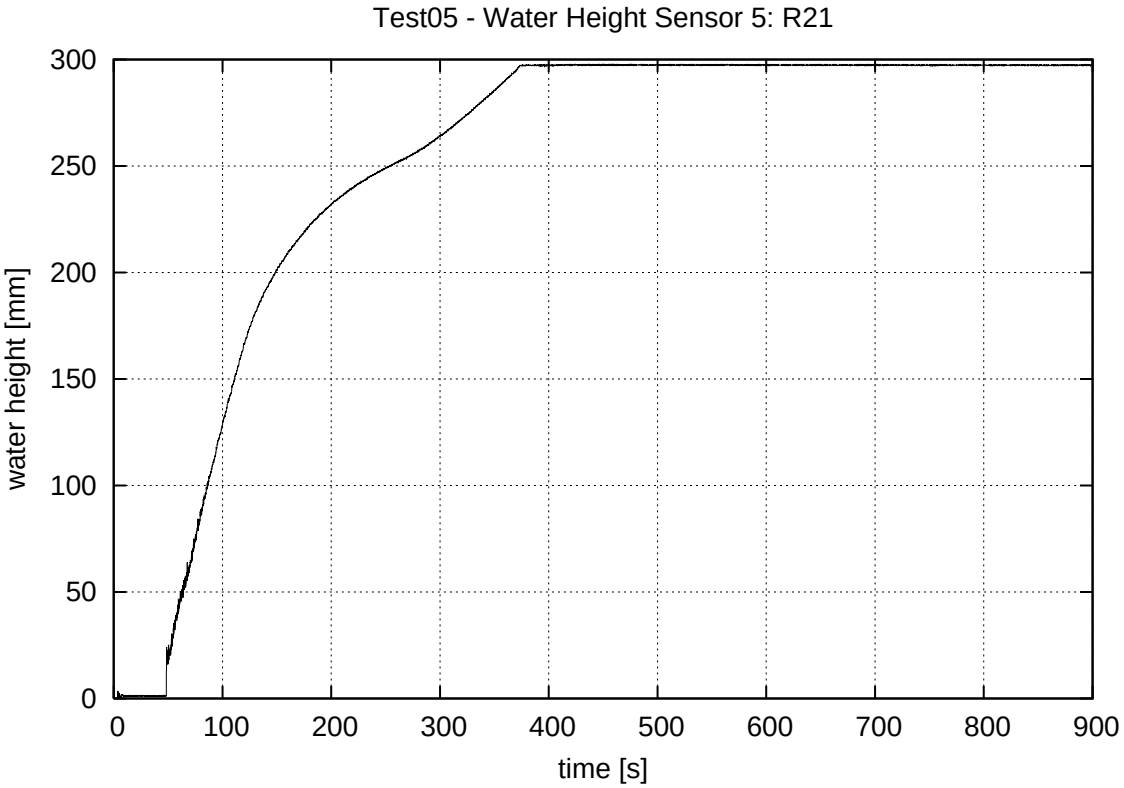

Figure 4.72 Test05 – water height in the room R21

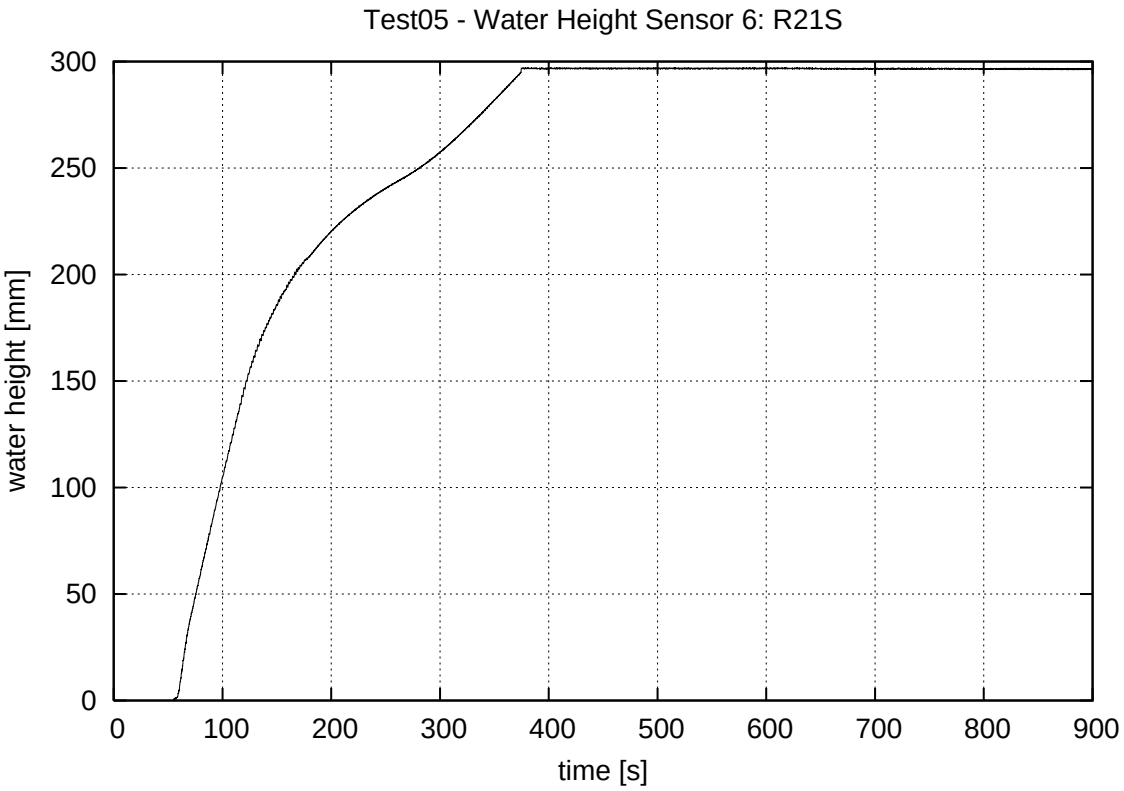

Figure 4.73 Test05 – water height in the room R21S

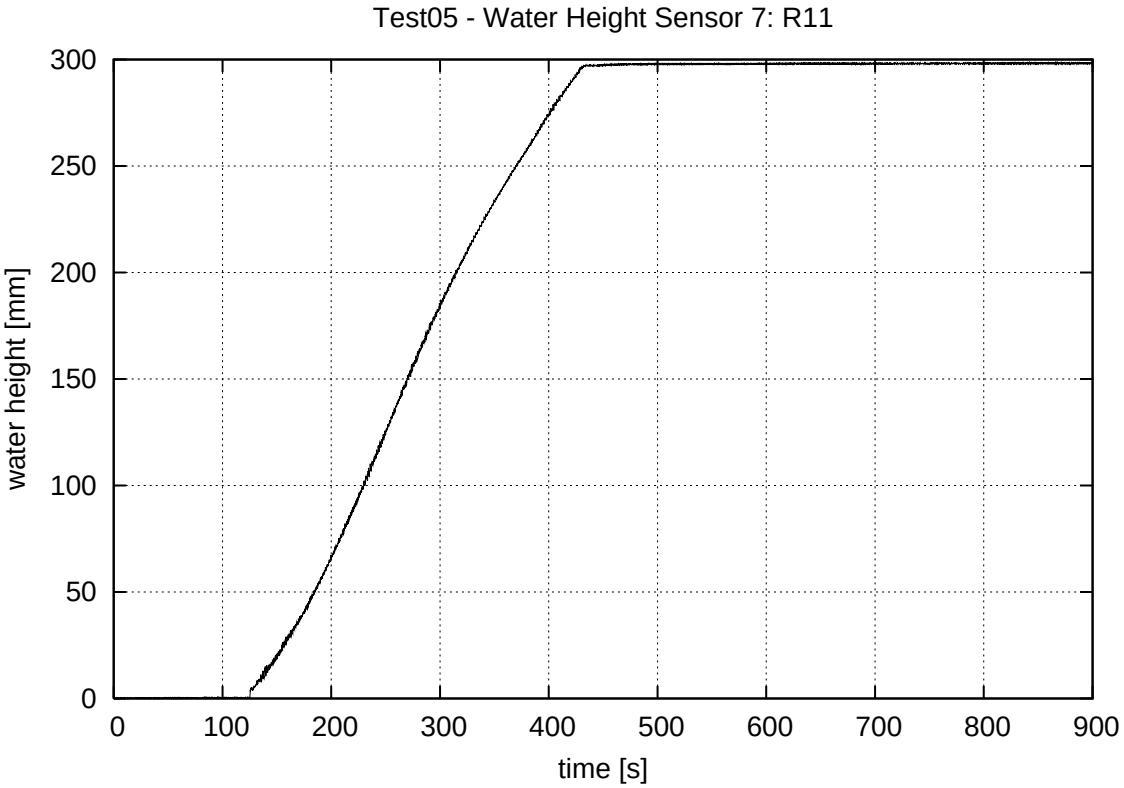

Figure 4.74 Test05 – water height in the room R11

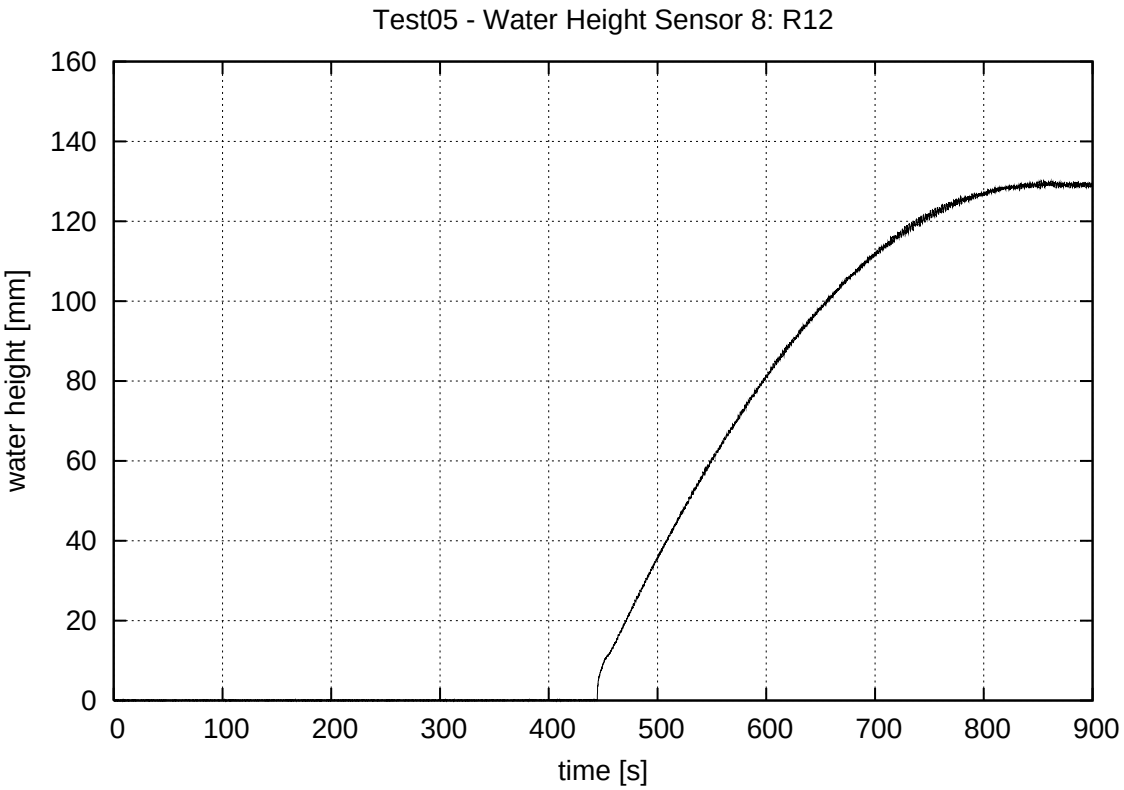

Figure 4.75 Test05 – water height in the room R12

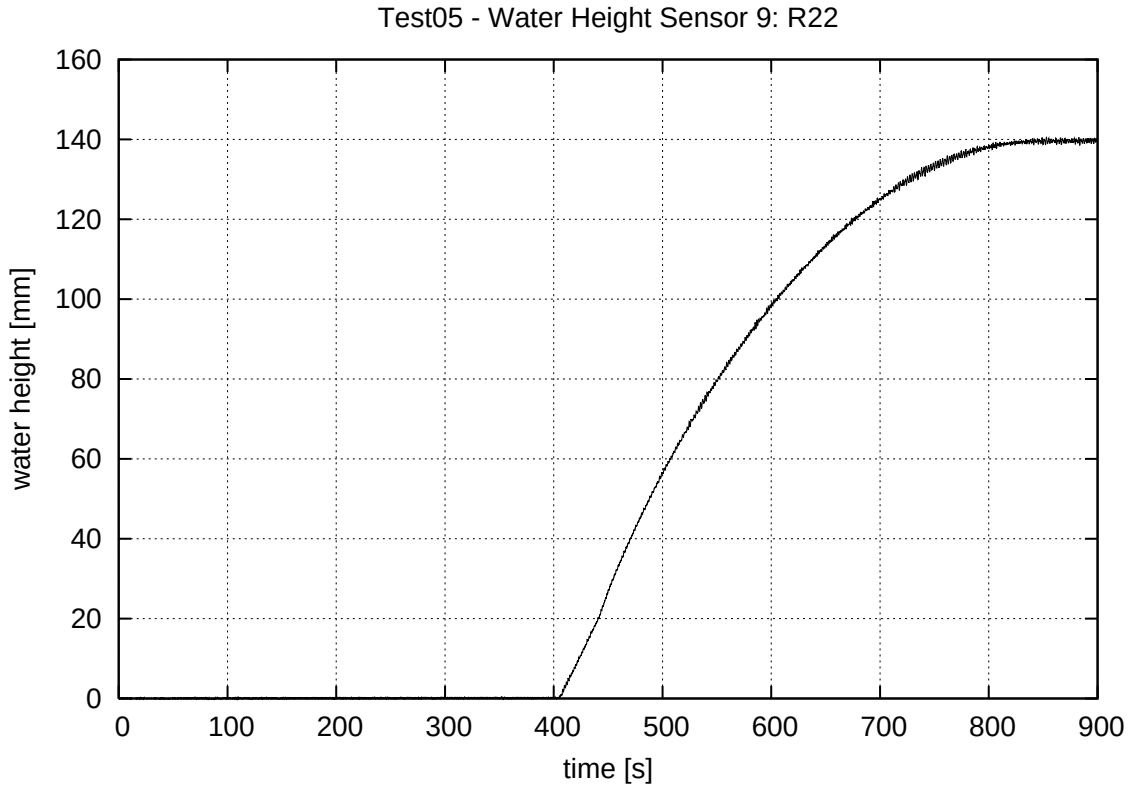

Figure 4.76 Test05 – water height in the room R21

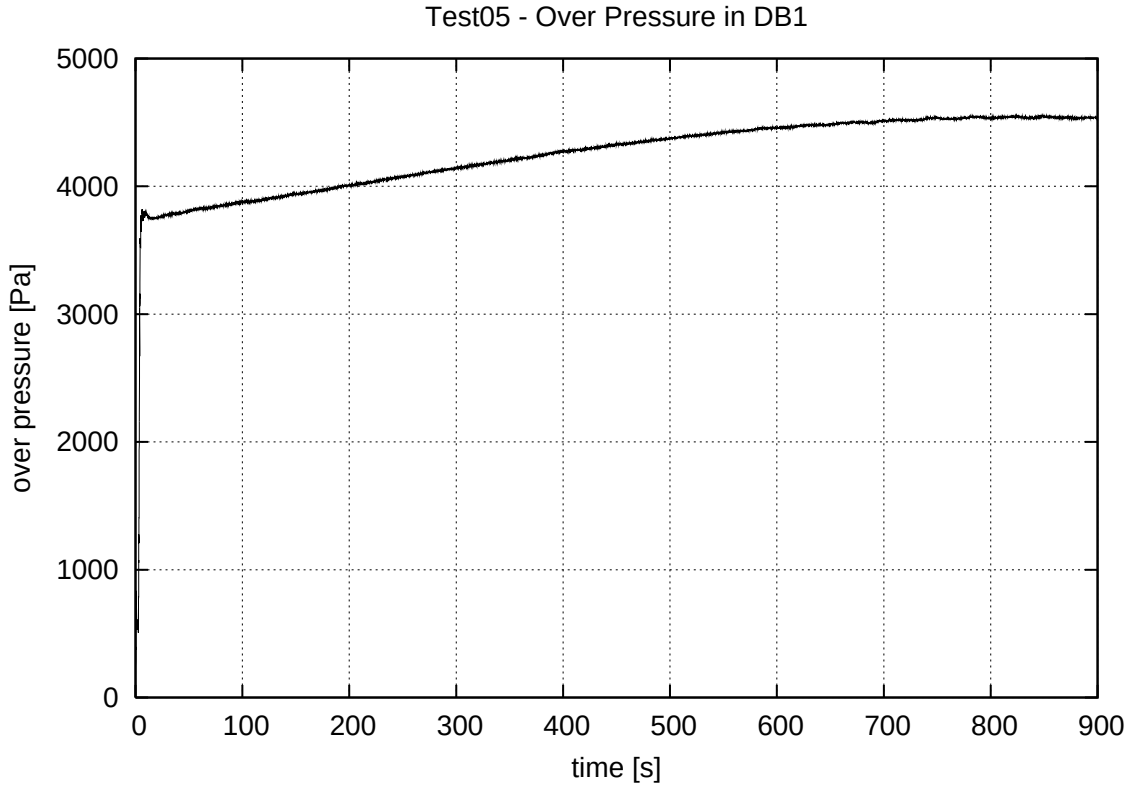

Figure 4.77 Test05 – air pressure in the damaged room DB1

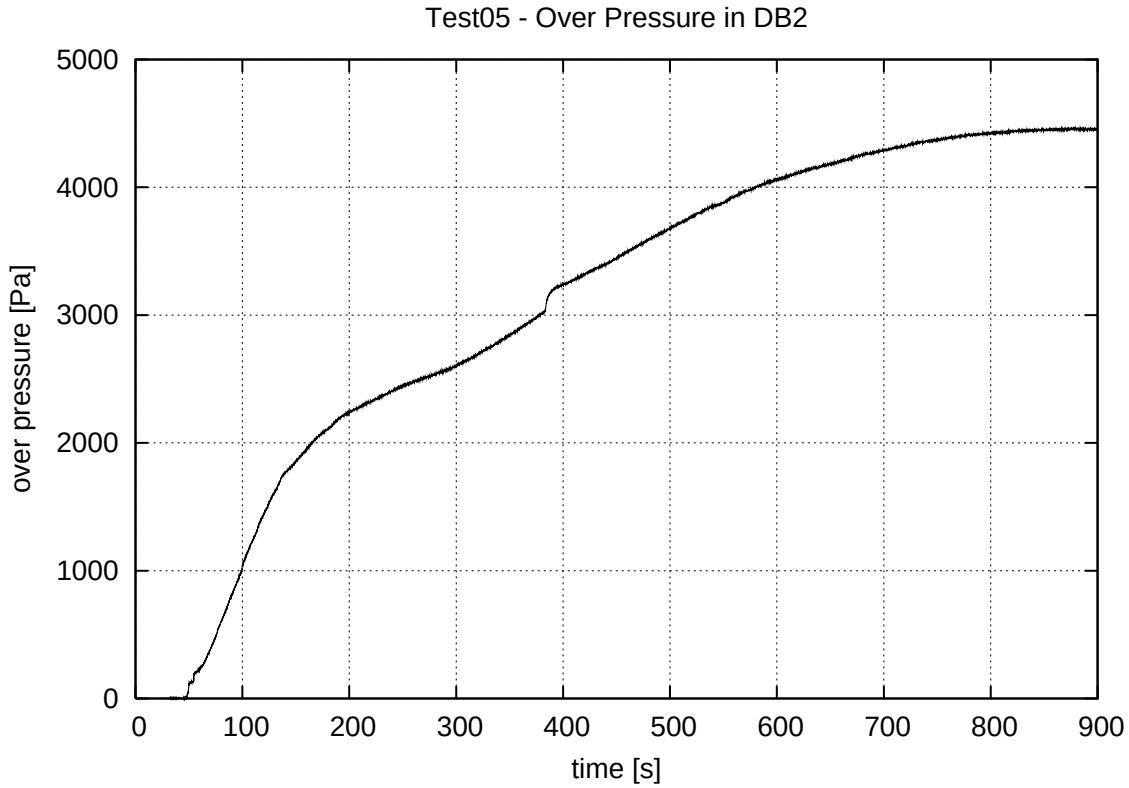

Figure 4.78 Test05 – air pressure in the room DB2

4.3 Side Damage

4.3.1 Large Damage Opening in the Forward Compartment (Test06)

The large damage opening (40 mm × 60 mm) is located on the side of the forward compartment in the room R21S. In the intact condition, the center of the damage opening is 185 mm below the waterline and in the center of the compartment in longitudinal direction.

In this test the down-flooding to the double bottom is prevented by closing the manhole that connects the rooms DB2 and R21 with a tight plate. Also the WT-door on the upper deck is closed with a tight plate.

The floodwater sprays directly from the “sea” to the room R21 through the damaged room R21S, and also further to R21P since the openings between these rooms are in line with the damage opening. Some video captures from this process are presented in Figure 4.79. Furthermore, the sizes of the openings connecting the side compartments (R21S and R21P) to the room R21 are of the same magnitude as the size of the damage opening. Therefore, the flooding process is actually not very asymmetrical in the transverse direction even through the damage opening is located on the side of the model. Therefore, the model does not heel significantly during the flooding. During the first 40 s the model rolls slightly with an

amplitude of just 0.7° and the average is approximately 0.0° (Figure 4.82). Thereafter, the roll amplitude is smaller.

Due to the large internal openings in the longitudinal bulkheads, there is no significant difference between the water levels in R21P, R21 and R21S during the flooding (Figure 4.84, Figure 4.85 and Figure 4.86, respectively). However, R21 is filled up 24 s after the damage opening is released, while the side compartments are filled up approximately 8 s later (Figure 4.80). These compartments are ventilated through relatively small pipes (inner diameter is 7 mm) while R21 is ventilated through a large opening (100 mm × 100 mm) to the upper deck. So when the water level reaches the opening to R21, air is probably compressed in these rooms. Unfortunately, air pressure was not measured in either of these rooms, so this hypothesis cannot be verified directly. However, the delayed increase of the water heights in the side compartments is a good indicator of air compression in those rooms.

Figure 4.79 Test06 – video captures from the early stages of the flooding; the plate that closes the manhole to the double bottom is clearly visible

Figure 4.80 Test06 – the free surfaces are parallel when the damage opening is fully submerged (left) and the side compartment R21P is not yet filled when the up-flooding to R22 starts (right)

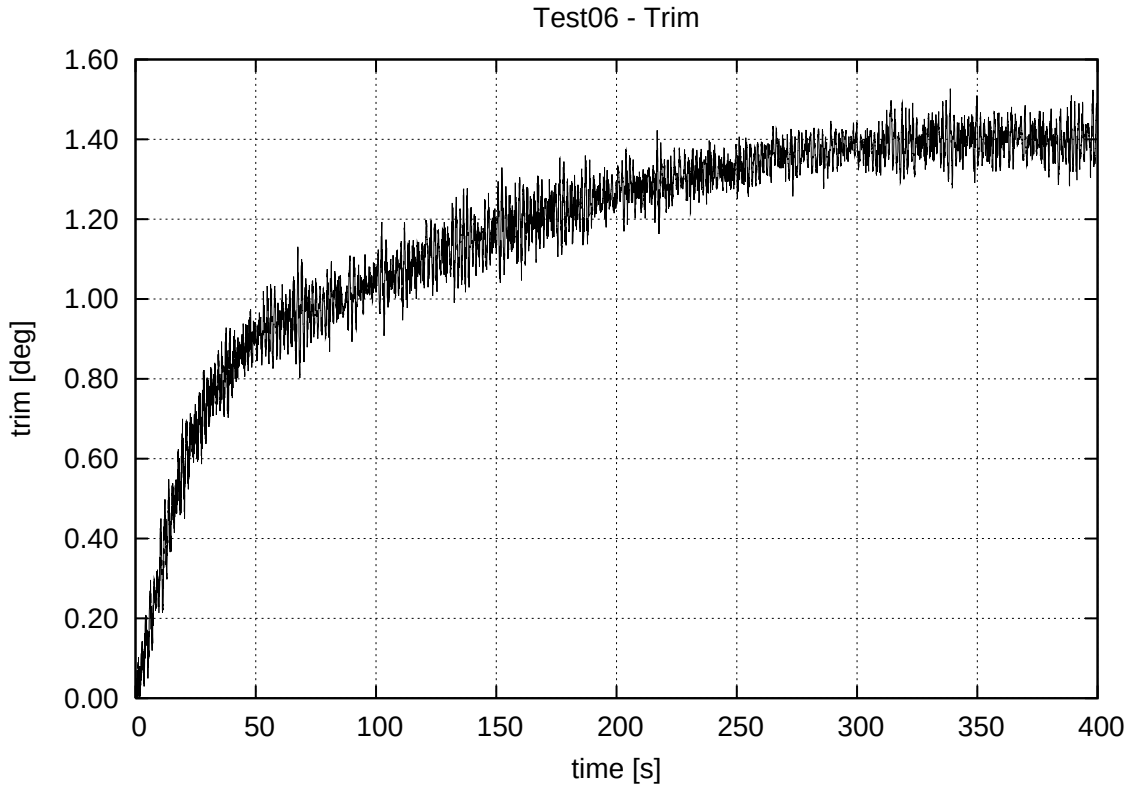

Figure 4.81 Test06 – measured trim angle

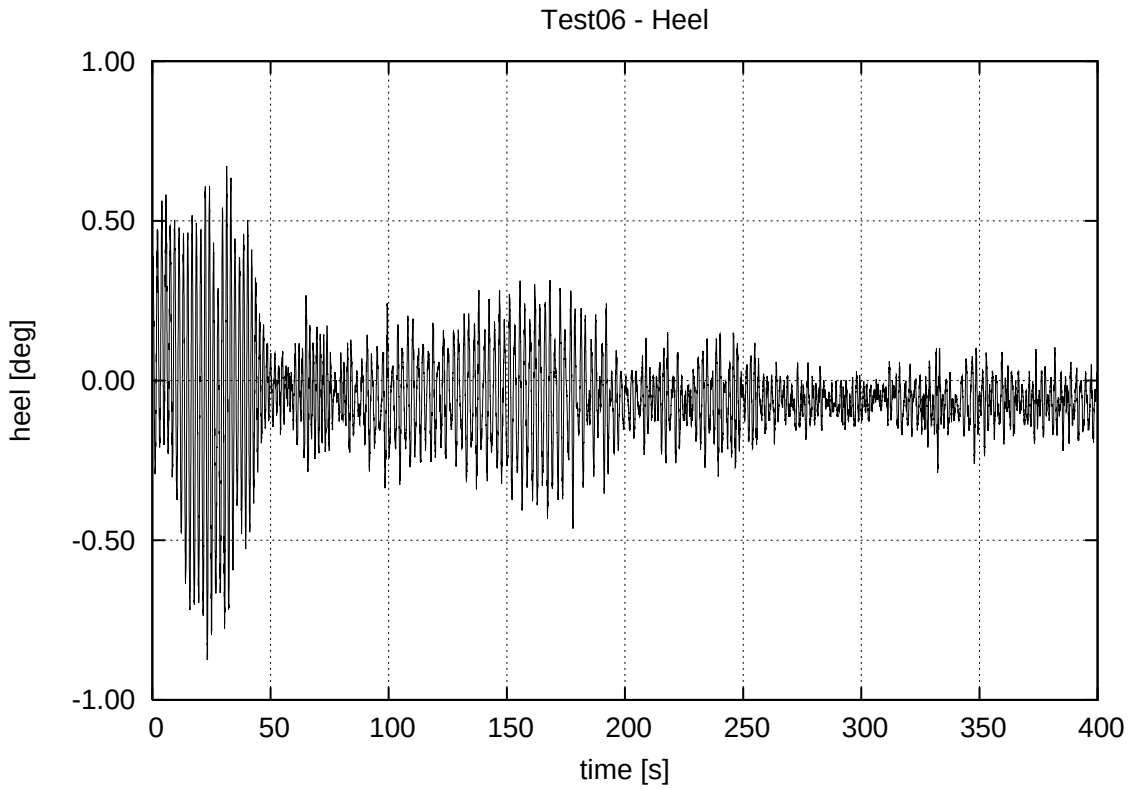

Figure 4.82 Test06 – measured heel angle

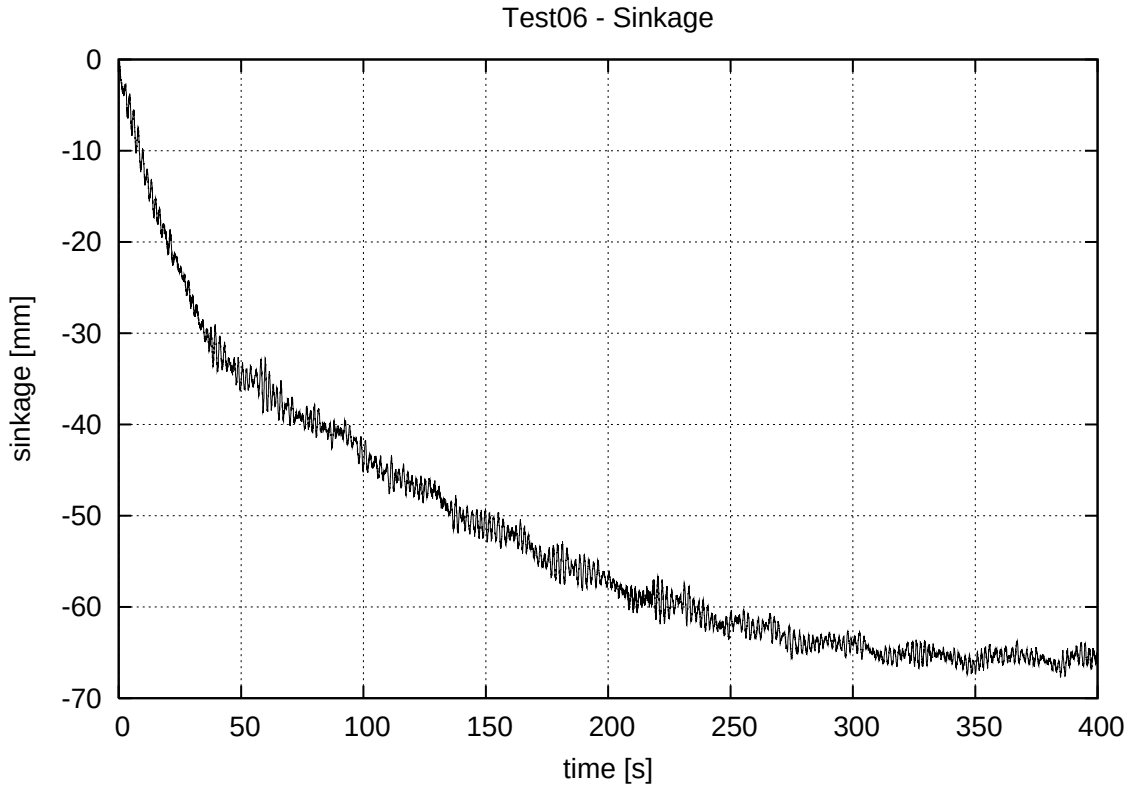

Figure 4.83 Test06 – measured sinkage of the c.o.g.

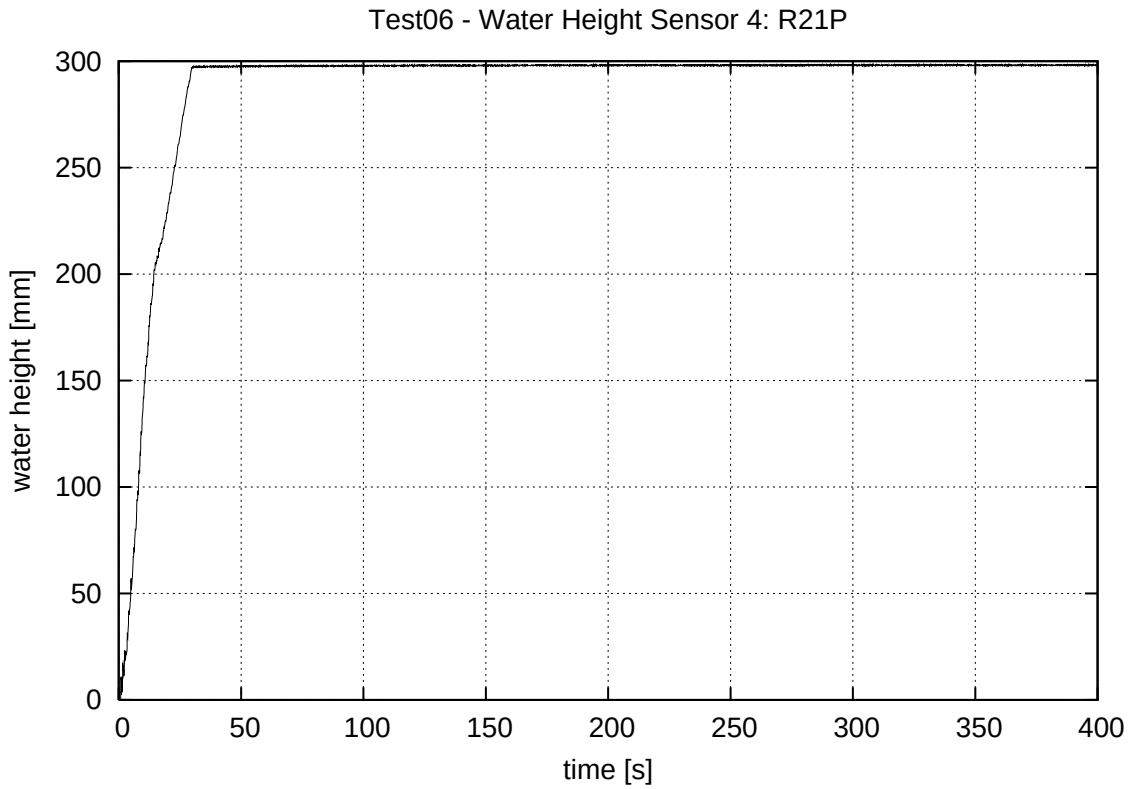

Figure 4.84 Test06 – water height in the room R21P

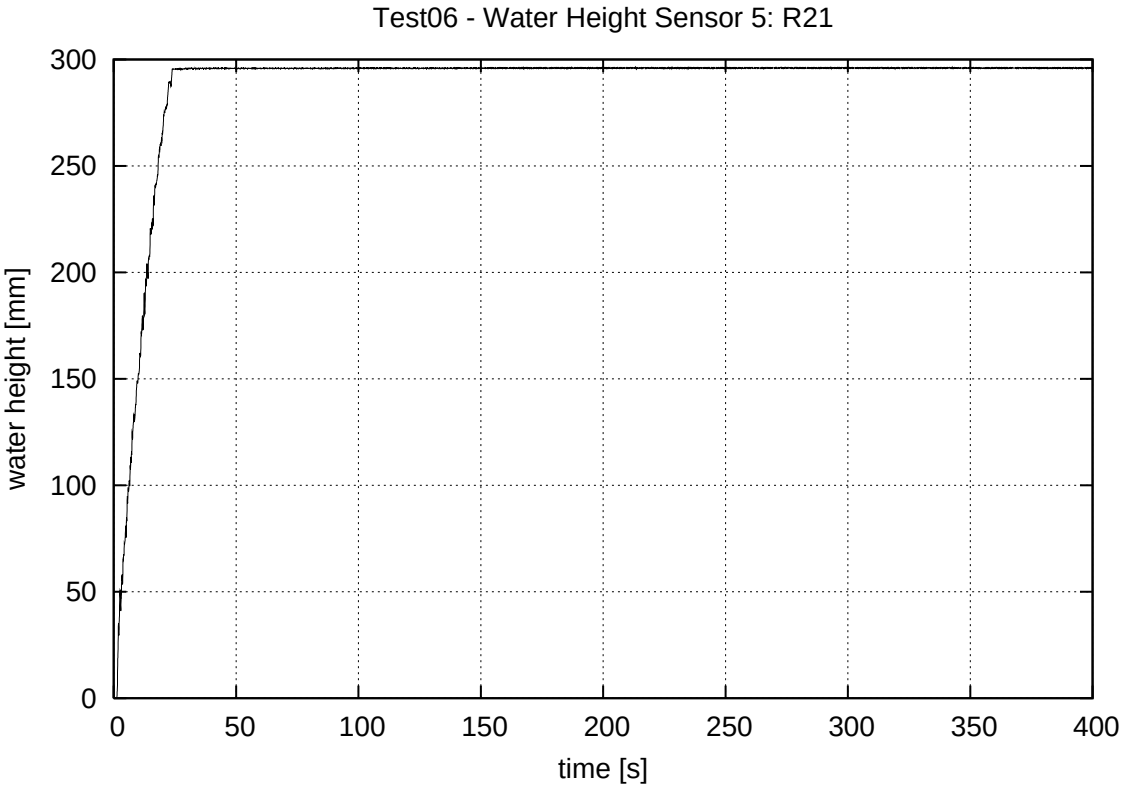

Figure 4.85 Test06 – water height in the room R21

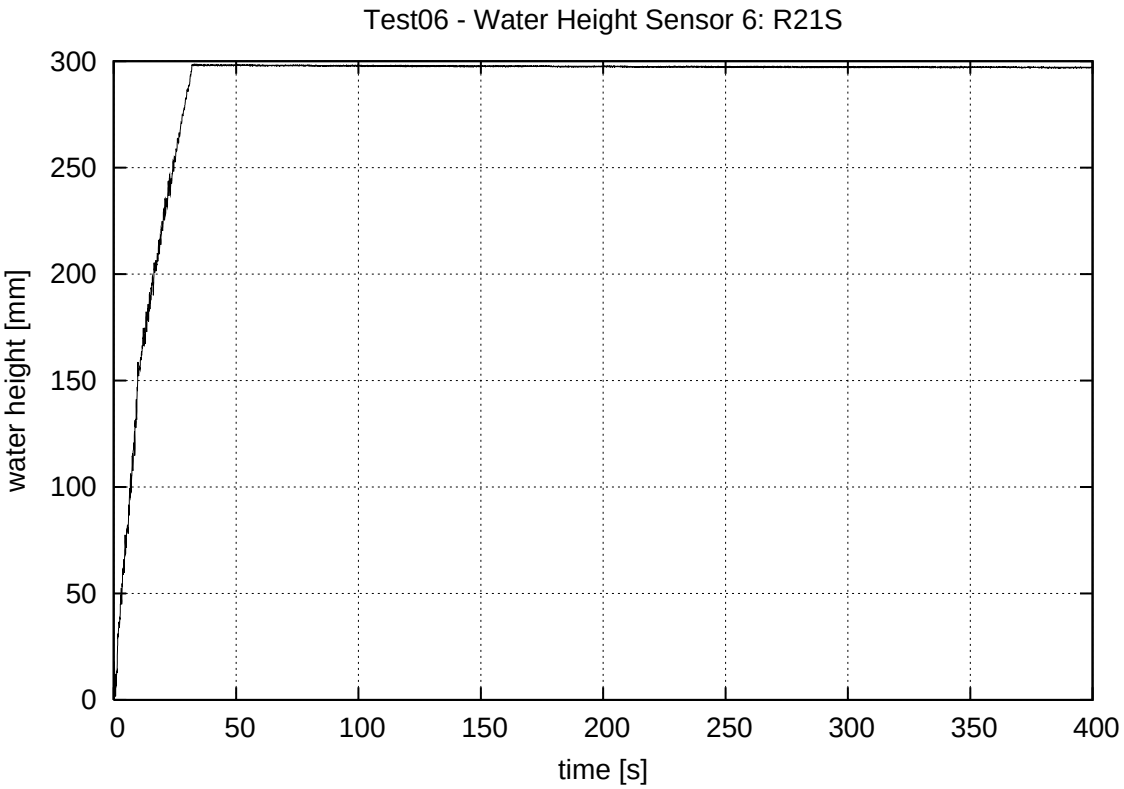

Figure 4.86 Test06 – water height in the damaged room R21S

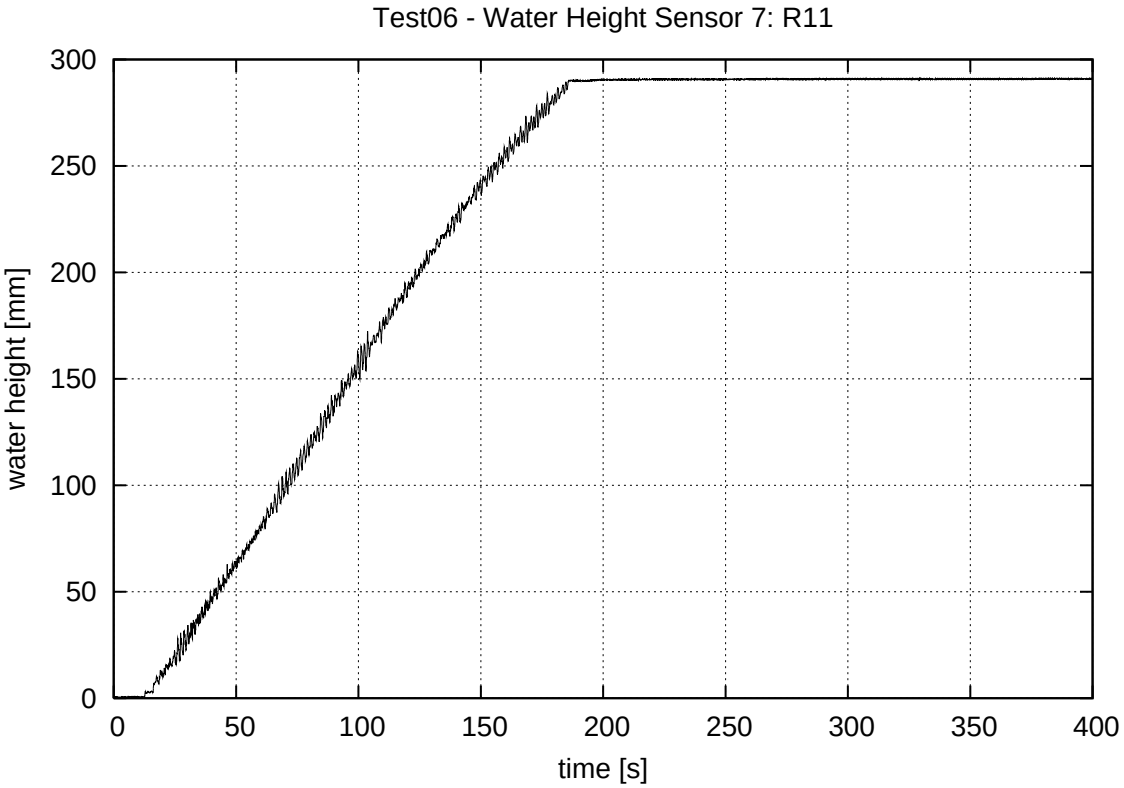

Figure 4.87 Test06 – water height in the room R11

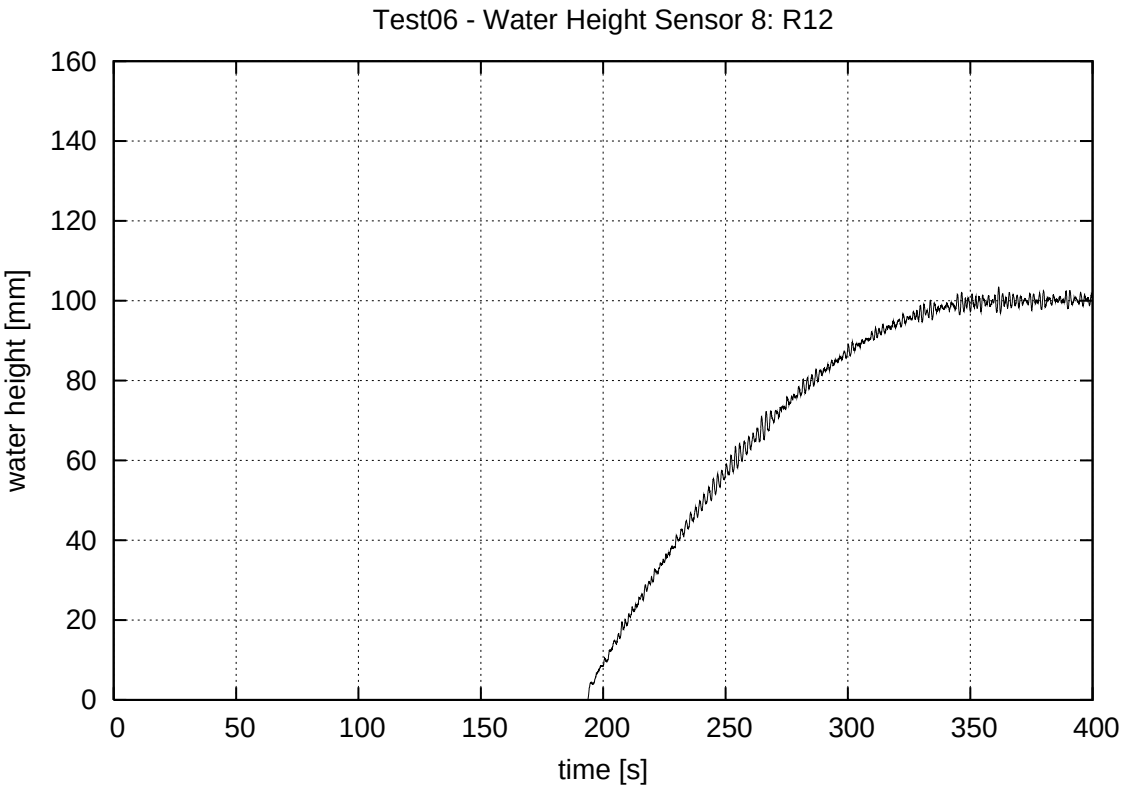

Figure 4.88 Test06 – water height in the room R21

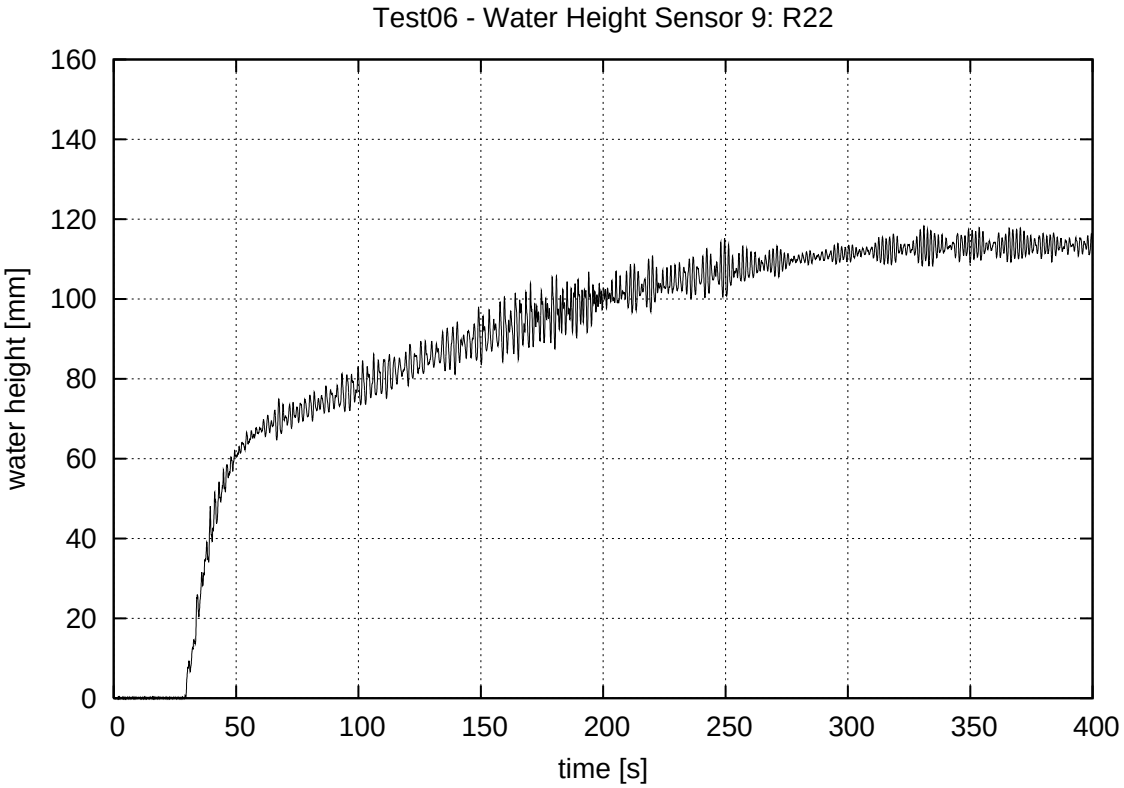

Figure 4.89 Test06 – water height in the room R22

4.4 Summary of the Results

The results of the performed tests are summarized in terms of the time-to-flood. The results are compared in order to assess the effects of the floating position and the damage size and location. The time-to-flood (TTF) and the final floating position (trim and sinkage) for the tests are listed in Table 4.2.

Table 4.2 Time-to-flood (TTF) and final floating position for all performed tests

	TTF [s]	Trim [°]	Sinkage [mm]
Test01	435	0.00	0.00
Test02	515	1.77	81.0
Test03	440	1.76	81.2
Test04	380	1.75	80.5
Test05	860	1.80	83.9
Test06	390	1.40	65.5

Floating position

The time-to-flood is 80 s (18 %) longer for the freely floating model (Test02) than for the fixed model (Test01). The damage size and location are the same but when the draft and trim are increased due to the floodwater, more water can flood in. As a result, the time-to-flood is longer and the total volume of flooded water is larger.

Damage size

The area of the large damage hole is 3.84-times larger than the area of the small damage hole. Larger damage size means shorter time-to-flood. With the small damage hole (25 mm × 25 mm) the TTF is 515 s (Test02) and with the large damage hole (60 mm × 40 mm) the TTF is only 380 s (Test04), i.e. 26 % shorter.

Damage location

In Test04 the large damage opening was located in the bottom of the forward compartment (DB2) and in Test05 in the bottom of the aft compartment (DB1). In the latter case the time-to-flood is 480 s (i.e. 126 %) longer. This is due to the longer chain of flooded compartments. Especially the opening between the double bottom compartments (DB1 and DB2) is so small that the flooding process becomes much slower. Apparently the air pocket in DB1 is smaller when this compartment is damaged (Test05) since both the trim angle and the vertical sinkage are larger than in Test04. This is reasonable, since in Test05 the double bottom DB1 is flooded much faster and the waves inside the compartment allow more air to escape from the air pocket (see section 4.2.5).

WT-door on the upper deck

The time-to-flood is 75 s (i.e. 15 %) shorter when the WT-door on the upper deck is open (Test03) since the aft compartment is flooded faster due to the additional opening in the transverse bulkhead. The equilibrium floating position is practically the same as in Test02 and Test03. This is how it should be since the status of the door (open/closed) should not affect the final volume of flooded water

Air Pockets.

In all the tests, where the double bottom was flooded (Test01 – Test05), an air pocket was formed in the aft compartment (DB2). On the other hand, the forward double bottom compartment (DB2) was practically filled up with water and the measured air compression took place only in the pipe to the pressure gauge.

In the testes, where the damage was located in DB2 (Test01 – Test04), air escaped in a bubble flow from the air pocket in DB1 through DB2 and R21 to the atmosphere. This bubbling was stopped when the water level in DB1 had risen to the top of the opening to DB2.

There is a sudden increase in the pressure of the air pocket when the compartment R21 is filled up with water. This might be partly explained by the increased resistance for the air bubble flow. However, in Test05 a similar pressure increase takes place in the pipe from DB2 to the pressure gauge. In this test, no air bubbling was observed. Therefore, it is possible that there is also a sudden increase in the hydrostatic pressure in DB2 when R21 is filled up, and the observed sudden pressure increase in the air pocket results from this.

5 Roll Decaying Tests in Damaged Condition

Roll decaying tests were performed after the Test03, Test05 and Test06. The results are compared to the roll decaying test in intact condition (see section 3.3) in Figure 5.1, Figure 5.2 and Figure 5.3, respectively.

The natural frequency ω_ϕ and the natural period T_ϕ of the roll motion and the critical damping ratio ξ are listed in Table 5.1 for the tested damage cases and for the intact condition. In the damaged condition, the model has a larger critical damping ratio and the natural period of roll motion is longer.

Table 5.1 Natural roll period and damping ratio after the tested damage cases

Case	Damage description	ω_ϕ [rad/s]	T_ϕ [s]	ξ [-]
Intact	-	3.25	1.93	0.019
Test03	Small bottom dam. comp 2	2.94	2.14	0.023
Test05	Large bottom dam. comp 1	2.95	2.13	0.023
Test06	Large side dam. comp 2	2.84	2.21	0.023

The natural period of roll motion is slightly longer for the flooded model. In Test06 the period is longer than in the other damage cases. In this case the double bottom compartments (DB1 and DB2) were not flooded. Therefore, the center of gravity for the floodwater inside the model is higher than in the tests, where also the double bottom was flooded. As a result, the initial metacentric height of the flooded model is smaller and the model is not as stable as it is after the other flooding tests. The natural period of roll motion is inversely proportional to the square root of the initial metacentric height (see e.g. *Matusiak, 1996*). Hence, the period is longer for the case, where the center of gravity is higher.

The critical roll damping ratio is 21 % larger for the flooded model. The damage case does not seem to affect this as the ratio is the same even if the double bottom is not flooded (Test06).

There is no notable difference in the natural period and critical damping ratio between Test03 and Test05. So it seems that the size and location of the damage opening does not have a major effect on the roll decaying in damaged condition. Therefore, it can be concluded that there is no significant ingress or egress of the floodwater as the ship rolls with small amplitude.

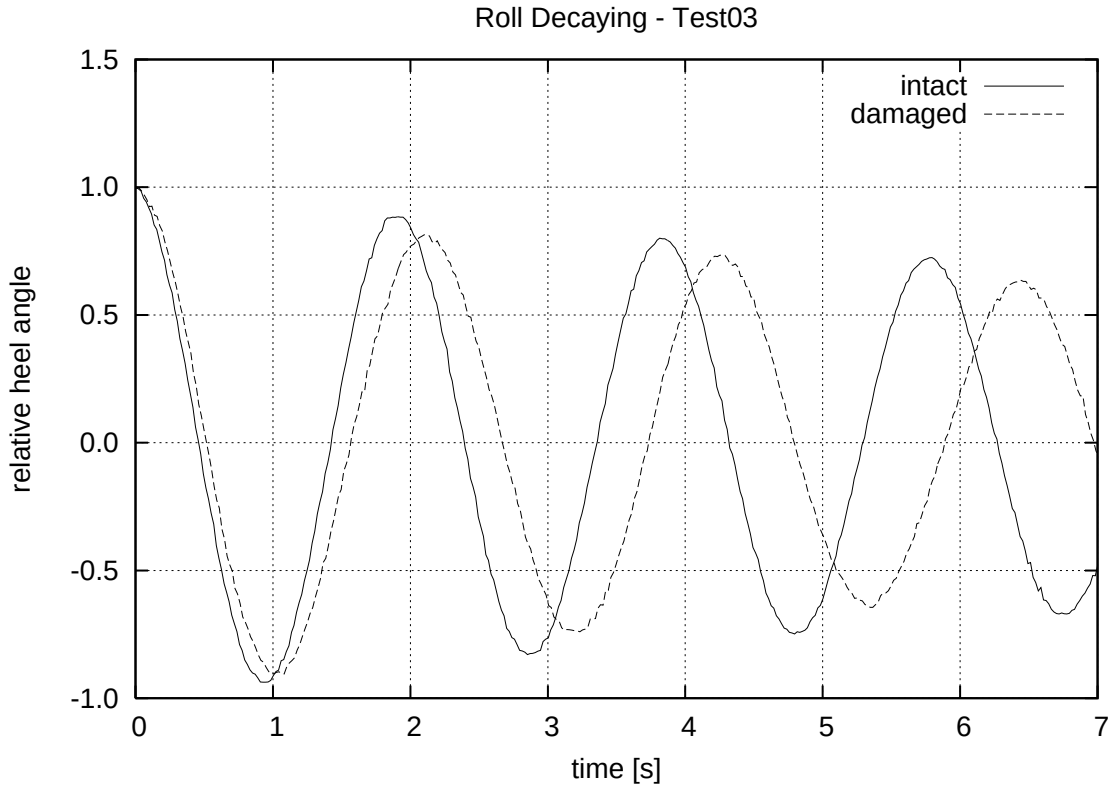

Figure 5.1 Roll decaying after damage (Test03) and in intact condition (initial heel angle was 2.8° in the damaged condition and 2.8° in intact condition)

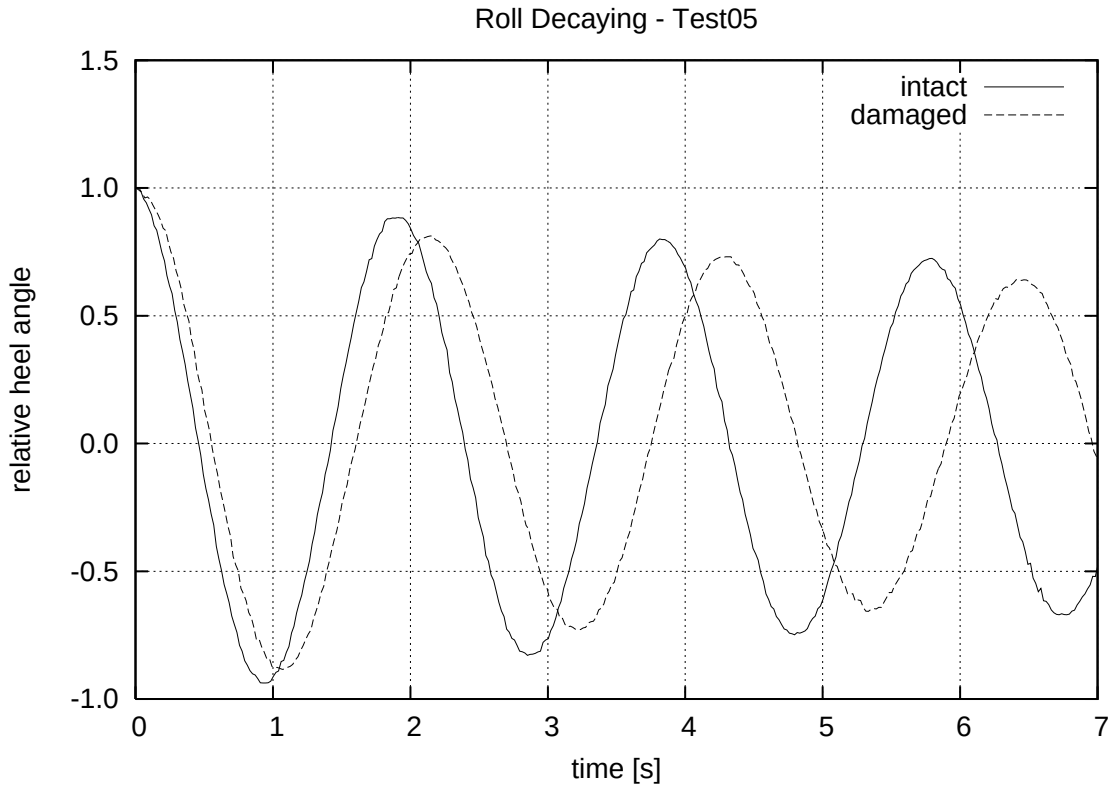

Figure 5.2 Roll decaying after damage (Test05) and in intact condition (initial heel angle was 3.2° in damaged and intact conditions)

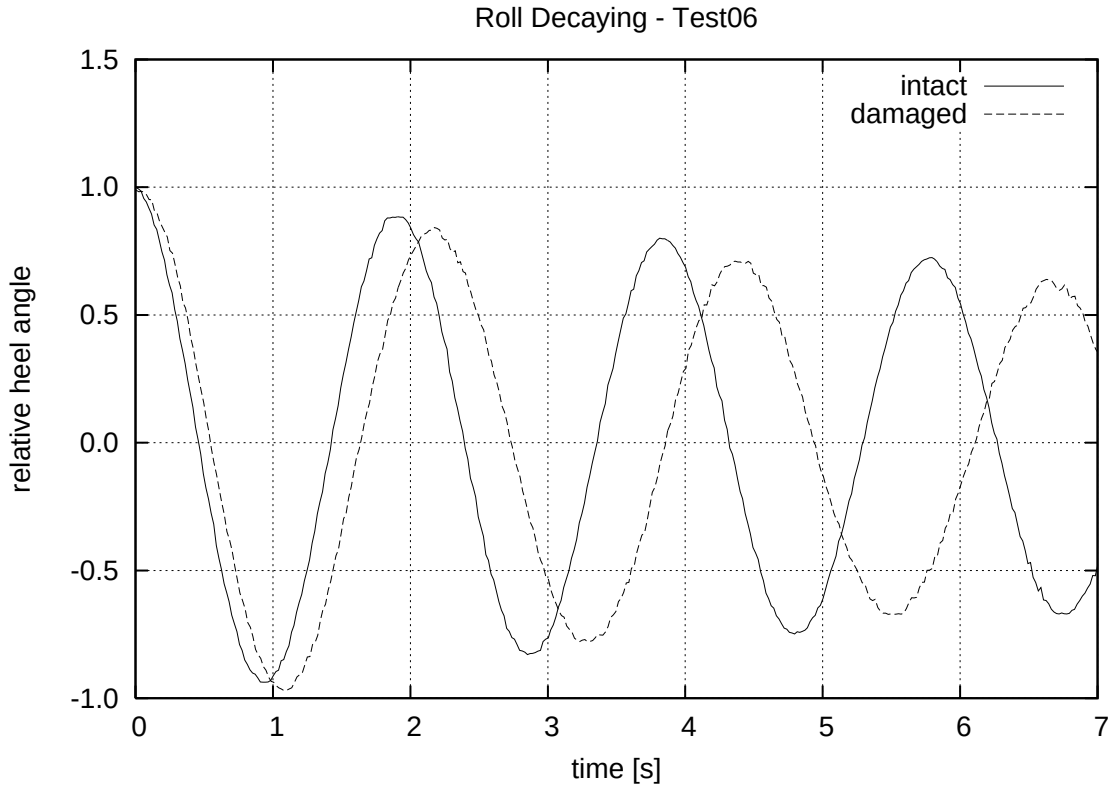

Figure 5.3 Roll decaying after damage (Test06) and in intact condition (initial heel angle was 2.4° in the damaged condition and 2.8° in intact condition)

6 Conclusions

Six different damage cases have been tested with a model of a box-shaped barge. Before the flooding tests, the initial metacentric height was evaluated by performing an inclining test for the fully loaded and instrumented model. The geometry of the hull of the model and the flooded compartments and openings are simple and accurately recorded.

The average discharge coefficients for all the openings in the model were evaluated experimentally by draining water through the openings. These results should be very useful input parameters when the flooding cases are simulated with a computational method.

During the flooding tests, the heel, trim and vertical sinkage of the model were measured. Water height was measured in every flooded room of the model and also the air pressures in the double bottom were measured.

The measured water heights show the progress of the floodwater and the results correspond to the visual observations that were obtained from the in-model video recordings.

The calibration of the water height sensors was found out to be challenging since the applied system was rather sensitive to the input voltage and the cables had to be plugged out and plugged in between the tests in order to empty the model from the flooded water. However, this problem was solved with the post-test calibrations and a careful analysis of the results.

Significant air bubbling was observed in the tests, where the damage opening was located in the bottom of the forward compartment. In general, it seems that air can escape from an air pocket as bubble flow if there is a partly submerged opening to the air pocket. In Test05 and Test06 such a situation did not exist, and also no air bubbling was observed.

Small sudden increases in the pressures of the air pockets in the double bottom were observed when room the R21 was filled up with water. This is can be, at least partly, caused by the increased resistance for the bubble flow. On the other hand, this can also indicate that there is sudden increase in the hydrostatic pressure in DB2.

The air bubbling caused high waves, especially in the room R21. The accuracy of the measurement of the water height in this room was somewhat reduced since the sensor was located rather close to the opening and the bubble flow.

The emptying of the model from the flooded water in between the tests was found out to be a slow and demanding process due to the complex structure of the flooded compartments. As a result, in Test01 and Test04 a very small volume of water was left inside some compartments from a previously performed test. These volumes of water were very small, and therefore, they did not have any effect on the flooding process.

The analysis of the results has shown that there was no need to measure the air pressure in the forward double bottom compartment DB2 since air compression was measured only after the compartment was already full of water. This means that the measured compression occurred in the pipe that lead to the pressure gauge.

The increase of the water heights in the side compartments R21S and R21P seems to slow down when the opening to R21 is submerged. This indicates that the air in these side compartments is slightly compressed due to the small ventilation pipes that slow down the outflow of air. Therefore, it would have been more useful to measure the air pressure in one of the side compartments than in the forward double bottom compartment.

In addition to the flooding tests, roll decaying test was performed for the flooded model after three flooding tests. The results show that the natural period of roll motion is slightly longer for the flooded model than for the intact model. Furthermore, roll damping is increased. The critical damping ratio was the same after all the three damage cases. The natural period of roll motion seems to depend mainly on the number of flooded compartments as the center of gravity depends on the volume of floodwater. No significant water ingress or egress was observed during the roll decaying tests. This is likely due to the relatively small size of the tested damage holes and the relatively small heel angles.

In general, the results of the measurements seem to correspond very well with the visual observations. Furthermore, the measurement of the water height in every compartment allowed a thorough analysis of the progress of the floodwater. Therefore, it is believed that the performed model tests provide valuable experimental data for the validation of numerical simulation methods for progressive flooding.

7 References

Matusiak, J. (1996): Laivan kelluvuus ja vakavuus (Ship Stability and Buoyancy), in Finnish, Otatieto 557, 177 p.

Ruponen, P. (2006): Pressure-Correction Method for Simulation of Progressive Flooding and Internal Air Flows, Schiffstechnik – Ship Technology Research Vol. 53, No. 2, pp. 63-73.

APPENDIX A

Evaluation of the Discharge Coefficient Based on the Discharging Time

Let us consider a tank with perpendicular walls that is discharging through an opening in the bottom of the tank. The area of free surface in the tank is *S*. The initial water height is H_1 and the final water height is H_2, measured from the level of the opening. The area of the opening is *A* and the discharge coefficient C_d is unknown. Instead, the discharging time *T* is known. A schematic picture of the system is presented in Figure A1. It is assumed that C_d is independent on the Reynolds number so that it is constant during the whole discharging time.

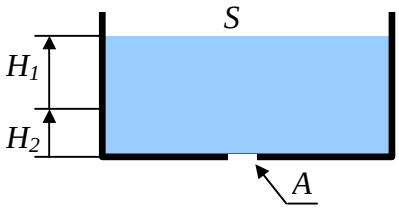

Figure A1 Draining tank

Bernoulli's equation along a streamline between point 1 and point 2 is:

$$p_1 + \frac{1}{2}\rho u_1^2 + \rho g H(t) = p_2 + \frac{1}{2}\rho u_2^2, \tag{A1}$$

where *p* is air pressure, ρ is density, *u* is flow velocity and *g* is the acceleration due to gravity. The point 2 is in the opening, and hence the water height *H* is present only on the left hand side.

In the case of fully vented system $p_1 = p_2$, and the air pressure has no effects on the discharge process. The velocity far from the opening can be taken as zero, i.e. $u_1 = 0$. Hence the flow velocity through the opening, solved from equation (A1), is:

$$u_2 = \sqrt{2gH(t)}. \tag{A2}$$

The instantaneous water height can be expressed as function of the volume of water since the area of free surface *S* is constant:

$$H(t) = \frac{V_w(t)}{S}, \tag{A3}$$

and the time derivative for the volume of water is the negation of the volumetric flow through the opening:

$$\frac{dV_w(t)}{dt} = -Q_w = -C_d A u_2. \tag{A4}$$

Therefore, the discharge process is governed by the following differential equation:

$$\frac{dV_w(t)}{dt} = -C_d A\sqrt{2g\frac{V_w(t)}{S}}\,, \tag{A5}$$

and the initial condition is:

$$V_w(0) = H_1 S\,, \tag{A6}$$

and the volume of water in the tank is decreasing. This can be solved analytically:

$$V_w(t) = \frac{{C_d}^2 A^2 g}{2S}\cdot\left[t^2 - \frac{2\sqrt{2gH_1}S}{C_d A g}\cdot t + \frac{2H_1 S}{gC_d^2 A^2}\right]. \tag{A7}$$

When a time period T has elapsed, the water level has decreased to H_2, and therefore:

$$V_w(T) = H_2 S\,. \tag{A8}$$

When this is substituted into equation (A7), the following equation is formed:

$$H_2 S = \frac{{C_d}^2 A^2 g}{2S}\cdot\left[T^2 - \frac{2\sqrt{2gH_1}S}{C_d A g}\cdot T + \frac{2H_1 S}{gC_d^2 A^2}\right]. \tag{A9}$$

This is a second order equation for the discharge coefficient and it can be rearranged, resulting in:

$$\frac{A^2T^2 g}{2S}{C_d}^2 - \sqrt{2gH_1}TA\cdot C_d + H_1 S - H_2 S = 0\,. \tag{A10}$$

The discharge coefficient can be solved:

$$C_d = \frac{AT\sqrt{2gH_0} \pm \sqrt{A^2T^2 2gH_0 - 4\cdot\frac{gA^2T^2}{2S}\cdot S(H_1 - H_2)}}{2\cdot\frac{gA^2T^2}{2S}} = \frac{S\sqrt{2gH_1}}{ATg} \pm \frac{S\sqrt{2gH_2}}{ATg}\,. \tag{A11}$$

Therefore, the following equation for the discharge coefficient is obtained:

$$C_d = S\frac{\sqrt{2gH_1} - \sqrt{2gH_2}}{ATg}\,. \tag{A12}$$

APPENDIX B

Results of the Calibration of Water Height Sensors

The initial calibration of the measurement system for the water heights was performed before the flooding test. Specially manufactured calibration sensors were used for this purpose. These sensors were practically identical to the ones that were installed in the model. The calibration sensor was connected to the measurement system. The sensor was then submerged to the water in the towing tank at certain intervals. The relative water height and the output voltage were recorded. A straight line was fitted to the results (see the figures below) and the slope of this line was used as the calibration factor for the measurement with the corresponding measurement card and channel. The obtained calibration factors and the correlations are given in the table below.

Sensor ID	Calibration factor [mm/V]	Correlation R^2
1	8.539	0.9999
2	7.811	0.9999
3	9.059	0.9998
4	20.823	0.9999
5	21.449	0.9999
6	16.933	0.9994
7	16.484	0.9999
8	16.549	0.9995
9	17.809	0.9995

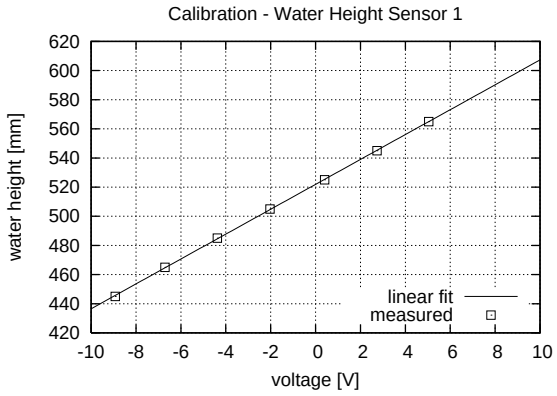

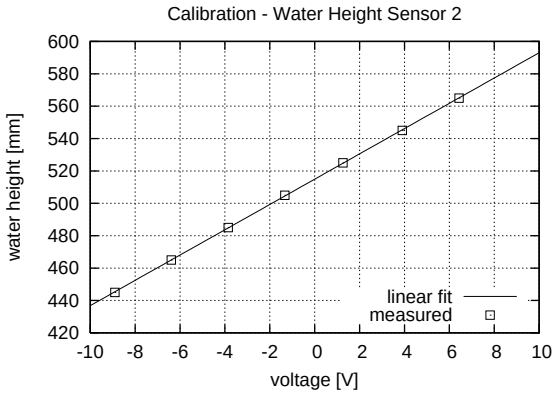

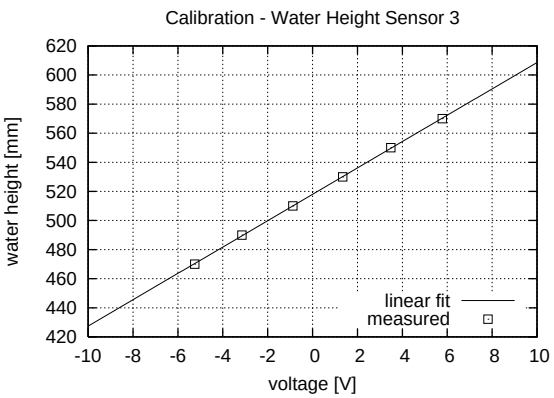
Calibration - Water Height Sensor 3
water height [mm]
voltage [V]
linear fit
measured

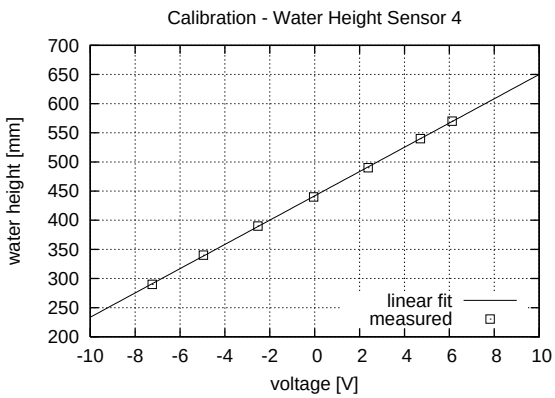
Calibration - Water Height Sensor 4
water height [mm]
voltage [V]
linear fit
measured

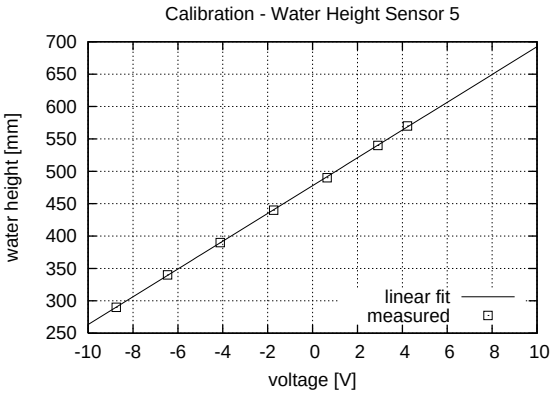
Calibration - Water Height Sensor 5
water height [mm]
voltage [V]
linear fit
measured

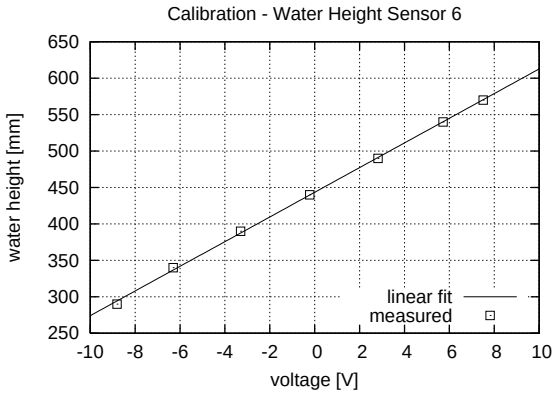
Calibration - Water Height Sensor 6
water height [mm]
voltage [V]
linear fit
measured

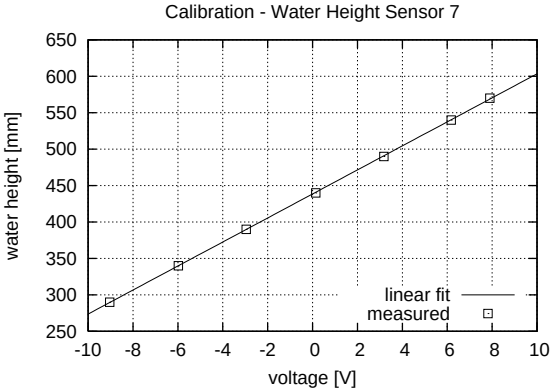
Calibration - Water Height Sensor 7
water height [mm]
voltage [V]
linear fit
measured

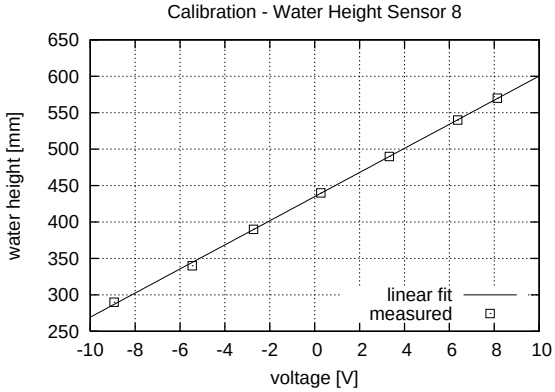
Calibration - Water Height Sensor 8
water height [mm]
voltage [V]
linear fit
measured

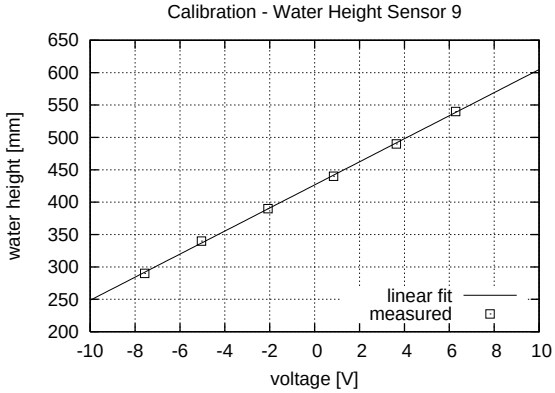
Calibration - Water Height Sensor 9
water height [mm]
voltage [V]
linear fit
measured

SHIP LABORATORY
Published M-series reports:

M-278 Heikki Remes, LABORATORY FATIGUE TESTS OF CO2-LASER HYBRID AND SUBMERGED ARC WELDED BUTT JOINT OF RAEX S275 LASER AND NVA. VOLUME 1 AND 2. Otaniemi 2003.

M-279 Pentti Häkkinen, LAIVAN SÄHKÖVERKKO. Otaniemi 2003.

M-280 Mikko Lensu, THE EVOLUTION OF RIDGED ICE FIELDS. Otaniemi 2003.

M-281 Juha Schweighofer, INVESTIGATION OF TWO-DIMENSIONAL TRANSOM WAVES USING INVISCID AND VISCOUS FREE-SURFACE BOUNDARY CONDITIONS AT MODEL- AND FULL SCALE SHIP REINOLDS NUMBERS. Otaniemi 2003.

M-282 J. Kajaste, P. Varsta, MECHANICS OF SHIP GROUNDING. Otaniemi 2003.

M-283 J. Kajaste, P. Varsta, J. Matusiak, DYNAMICS OF SHIP-GROUNDING. Otaniemi 2004.

M-284 T. Tamminen, H. Remes, FATIGUE TESTS OF LASER, LASER HYBRID AND ARC WELDED BUTT AND T-JOINTS OF RAEX S275 LASER, RAEX 420MC LASER, RAEX 700 OPTIM, GL-A36TM AND NVA STEELS. Otaniemi 2003.

M-285 A. Klanac, BENDING OF STEEL SANDWICH PANELS UNDER LATERAL LOADING. Otaniemi 2004

M-286 J. Matusiak, HYDRODYNAMIIKAN SOVELLUKSET SOTA-ALUKSISSA – ENNUSTE VUOTEEN 2020. Otaniemi 2004.

M-287 T. Leiviskä; LAIVAN PROPULSIOKERTOIMET JÄISSÄ JA AVOVESISSÄ. OSA 1: KEVÄÄN 2002 MALLIKOESARJAN MITTAUSRAPORTTI. OSA 2: MITTAUSTULOSTEN ANALYYSI JA PROPULSIOKERTOIMIEN TARKASTELU. Otaniemi 2004.

M-288 J. Romanoff, A. Klanac; DESIGN FORMULATION FOR FILLED STRUCTURAL SANDWICH PANES. Otaniemi 2005.

M-289 J. Matusiak; LAIVAN KULKUVASTUS. Otaniemi 2005.

M-290 J. Kajaste-Rudnitski, P. Varsta, J. Matusiak; SOME FE ESTIMATES OF SHIP COLLISION EVENT. Otaniemi 2005.

M-291 J. Romanoff, H. Remes, G. Socha, M. Jutila; STIFFNESS AND STRENGTH TESTING OF LASER STAKE WELDS IN STEEL SANDWICH PANELS. Otaniemi 2006.

ISBN 921-22-8228-3
ISSN 1456-3045